INFORMATION TO USERS

This manuscript has been reproduced from the microfilm master. UMI films the text directly from the original or copy submitted. Thus, some thesis and dissertation copies are in typewriter face, while others may be from any type of computer printer.

The quality of this reproduction is dependent upon the quality of the copy submitted. Broken or indistinct print, colored or poor quality illustrations and photographs, print bleedthrough, substandard margins, and improper alignment can adversely affect reproduction.

In the unlikely event that the author did not send UMI a complete manuscript and there are missing pages, these will be noted. Also, if unauthorized copyright material had to be removed, a note will indicate the deletion.

Oversize materials (e.g., maps, drawings, charts) are reproduced by sectioning the original, beginning at the upper left-hand corner and continuing from left to right in equal sections with small overlaps. Each original is also photographed in one exposure and is included in reduced form at the back of the book.

Photographs included in the original manuscript have been reproduced xerographically in this copy. Higher quality 6" x 9" black and white photographic prints are available for any photographs or illustrations appearing in this copy for an additional charge. Contact UMI directly to order.

UMI

A Bell & Howell Information Company
300 North Zeeb Road, Ann Arbor MI 48106-1346 USA
313/761-4700 800/521-0600

Hydrodynamic and Thermal Analysis of A Fluidized Bed Drying System

by

Ebrahim Hajidavalloo

A Thesis Submitted to the
Faculty of Engineering
in Partial Fulfillment of the Requirements
for the Degree of

DOCTOR OF PHILOSOPHY

Major Subject: Mechanical Engineering

APPROVED:

[redacted]

Feridun Hamdullahpur, Supervisor

[redacted]

Julio Militzer

[redacted]

K. Chris Watts

[redacted]

Ibrahim Dincer, King Fahd University of Petroleum and Minerals,
Saudi Arabia, External Examiner

DALHOUSIE UNIVERSITY-DALTECH

Halifax, Nova Scotia

1998

DALTECH LIBRARY

"AUTHORITY TO DISTRIBUTE MANUSCRIPT THESIS"

TITLE:

Hydrodynamic and Thermal Analysis of Fluidized Bed Drying System

The above library may make available or authorized another library to make available individual photo/microfilm copies of this thesis without restrictions.

Full Name of Author: Ebrahim Hajidavalloo

Signature of Author: 

Date: July/6/1998

TABLE OF CONTENTS

Page

LIST OF TABLES viii

LIST OF FIGURES ix

LIST OF SYMBOLS AND ABBREVIATIONS xvi

ACKNOWLEDGMENTS xxiii

ABSTRACT xxiv

1. INTRODUCTION 1

   1.1 Principles of Drying 2

   1.2 Fluidized Bed Drying 4

   1.3 Scope of the Study 6

2. LITERATURE REVIEW 8

   2.1 Introduction 8

   2.2 Prior Works in Fluidized bed Drying 8

3. EQUIPMENT, MATERIALS AND PROCEDURE 16

   3.1 Experimental Setup 16

      3.1.1 The Heater 18

      3.1.2 The Balance 18

      3.1.3 Data Acquisition System 18

   3.2 Material Properties 19

      3.2.1 Wheat 19

      3.2.2 Corn 21

   3.3 Method of Grain Conditioning 22

   3.4 Moisture Content Determination of Grain 22

   3.5 Drying Run Procedure 23

4. EFFECT OF SWIRLING INDUCED DISTRIBUTOR PLATE ON HYDRODYNAMICS OF FLUIDIZED BED 25

4.1 Introduction 25

4.2 Experimental Setup and Materials 27

4.2.1 Materials 29

4.3 Distributor Plate Design 30

4.4 Theoretical Background 30

4.4.1 Probability Distribution 31

4.4.2 Correlation 32

4.4.3 Power Spectral Density 32

4.5 Results for Low Density Materials (Wheat) 33

4.5.1 Minimum Fluidization Velocity 33

4.5.2 Signal Processing of Pressure Fluctuations 33

4.5.2.1 Effect of Bed Height 38

4.5.2.2 Effect of Distributor Plate Pressure Drop 39

4.6 Results for High Density Materials (Sand) 39

4.7 Discussion and Conclusions 44

5. EFFECT OF MOISTURE CONTENT OF PARTICLES ON THE HYDRODYNAMICS OF FLUIDIZED BED 45

5.1 Introduction 45

5.2 Theoretical Analysis 46

5.2.1 Adhesion Force Due to Capillary Action 48

5.2.1.1 Pendular-Bond Strength 48

5.2.2 Minimum Fluidization Velocity 52

5.3 Experimental Results 54

5.3.1 Pressure Drop versus Gas Velocity 55

5.3.2 Comparison of Bed Pressure Drop for Dry and Moist Particles 56
5.3.3 Effect of Moisture Content of Particles on Minimum Fluidization Velocity 60
5.4 Discussion and Conclusions 62

6. MATHEMATICAL MODELING OF FLUIDIZED BED DRYING 64
6.1 Introduction 64
6.2 Gas Flow Pattern in Fluidized Bed 65
6.2.1 Group D Particles 65
6.2.2 Group A Particles 70
6.2.3 Group B Particles 73
6.3 The Interstitial Gas Phase 75
6.4 The Bubble Phase 80
6.5 The Solid Phase 82
6.5.1 The Falling Rate Drying 83
6.5.2 The Constant Rate Drying 87
6.6 The Wall Effect 88

7. NUMERICAL ANALYSIS OF NONLINEAR SET OF PARTIAL DIFFERENTIAL EQUATIONS 90
7.1 Discretization of Differential Equations 90
7.1.1 Interstitial Gas Phase 91
7.1.2 The Bubble Phase 94
7.1.3 The Solid Phase 94
7.2 Method of Solution 100
7.3 Under-relaxation 102

8. NUMERICAL SOLUTIONS AND COMPARISON WITH EXPERIMENTAL RESULTS 104
8.1 Introduction 104
8.2 Assumptions 104
8.3 Comparison of Model and Experimental Results for Wheat Particles 105
8.3.1 General Agreement 105
8.3.1.1 Comparison of Results at T=49.5 °C 106
8.3.1.2 Comparison of Results at T=65.0 °C 113
8.3.2 Effect of Temperature 118
8.3.3 Effect of Bed Hold Up 121
8.3.4 Effect of Gas Velocity 123
8.3.5 Effect of Initial Moisture Content 125
8.4 Comparison of Model and Experimental Results for Corn Particles 129
8.4.1 General Agreement 129
8.4.2 Effect of Temperature 135
8.4.3 Effect of Bed Hold Up 137
8.4.4 Effect of Gas Velocity 139
8.4.5 Effect of Initial Moisture Content 141
8.5 Effect of Hydrodynamic Modeling on Drying Characteristics 143
8.6 Discussion and Conclusions 146

9. METHODS FOR INCREASING THERMAL EFFICIENCY OF FLUIDIZED BED DRYING 149
9.1 Thermal Efficiency 149
9.2 Recycling of Exhaust Gas 150
9.3 Intermittency 156

9.4 Discussion and Conclusions 160

10. CONCLUSIONS AND RECOMMENDATIONS 162

10.1 Conclusions 162

10.2 Recommendations 165

REFERENCES 167

LIST OF TABLES

Page

Table 1.1 Overall research program on the fluidized bed drying systems 7

Table 3.1 Specification of the thermocouples 18

Table 3.2 Specification of humidity transducer 18

Table 3.3 ASAE standard for drying of the grains 22

Table 4.1 Specification of particles used in the experiment 29

Table 5.1 Physical properties of various bed materials before and after conditioning 54

Table 8.1 Experimental conditions for investigating the effect of temperature 119

Table 8.2 Experimental conditions for investigating the effect of bed hold-up 121

Table 8.3 Experimental conditions for investigating the effect of velocity 123

Table 8.4 Experimental conditions for investigating the effect of initial moisture content 126

Table 8.5 Experimental conditions for investigating the effect of temperature 135

Table 8.6 Experimental conditions for investigating the effect of bed hold up 137

Table 8.7 Experimental conditions for investigating the effect of velocity 139

Table 8.8 Experimental conditions for investigating the effect of initial moisture content 141

LIST OF FIGURES

Page

Figure 3.1 Schematic diagram of experimental setup 17

Figure 3.2 Sorption isotherm of wheat particles at different temperatures, based on Fortes et al. [1981] Equation 20

Figure 3.3 Comparison of sorption isotherm curves of different authors 20

Figure 4.1 Experimental set up for analyzing the pressure fluctuation 28

Figure 4.2 (a) Cross section of a tuyere, (b) Half hole layout of the distributor and gas outlet direction 29

Figure 4.3 Effect of bed height on minimum fluidization velocity of wheat 33

Figure 4.4 Typical pressure fluctuation signal in the bed for wheat particles 34

Figure 4.5 Power spectral density function of pressure fluctuations for wheat 35

Figure 4.6 Autocorrelation function of pressure fluctuations for wheat 36

Figure 4.7 PDF of pressure fluctuations for wheat 37

Figure 4.8 Probability distribution of fluctuations for wheat 37

Figure 4.9 Power spectral density of fluctuations for wheat 38

Figure 4.10 Autocorrelation function of fluctuations for wheat 40

Figure 4.11 Power spectral density function of fluctuations for wheat 40

Figure 4.12 Power spectral density function of fluctuations for sand 42

Figure 4.13 Autocorrelation of pressure fluctuations for sand 42

Figure 4.14 PDF of pressure fluctuations for sand 43

Figure 4.15 Power spectral density of pressure fluctuations for sand 43

Figure 5.1 Balance of forces on a single particle in the fluidized bed 47

Figure 5.2 State of liquid bonding in a material, (a) pendular state, (b) funicular state, (c) capillary state 47

Figure 5.3 Geometrical representation of the pendular liquid bridge between equal-sized spheres 49

Figure 5.4 General pattern of bed pressure drop for sand and wheat particles with high moisture content. (Horizontal lines show the pressure drop equivalent to weight of bed material) 55

Figure 5.5 Comparison of bed pressure drop for sand with different moisture content 56

Figure 5.6 Mean amplitude of pressure fluctuation versus superficial gas velocity for sand 57

Figure 5.7 Comparison of bed pressure drop for wheat with different moisture content 59

Figure 5.8 Mean amplitude of pressure fluctuation versus gas velocity for wheat 60

Figure 5.9 Effect of moisture content on u_{mf} for sand particles 61

Figure 5.10 Effect of moisture content on u_{mf} for wheat particles 61

Figure 6.1 Different models for bubble behaviour inside bed: (a) mean bubble size (b) variable bubble size in axial direction (c) variable bubble size in axial and lateral directions 67

Figure 6.2 Voidage phase distribution inside the bed, (a) constant phase voidage, (b) variable phase voidage 67

Figure 6.3 One-dimensional control volume for interstitial gas mass transfer analysis 76

Figure 6.4 One-dimensional control volume for interstitial gas heat transfer analysis 78

Figure 7.1 Control volumes and grid-point cluster inside the bed 91

Figure 7.2 Control volumes and grids in spherical coordinates 95

Figure 7.3 Half control volume at boundary condition for mass exchange at the surface 97

Figure 7.4 Half control volume at boundary condition for heat exchange at the surface 99

Figure 8.1 Comparison between experimental data and model predictions for moisture content vs. time 107

Figure 8.2 Comparison between experimental data and model predictions for drying rate vs. time 107

Figure 8.3 Comparison between experimental data and model predictions for drying rate vs. moisture content 108

Figure 8.4 Comparison between experimental data and model predictions for relative humidity of exit air vs. time 108

Figure 8.5 Predicted moisture distribution profiles inside the wheat kernel 109

Figure 8.6 Predicted moisture distribution profiles inside a wheat kernel vs. time 109

Figure 8.7 Predicted temperature distribution profiles inside the wheat kernel 110

Figure 8.8 Comparison between experimental data and model prediction for gas temperature at h= 2 cm 111

Figure 8.9 Comparison between experimental data and model predictions of exit gas temperature 112

Figure 8.10 Comparison between model predictions and experimental data for gas temperatures as a function of bed height at different time 112

Figure 8.11 Comparison between experimental data and model predictions for moisture content vs. time 113

Figure 8.12 Comparison between experimental data and model predictions for drying rate vs. time 114

Figure 8.13 Comparison between experiment and model predictions for drying rate vs. moisture content 114

Figure 8.14 Comparison between experiment and model predictions for relative humidity of exit air vs. time 115

Figure 8.15 Predicted moisture distribution profiles inside the wheat kernel 115

Figure 8.16 Predicted moisture distribution profiles inside the wheat kernel vs. time 116

Figure 8.17 Predicted temperature distribution profiles inside the wheat kernel 116

Figure 8.18 Comparison between experimental data and model prediction for gas temperature at h=2 cm 117

Figure 8.19 Comparison between experimental data and model predictions for gas temperature at exit 117

Figure 8.20 Comparison between model predictions and experimental data for gas temperature as a function of bed height at different time 118

Figure 8.21 Effect of inlet air temperature on drying and comparison between experimental and numerical results for wheat 119

Figure 8.22 Effect of inlet air temperature on drying rate and comparison between experimental and numerical results for wheat 120

Figure 8.23 Effect of inlet air temperature on drying rate and comparison between experimental and numerical results for wheat 120

Figure 8.24 Effect of bed hold up on drying and comparison between experimental and numerical results for wheat 122

Figure 8.25 Effect of bed hold up on drying rate and comparison between experimental and numerical results for wheat 122

Figure 8.26 Effect of bed hold up on drying rate and comparison between experimental and numerical results for wheat 123

Figure 27 Effect of gas velocity on drying and comparison between experimental and numerical results for wheat 124

Figure 8.28 Effect of gas velocity on drying rate and comparison between experimental and numerical results for wheat 124

Figure 8.29 Effect of gas velocity on drying rate and comparison between experimental and numerical results for wheat 125

Figure 8.30 Effect of initial moisture content on drying and comparison between experimental and numerical results for wheat (top curves are normalized and bottom curves are actual M_p) 126

Figure 8.31 Effect of initial moisture content on drying rate and comparison between experimental and numerical results for wheat 127

Figure 8.32 Effect of initial moisture content on drying rate and comparison between experimental and numerical results for wheat 127

Figure 8.33 Effect of initial moisture content on drying rate and comparison between experimental and numerical results for wheat 128

Figure 8.34 Comparison between experimental data and model predictions for moisture content vs. time 130

Figure 8.35 Comparison between experimental data and model predictions for moisture content vs. time 130

Figure 8.36 Comparison between experimental data and model predictions for drying rate vs. moisture content 131

Figure 8.37 Comparison between experimental data and model predictions for relative humidity of exit air vs. time 131

Figure 8.38 Predicted moisture distribution profiles inside the corn kernel 132

Figure 8.39 Predicted moisture distribution profiles inside the corn kernel vs. time 132

Figure 8.40 Predicted temperature distribution profiles inside the wheat kernel 133

Figure 8.41 Comparison between experimental data and model prediction for gas temperature at h=2 cm 133

Figure 8.42 Comparison between experimental data and model predictions of exit gas temperature 134

Figure 8.43 Comparison between model predictions and experimental data for gas temperature as a function of bed height at different time 134

Figure 8.44 Effect of inlet air temperature on drying and comparison between experimental and numerical results for corn 135

Figure 8.45 Effect of inlet air temperature on drying rate and comparison between experimental and numerical results for corn 136

Figure 8.46 Effect of inlet air temperature on drying rate and comparison between experimental and numerical results for corn 136

Figure 8.47 Effect of bed hold up on drying and comparison between experimental and numerical results for corn 137

Figure 8.48 Effect of bed hold up on drying rate and comparison between experimental and numerical results for corn 138

Figure 8.49 Effect of bed hold up on drying rate and comparison between experimental and numerical results for corn 138

Figure 8.50 Effect of gas velocity on drying and comparison between experimental and numerical results for corn 139

Figure 8.51 Effect of gas velocity on drying rate and comparison between experimental and numerical results for corn 140

Figure 8.52 Effect of gas velocity on drying rate and comparison between experimental and numerical results for corn 140

Figure 8.53 Effect of initial moisture content on drying and comparison between experimental and numerical results for corn (top curves are normalized and bottom curves are actual M_p) 141

Figure 8.54 Effect of initial moisture content on drying rate and comparison between experimental and numerical results for corn 142

Figure 8.55 Effect of initial moisture content on drying rate and comparison between experimental and numerical results for corn 142

Figure 8.56 Effect of initial moisture content on drying rate and comparison between experimental and numerical results for corn 143

Figure 8.57 Effect of hydrodynamics modeling on the drying curve of wheat 144

Figure 8.58 Effect of hydrodynamics modeling on the drying rate of wheat 145

Figure 8.59 Effect of hydrodynamics modeling on the drying curve of corn 145
Figure 8.60 Effect of hydrodynamics modeling on the drying rate of corn 146
Figure 9.1 Effect of percentage of air recycled on the moisture content of particles 151
Figure 9.2 Effect of percentage of air recycled on the efficiency of drying 152
Figure 9.3 Effect of percentage of air recycled on the drying time 152
Figure 9.4 Variation of time vs. efficiency when the percentage of air recycled increases 153
Figure 9.5 Effect of percentage of air recycled on the exit relative humidity of gas 154
Figure 9.6 Effect of percentage of air recycled on the drying rate of process 154
Figure 9.7 Thermal efficiency as a function of inlet air temperature and bed height 155
Figure 9.8 Typical variation of moisture inside the grain during the drying 156
Figure 9.9 Prediction of drying curve in the intermittent scheme 157
Figure 9.10 Drying rate vs. time in the intermittent scheme 159
Figure 9.11 Predicted moisture distributions for intermittent scheme (solid lines are at the end of "on" period and dashed lines are at the end of "off" period) 159
Figure 9.12 Predicted relative humidity vs. time in the intermittent scheme 160
Figure 9.13 Predicted temperature of grain and air at h=2 cm, vs. time in the intermittent scheme 160

LIST OF SYMBOLS AND ABBREVIATIONS

A_b Bubble surface area (m^2)

A_o Distributor plate area per orifice (m^2)

A_p Particle surface area (m^2)

A_t Bed cross-section area (m^2)

A_{wi} Contact area between wall and interstitial gas (m^2)

A_{wp} Contact area between wall and particles (m^2)

C Air specific heat at constant pressure (J/ kg °K)

C_i Interstitial gas specific heat at constant pressure (J/ kg °K)

C_p Particle specific heat (J/ kg °K)

C_v Vapor specific heat at constant pressure (J/ kg °K)

C_{wl} Wall specific heat (J/ kg °K)

D Moisture diffusion coefficient (m^2/s)

D_v Diffusivity of vapor (m^2/s)

d_b Bubble diameter (m)

d_{b_j} Bubble diameter at control volume j (m)

d_{bm} Maximum bubble diameter (m)

d_{bo} Initial bubble diameter (m)

d_{or} Hole diameter of distributor plate (m)

d_p Particle volume diameter (m)

dr Grid interval in particle (m)

d_t Bed or tube diameter (m)

dt Time interval (s)

dv Volume of control volume in the bed (m)

dy Height of control volume in the bed (m)

H Bed height (m)

H_{cb} Overall heat transfer coefficient between cloud and bubble (1/s)

H_{ib} Overall heat transfer coefficient between interstitial gas and bubble (1/s)

H_f Bed height after fluidization (m)

H_j Height of control volume j from distributor plate (m)

H_{mf} Bed height at minimum fluidization (m)

Htap Tap height from distributor plate (m)

h_b Heat transfer coefficient of bubble and interstitial gas (W/m^2 °K)

h_{fg} Latent heat of vaporization of water (J/kg water)

h_p Heat transfer coefficient of particle and interstitial gas (W/m^2 °K)

h_{pw} Heat transfer coefficient of particle and wall (W/m^2 °K)

h_{wa} Heat transfer coefficient of wall and air ambient (W/m^2 °K)

h_{wi} Heat transfer coefficient of wall and interstitial gas (W/m^2 °K)

h_s Heat transfer coefficient of wall surface and interstitial gas (W/m^2 °K)

L Hole pitch of distributor plate (m)

f Frequency (Hz)

F_A Adhesive force (N)

F_{At} Total adhesive force (N)

F_b Buoyancy force (N)

F_d Drag force (N)

F_g Gravity force (N)

F_p Pressure difference force due to curvature of meniscus (N)

F_s Surface tension force along the wetted area (N)

g Gravity acceleration (m/s^2)

K Matrix of coupling coefficient (m^2/s)

K_{bc} Overall coefficient of gas interchange between bubble and cloud (1/s)

K_{ci} Overall coefficient of gas interchange between cloud and interstitial gas(1/s)

K_{ib} Overall coefficient of gas interchange between interstitial gas and bubble (1/s)

K_{ij} Element of matrix of coupling coefficient (m^2/s)

k_{ib} Mass transfer coefficient of interstitial gas and bubble (m/s)

k_p Mass transfer coefficient between gas and particles (m/s)

k_t Thermal conductivity of particle (W/m °K)

k_{ta} Thermal conductivity of air (W/m °K)

M_f Final moisture content of particle, dry basis (kg water/kg solid)

M_p Particle moisture content, dry basis (kg water/kg solid)

M_{pi} Initial particle moisture content, dry basis (kg water/kg solid)

M_{pwb} Particle moisture content, wet basis (kg water/kg wet solid)

M_w Molecular weight of water (kg/kmol)

$\overline{M}$ Averaged moisture content of a particle, dry basis (kg water/kg solid)

$\dot{m}_{conv.}$ Mass evaporation from surface of a particle (kg water/s)

N_{or} Number of orifices per unit area of distributor (m^{-2})

n_c Coordination number (-)

n_p Number of particles in the bed (-)

P Pressure (Pa)

P_p Pressure inside the solid particle (Pa)

$P(x_1)$ Probability Distribution Function (-)

p(x) Probability Density Function (-)

P_{sat} Saturated vapor pressure of air (Pa)

P_v Vapor pressure of air (Pa)

P_{wp} Wetted perimeter (m)

Q_b Bubble flow rate (m^3/s)

$\dot{q}_{evap.}$ Heat transfer due to water evaporation (W)

$\dot{q}_{pi}$ Heat transfer rate between particle and interstitial gas (W)

$\dot{q}_{pw}$ Heat transfer rate between particle and wall (W)

$\dot{q}_{wi}$ Heat transfer rate between wall and interstitial gas (W)

$\dot{q}_{wa}$ Heat transfer rate between wall and ambient air (W)

r Radius (m)

R Particle radius (m)

R_f Radius of particle surface roughness (μm)

R_{cons} Universal ideal gas constant (8314 J/mol °K)

RH	Relative humidity (%)
$R(\tau)$	Autocorrelation function ($[InH2o]^2$)
S	Projected area (m^2)
S(f)	Power spectral density function (Pa^2)
S_L	Liquid saturation of particle (-)
T	Inlet air temperature (°K)
T_a	Ambient air temperature (°K)
T_b	Bubble temperature (°K)
T_i	Interstitial gas temperature (°K)
T_p	Particle temperature (°K)
T_{pf}	Final particle temperature (°K)
T_{pi}	Initial particle temperature (°K)
T_{ps}	Surface temperature of particle (°K)
Ts	Duration of sampling (s)
T_{wl}	Wall temperature (°K)
t	time (min.)
V_b	Bubble volume (m^3)
W_A	Weight of grain after drying (kg)
W_B	Weight of grain before drying (kg)
W_b	Mass of particles inside the bed (kg)
u	Superficial gas velocity (measured on an empty vessel basis) (m/s)
$\underset{\sim}{u}$	Vector standing for M_p, T_p, P of particle
u_b	Bubble velocity (m/s)
u_{br}	Bubble rise velocity with respect to the emulsion phase (m/s)
u_i	Interstitial gas velocity (m/s)
u_{b_j}	Bubble velocity at control volume J (m/s)
u_{i_j}	Interstitial gas velocity at control volume J (m/s)
u_{mf}	Superficial gas velocity at minimum fluidization conditions (m/s)

X_i Interstitial gas absolute humidity (kg water vapor/kg dry air)

X_b Bubble absolute humidity (kg water vapor/kg dry air)

X_{sp} Absolute humidity of air adjacent to the particle surface (kg water vapor/kg dry air)

x(t) Pressure Fluctuation Signal (In H_2O)

Greek Symbols

α Thermal diffusivity (m^2/s)

β Coefficient of volumetric thermal expansion of air (K^{-1})

ν Kinematic viscosity (m^2/s)

η_{th} Thermal efficiency (-)

ε_{b_j} Bubble volume fraction at control volume J (-)

$\varepsilon_{b_{av}}$ Average bubble volume fraction (-)

ε_e Emulsion phase volume fraction in bed (-)

ε_i Interstitial gas volume fraction in bed (-)

ε_{e_j} Emulsion phase volume fraction at control volume J (-)

ε_{i_j} Interstitial volume fraction at control volume J (-)

ε_p Particle volume fraction in bed (-)

ε_{mf} Bed voidage at minimum fluidization (-)

ρ_a Air density (kg/m^3)

ρ_g Gas density (kg/m^3)

ρ_p Dry particle density (kg/m^3)

ρ_v Vapor density (kg/m^3)

ρ_w Water density (kg/m^3)

ρ_{wl} Wall density (kg/m^3)

ΔP Pressure difference due to curvature of meniscus (Pa)

ΔP_b Bed pressure drop (Pa)

θ Contact angle (-)

φ Bridge angle (-)

φ_s Sphercity of a particle (-)

ϕ Open area ratio of the distributor plate (-)

ϕ_m Logarithmic mean fraction of the inert or nondiffusing component (-)

σ Vapor-liquid surface tension (N/m)

μ_g Dynamic viscosity of gas (kg/m s)

μ_v Dynamic viscosity of vapor (kg/m s)

ω Under-relaxation coefficient (-)

τ Time Shift variable in Autocorrelation (s)

Subscripts

a Air

b Bubble or bed

i Interstitial gas

in Inlet

j location of control volume in the bed

g Gas

mb Minimum bubbling

mf Minimum fluidization

or Orifice

p Particle

ps Particle surface

s Surface

sat Saturated vapor

v Vapor

w Water

wl Wall

Abbreviation

PDF Probability Density Function

Amp Amplitude of pressure fluctuation

SFB Swirling Fluidized Bed

Dimensionless Numbers

Ar Archimides number, $Ar = \frac{d_p^3 \rho_g (\rho_p - \rho_g) g}{\mu_g^2}$

Ad Adhesion number, $Ad = \frac{49.5 \rho_g n_c R}{\pi \mu_g^2} \sqrt{\frac{\rho_p M_p}{\rho_w}} \left[\sigma - \frac{\rho_w R_{cons} T}{2 M_w} R \ln\left(\frac{P_v}{P_{sat}} \right) \right]$

Bi_h Heat transfer Biot number, $Bi_h = \frac{h_p R}{k_t}$

Bi_m Mass transfer Biot number, $Bi_m = \frac{k_p R}{D}$

Re_{mf} Reynolds number at minimum fluidization state based on particle diameter,

$$Re_{mf} = \frac{d_p u_{mf} \rho_g}{\mu_g}$$

Re_p Reynolds number based on particle diameter, $Re_p = \frac{d_p u \rho_g}{\mu_g}$

Sc Schmidt number, $Sc = \frac{\mu_v}{\rho_v D_v}$

Sh Sherwood number, $Sh = \frac{k_p d_p \phi_m}{D_v}$

ACKNOWLEDGEMENTS

Now, that I have finished this project, I would like to thank to those people who were involved in my project. Especially, I would like to express my sincere gratitude and appreciation to my thesis supervisor Dr. F. Hamdullahpur whose guidance, understanding, and continued support provided the necessary enthusiasm for the successful completion of this work. I wish him the best.

Also, the discussion, advice, and support by members of the guiding committee, Dr. K. C. Watts, and J. Militzer during the course of this project, are gratefully acknowledged. My gratitude and appreciation is extended to my friends in the university and also to Mechanical Engineering staff, Mr. G. Jollimore, Mr. S. Carr, Mr. F. Roma, and Mr. A. McPherson, who helped me in different ways in the course of this work.

I would also like to thank to Ministry of Culture and Higher Education of the Islamic Republic of Iran Government who provided a scholarship during the course of this study.

Last, but not least, I am very grateful to my wife and my children for their patience and supports during the term of this project without which this work would not have been accomplished.

ABSTRACT

Characteristics of the drying process of granular materials in the fluidized bed system has been studied. Experimental and theoretical approaches are used to undertake the study. Experiments are conducted in the laboratory scale fluidized bed to investigate the effect of the swirling outlet of air from the distributor plate, and the effect of initial moisture content of materials on the hydrodynamics of fluidized bed.

Digital signal processing of pressure fluctuations is used to understand and analyze the effect of swirling induced distributor plate on the hydrodynamics of the bed. The results obtained from the power spectral density function, autocorrelation, and probability density function analyses of pressure fluctuation signals show that the swirling induced distributor plate may significantly improve the contact efficiency of the fluidized bed by reducing the bubble size, in the case of shallow bed or low density materials in the bed.

Experimental investigations on the fluidization of moist material reveal that the moisture content of the bed material is directly proportional to the bed pressure drop. The pressure drop vs. velocity curve for wet particles exhibits a different pattern from that of the dry particles case. Also, increasing the moisture content of materials increases the minimum fluidization velocity because of the existence of interparticle adhesive force caused by liquid bridge of isolated capillaries. It is also found the pressure drop along the fixed bed of moist particles is smaller than the one for dry bed, suggesting the existence of microchannels in the beds.

In the theoretical section, a comprehensive mathematical model for simulation of simultaneous heat and mass transfer in fluidized bed drying is developed. The model considers the presence of different phases inside the bed, and their physical variation along the bed. A set of coupled non-linear partial differential equations is employed to accurately model the drying process without using any adjustable parameters. A

numerical code is developed to solve the governing partial differential equations using a control volume based discretization approach.

Results of the model predictions show very good agreement with a large number of experimental data obtained in the drying of two types of grains (wheat and corn). The agreement of model prediction and experimental data indicates that the model is fully predictable for drying of other materials in the fluidized bed with no restriction in the range of operational condition such as the air temperature and the relative humidity. The model can be applied to the other type of processes such as spouted bed and fixed bed drying with slight modification.

It is found that the drying of grain materials is usually controlled by internal mass transfer parameters. The inlet air temperature has an important effect on the magnitude of drying rate while the gas velocity and bed hold up do not show significant contribution on the drying rate. The initial moisture content of the bed materials can have an important effect on the drying rate depending on the physical properties of bed materials.

Different schemes for increasing the thermal efficiency of fluidized bed drying are introduced in the mathematical model including the recycling and intermittent schemes. It is found that the recycling scheme may increase the thermal efficiency of fluidized bed system substantially without considerable increase in the drying time. Intermittent scheme can also improve the thermal efficiency of the fluidized bed and the quality of dried products. The amount of increase in thermal efficiency depends on the intermittency scheme, but it is usually lower than the recycling scheme.

CHAPTER 1
Introduction

Of all the unit operations used by the process industries, drying is probably the oldest and the most common one found in diverse fields such as agricultural, chemical, food, pharmaceutical, pulp and paper, mineral, polymer, ceramic, and textile industries. Industrial dryers consume a significant fraction of the total energy used in many manufacturing process, on average some 12%. For an individual dryer, energy costs account for the bulk of the overall costs, typically some 60-70% [Bahu, 1991]. At the most fundamental level, the process of drying requires latent heat of vaporization to evaporate moisture. Considering the cost of fuel and its heating value, it is easy to see how important the rate of energy consumption is in any type of drying process.

Despite this intensive energy consumption, and even after more than half a century of investigation at universities and in industry, the drying of wet solid is still as much art as science [Cook, 1997]. This is so because drying is one of the most complex and least understood operations which often involves simultaneous and coupled multiphase flow, and there are difficulties and deficiencies in the mathematical description of the phenomenon of simultaneous and coupled heat, mass, and momentum transfer in solid media.

Fundamental research with the aid of mathematical modeling and numerical simulation provides an extremely powerful and cognitive tool for investigating the complicated physics that evolve during the drying of wet porous materials [Turner and Mujumdar 1997]. The results of this simulation can be used subsequently by drying engineers and practitioners to guide further experimental design, and perhaps most importantly, to provide a better understanding of the drying process as a whole. The strategy of modeling followed by system optimization and overall experimental validation of the results is a cost-effective and efficient method for furthering drying technology.

In the past, analytical solutions to this problem were confined to simple drying configurations and were valid only under a very stringent set of assumptions. In general, numerical simulation is the only possible solution strategy which can overcome the inherent nonlinearity of governing set of partial differential equations. Due to tremendous increase in computational capabilities, the possibilities for obtaining fast and accurate solutions to many of the previously intractable drying problems are becoming a reality.

However, the way of developing an efficient and effective solution strategy for the drying equations is by no means straightforward. There are numerous stumbling blocks which should be overcome before the implementation task is completed. For example, some of the more formidable tasks are: identification of the best discretization strategy to use, solution of the nonlinear set of equations, convergence criteria, grid generation, time step control, experimental validation, and, finally, the best means of graphically visualizing the results. One of the main objectives of this work concerns the analysis and state-of – the-art numerical methods that can be used to assist with the implementation of the above-mentioned tasks.

1.1 Principles of Drying

When a wet solid subjected to thermal drying, two processes occur simultaneously [Mujumdar, 1987];

1. Transfer of energy from the surrounding environment to the solid to evaporate the surface moisture. This depends on external conditions i.e. air temperature, humidity, velocity, pressure, and the exposed surface area.
2. Transfer of internal moisture to the surface of the solid and its subsequent evaporation due to process 1. This is a function of physical properties of the solid, the temperature, and its moisture content.

The rate at which drying is accomplished is governed by the rate at which the two processes proceed. In a drying operation, any one of these processes may be the limiting factor governing the rate of drying, although they both proceed simultaneously throughout the drying cycle. Measurement of sample temperature during drying can help to identify whether a process is controlled by energy (external) or mass (internal) transfer. A sample temperature equal to the wet bulb temperature of the surrounding medium is characteristic of energy transfer control. If the sample reaches the dry bulb temperature of the drying medium, mass transfer control is suggested. Usually, when the first process is the limiting factor, namely transfer of energy from the surrounding environment to the solid, drying takes place at a constant rate and is known as constant rate drying. If the second process is the limiting factor, namely transfer of internal moisture to the surface of the solid, drying takes place at a logarithmicly decreasing rate and is known as falling rate. Existence of any of these two process depend on many parameters such as type of material, moisture content, sorption isotherm, diffusion coefficient and other transport coefficients. The critical moisture content occurs between the falling rate period and the constant rate period [Hall, 1980]. The critical moisture content is the minimum moisture content of the grain that will sustain a rate of flow of free water to the surface of the grain equal to the maximum rate of removal of water vapor from the grain under the drying conditions. The critical moisture content can vary with air temperature and the properties of the material.

Generally, non-hygroscopic materials dry mostly at a constant rate period and have short time of falling rate period at the end of the drying process. Moisture in this type of materials is not bonded (i.e. it is free moisture) and exists inside the relatively large size pores inside the particles. Therefore, the vapor pressure of the moisture is identical to the saturated vapor pressure of water.

On the other hand, hygroscopic materials dry mostly in the falling rate period and have only a very short time of constant rate period initially. Moisture for this type of material

is bonded inside the material (bound moisture), and therefore, its migration to the surface can not takes place easily. If the moisture content is lower than a specified value the vapor pressure of moisture is not identical to the saturated vapor pressure, and should be specified through the sorption isotherm.

Different mechanisms have been proposed for moisture migration inside the particle in the falling rate period such as [Brooker et al., 1974, and Waananen et al., 1993]:

1. Liquid movement due to surface forces (capillary flow);
2. Liquid movement due to moisture concentration differences (liquid diffusion);
3. Liquid movement due to diffusion of moisture on the pore surface (surface diffusion);
4. Vapor movement due to moisture concentration differences (vapor diffusion);

Modeling of the drying process is complicated because more than one mechanism may contribute to the total process, and the contribution of different mechanism may change as the drying process proceeds. The development of a generally applicable drying model requires the identification and inclusion of all contributing mechanisms. Most models apply the liquid diffusion mechanism with sufficient accuracy.

1.2 Fluidized Bed Drying

Fluidizing with hot air is an attractive means for drying many moist powders and granular products. The first commercial unit was installed in the United States in 1948 to dry dolomite [Becken, 1960], and currently this technique enjoys widespread popularity for drying grain, chemicals, pharmaceutical, polymer, mineral and many other industrial products. The main advantages offered by this technique of drying are as follows:

(1) Rapid mixing of solids leads to nearly uniform moisture content and temperature of solids throughout the bed.

(2) The lack of moving parts results in the low maintenance cost and low equipment costs.
(3) The fluidity of particles provides an excellent condition for handling and moving the particles under automatic or manual control.
(4) Heat transfer rate between fluidized particles and any submerged surface is very high, thus enabling the use of the heating or cooling surface to improve the process efficiency.
(5) High thermal efficiency when using newer designs of fluidized bed such as steam fluidized bed, indirect heating fluidized bed by using heating surfaces, vibrofluized bed, combined fluidized bed and spray drying

The main disadvantages or limitations of fluidized bed dryers are as follow:

(1) There is excessive loss of kinetic energy due to high superficial gas velocity.
(2) The material being dried must be fluidizable.
(3) Some fragile materials might break due to attrition and intense mixing.

Although fluidized bed drying systems are extensively used in different sectors of industries, fundamental research on fluidized bed drying has not made similar progress and the design of an industrial fluid bed dryer is still very much an art based upon empirical knowledge [Hovmand, 1987]. Most of the models presented in the literature use many simplifications to solve the governing equations analytically and those works which used the numerical solution consider many other assumptions which may not present a through analysis of drying process and what is required in the industrial designs. Much more work on the detail analysis of different fluidized bed drying system is necessary to increase our understanding from processes involved in this technique.

In this work, all processes taking place inside the fluidized bed, and other related parameters that are important from practical point of view are considered in the analysis

of drying process. This approach will provide a more comprehensive picture about the effective variables and factors during the process of drying and may shorten the gap between fundamental research and practical design in fluidized bed drying.

1.3 Scope of the Study

This study is carried out in two separate but interrelated sections, (a) experimental section, (b) theoretical section. The components of experimental section are as follow:

1. To design and build a swirling induced distributor plate and investigate its effect on the hydrodynamic of fluidized bed.
2. To investigate the effect of moisture content of particles on the hydrodynamic of fluidized bed.
3. To provide experimental data on the drying kinetics of grains in fluidized bed (wheat and corn) in order to evaluate the results of mathematical model and also introduce reliable data for other researches in this area.

The theoretical part of the study includes:

1. The development of a comprehensive mathematical model for simulation of fluidized bed dryers.
2. The investigation of the effect of recycling scheme on the kinetics of drying and the thermal efficiency of fluidized bed.
3. The investigation of the effect of intermittent scheme on the kinetics of drying and the thermal efficiency of fluidized bed.
4. The development of a reliable and stable numerical code for solving the set of governing partial differential equations of drying process under different schemes.

The overall research program is outlined in Table 1.1.

Table 1.1 Overall research program on the fluidized bed drying system.

"Hydrodynamic and Thermal Analysis of Fluidized Bed Drying"

- A) Experimental
  - 1. On Hydrodynamic of Bed
    - Effect of Distributor Plate Outlet Geometry
    - Effect of Moisture Content
      - Hygroscopic Material
      - Non - Hygroscopic Material
  - 2. On Drying Kinetic
    - Wheat
      - 1. Effect of Temperature
      - 2. Effect of Particle Hold - up
      - 3. Effect of Air Velocity
      - 4. Effect of Initial Moisture Content
    - Corn
      - Same As Wheat
- B) Theoretical
  - 1. Mathematical Modeling of Fluidized Bed Dryers
    - 1. Group A
    - 2. Group B
    - 3. Group D
  - 2. Recycling of Air
    - 1. Partial Recycling
    - 2. Total Recycling
  - 3. Intermittent Drying

CHAPTER 2
Literature Review

2.1 Introduction

This chapter provides a brief review of pertinent works with respect to the experimental investigations and mathematical modeling of the fluidized bed drying systems. It is crucial to have an understanding of previous works in these areas so that we can build upon these contributions to develop a better and more precise model for this type of dryer.

Literature review on the effect of swirling induced distributor plate and moisture content of particles on the hydrodynamic of fluidized bed is discussed separately in the introduction section of corresponding chapters of this thesis.

2.2 Prior Works in Fluidized Bed Drying

One of the primary works in fluidized bed drying belongs to Vanecek et al. [1966]. They proposed a design procedure for fluidized bed dryers based merely on the total heat and mass balance of the whole apparatus, and on the results of some runs with granular material in a laboratory-scale unit. In fact, the fluidized bed has been treated as a homogenous system, without considering bubbles, and its interactions in the bed. Hoebink and Rietema [1980a] developed a model for fluidized bed drying and described the heat and mass transfer between the dense phase, the cloud, and the bubbles with the assumption of no diffusion limitation inside the solids. They described the moisture transport between particles and gas with a single and constant overall mass transfer coefficient which is useful for constant rate drying. In their second model, Hoebink and Rietema [1980b], extended the first model to include a more general case where due to a severe diffusion limitation inside the particles, the concept of a constant mass transfer coefficient was no longer adequate to describe the moisture transport of solids. However, mass transfer was considered to be fast in the dense phase, and also equilibrium between

the solid particles and interstitial gas was assumed. Reay and Allen [1982] developed simple rules for estimating the effect of bed depth, gas velocity and bed temperature on fluidized bed drying curves. Furthermore, they proposed a procedure for simulating the performance of a continuous well-mixed fluid bed dryer from batch tests under isothermal inlet conditions. They verified it experimentally for iron ore, ion exchange resin and wheat particles.

Plancz [1983] proposed a mathematical model for continuous fluidized bed drying by employing a Kunii-Levespiel type, three-phase model inside the bed. The bubble phase was assumed to be in plug flow while the interstitial gas, as well as the solid particles was considered to be perfectly mixed. He assumed a simplified lumped model for solid particles and studied the effects of the process parameters on the moisture content of solids. However, he mentioned that the lumped model for solid particles was not realistic and recommended to improve the lumped particle model by taking into account the internal resistance to the heat and mass transfer inside the moisture solid. Uckan and Ulku [1986] studied the effects of air temperature and velocity on the corn drying in a batch fluidized bed and developed a model based on the diffusion theory. They suggested an empirical formula for the drying of corn based on the results of their model and experimental finding. The authors found out that the drying medium velocity had no particular effect on the drying rate and the dominant factor in corn drying was diffusion controlled. In their model, they assumed that the drying air left the bed in mass and thermal equilibrium with the grain, and that the presence of bubbles and their interactions with other phases was ignored.

Alebregtse [1986] presented a model for hydrodynamics and mass transfer for constant rate drying in a fluidized bed in which the heat and mass limitation was not inside the solid particles. He considered the interaction of bubble phase, interstitial gas phase and solid phase based on the two-phase theory of fluidization. He reported that above a certain bed height the drying rate was almost a reciprocal function of the bed height and

the catchment area of distributor plate. He mentioned that the model had two shortcomings. The first one is the major assumption of the two-phase theory of fluidization, which is not a reliable model for large size particles. The second shortcoming is that the model does not account for the difference in fluidization behaviour for wet and dry products. Giner and Calvelo [1987] studied drying of wheat in batch fluidized bed dryer and proposed a model similar to Becker and Isaacson [1970] model. They used the kinetic parameters, obtained from the thin-layer experiments, in their model, and showed that drying times could be decreased fourfold by raising the air temperature from 40 °C to 70 °C. They suggested that in order to increase the thermal efficiency, inlet air temperatures much higher than the critical temperature (temperature at which damage to the internal structure of grain may take place), could be used without deterioration of grains during the first stage of drying and then reduced the temperature to the specified value. They proposed using the recirculation of air as a means to improve the low thermal efficiency of the drying process. They, however, did not consider the presence of bubbles inside the bed and assumed a thermal equilibrium model between gas and gas. Chandran et al. [1990] presented a model for the drying kinetics of solid particles in batch fluidized bed dryer incorporating a constant rate period followed by a falling rate period. They combined the drying kinetics and the residence time density function appropriate for the mixing of solids in the bed to predict the average moisture content of the products for a continuous fluidized bed. They reported a satisfactory match between the experimental data and the model predictions for single and spiral fluidized bed.

Abid et al. [1990] performed an experimental and theoretical analysis of the mechanism of heat and mass transfer during drying of corn in a fluidized bed containing inert particles. They used the principle of irreversible thermodynamics in their model. They accounted for the transfer of water by diffusion under the influence of a concentration gradient of the moisture, and by thermodiffusion under the influence of a temperature gradient. They found the external conditions such as the humidity and velocity of the gas

have only a small effect on the rate of drying. By a sensitivity analysis for the coefficient of thermal gradient, they verified that the transfer of water by thermodiffusion was negligible compared to the one by ordinary diffusion.

Stakic and Milojvic [1992] developed a numerical simulation of heat and mass transfer in fluidized bed drying using a control volume method to discretize the differential equations. They used the classic two-phase theory of fluidization for the hydrodynamics of fluidized bed, and a known equation from the drying kinetic for mass transfer of particles. They reported a successful match between the results of the mathematical model with the experimental data available in the literature and with their own experimental results for which unrefined sugar was used. Thomas and Varma [1992] proposed a pseudo-steady state receding core model for drying kinetics of granular cellular materials –green pepper, black pepper and mustard. They indicated that intraparticle diffusion controls the drying process and the falling rate might be nonlinear depending upon the nature of material. They predicted the performance of the continuous fluidized bed drying from the kinetic data obtained, using a batch fluidized bed dryer and assuming ideal mixing of solids. Hemati et al. [1992] studied the drying of maize in a flotation fluidized bed, where the corn kernels were immersed in a hot fluidized bed of sand particles. They used an intermittent scheme to increase the efficiency of the bed and reported that under isothermal conditions it leads to 50% reduction of energy consumption.

Srinivasa Kannan et al. [1994] presented a model for drying of solids in a batch fluidized bed considering the heat and mass transfer among the bubble, interstitial gas, and solid phases. They used an analytic solution of diffusion equation to predict the moisture distribution inside the particle with the assumption of uniform temperature for solids in equilibrium with the interstitial gas (equilibrium model). They studied the effect of different experimental conditions, such as the temperature and flow rate of the air, the initial moisture content of solids, and solids hold up on the drying of material such as millet, ragi, and poppy seeds. They reported a good agreement between their model and

the experimental data and concluded that heat transfer is the controlling mechanism during the constant rate period, while intraparticle diffusion of moisture controled the falling rate period. However, they used a simplified model for mass and energy equation of interstitial gas and bubble phases. They also used the equilibrium assumption between gas and solid particles and evaluated the effective diffusivity of the solid particles by matching the experimental data with the model. Srinivasa Kannan et al. [1995] experimentally investigated the fluidized bed drying of solids in the constant and the falling rate. They compared the performance of batch and different types of continuous fluidized bed dryers. They reported the spiral fluidized bed dryer has an advantage over the single-stage continuous dryer and that of multistage dryers over the batch fluidized bed dryer.

Zahed et al. [1995] presented a model for a fluidized bed dryer with allowance for the diffusional moisture transport in the particles and for interstitial gas-to-particle mass transfer within the dense phase, as well as interphase exchange resistance between gas bubbles and the dense phase. They predicted the bed temperature and moisture content of the solids under various batch drying conditions. They did not conducted experiments to verify their numerical results and also could not compare their results with experimental results in the literature since they reported a few experimental data published on fluidized bed drying and those that had been published did not allow adequate information for comparison. However, like Srinivasa Kannan [1994], they neglected the unsteady term in the mass and energy equations for interstitial gas and bubble phases and also assumed a thermal equilibrium model and constant bubble size.

Ciesielczyk [1996] used the Kunii-Levenspiel bubbling bed model to calculate the interfacial coefficient of heat and mass transfer in the constant rate period of fluidized bed dryers. Alvarez and Shene [1996] presented a methodology to estimate the heat transfer coefficient using drying data in the constant rate period. They reported a much lower heat transfer coefficient than those reported in the literature. Theologos et al.

[1997] developed a model based on two-phase flow theory which consisted of the full set of partial differential equations for describing the conservation of mass, momentum, and energy for the solid and gas phases. However, they did not use the partial differential equation for mass and heat transfer inside the solid. Instead they used the drying kinetics model of Maroulis et al. [1996]. They used the PHONICS software to solve the set of partial differential equations and predicted the pressure drop, bed void fraction, temperature distribution in gas and solid phases as well as air humidity and particle moisture in the fluidized bed.

van Ballegooijen et al. [1997] developed a numerical model for the prediction of the drying process in a fluidized bed dryer of materials with diffusion limited behaviour. They compared the results of the numerical model with laboratory experiments for silica-gel particles and found a large discrepancy. They attributed this difference to wrong diffusion coefficient for silica-gel and proposed a diffusion coefficient to match their results with the experiments. Kiranoudis et al. [1997] designed a procedure for fluidized bed and rotary dryers to optimize the total cost of each system for a given production capacity. They used a simple mathematical model to describe the convective drying process for both types of dryers. Rotary dryers turned out to be rather expensive compared to fluidized bed dryers, regarding design structure. On operational grounds, however, it was the other way around due to the understandably favored heat transfer achieved in rotary dryer. They used both food products and inorganic material to test the effectiveness of the approach.

Soponronnarit et al. [1997] investigated the drying characteristics of corn in a small batch fluidized bed dryer. They recycled a fraction of the air to increase the thermal efficiency of the bed. They tried many empirical thin layer drying equations to correlate with their experimental results and found that the Wang and Singh [1977] equation could describe the results with sufficient accuracy.

Grabowski et al. [1997] experimentally examined the drying of yeast in a laboratory scale fluidized bed and spouted bed dryers. They reported that the spouted bed needed about 25% higher flow rate than the fluidized bed. However, they found that, based on fluidization and spouting behaviour, drying kinetics, and viability determination, drying in a spouted bed or combination of spouted bed and fluidized bed was better than only fluidized bed. Jumah et al. [1997] studied the effect of different intermittent schemes on the average moisture content of the particles in a novel rotating jet spouted bed drying system. They showed that significant energy and quality advantages may accrue from intermittent drying of heat sensitive particles.

A close examination of the previous modeling studies revealed that many assumptions have been made in order to simplify the analysis of drying process. First, in almost all of the works it has been assumed that for all particle groups with different specifications, the hydrodynamics of the fluidized beds is identical and the two-phase theory of fluidization can be used for the modeling purpose. Also, the bubble diameter and velocity are assumed to be constant along the bed height. These assumptions are at odds with the well recognized fact that the hydrodynamics of a fluidized bed is dependent on particle specifications and each particle group manifests its own behaviour in the bed. It is a well-known fact that the two-phase theory of fluidization is suitable for group A particles and cannot be used for other particle groups without a significant error. Geldart [1986] reported that the application of two-phase theory for group D particles, the group that is mostly used in drying processes, resulting up to 50% error in the bubble flow rate.

Second, in most of the works the temperature variation of the air along with the bed is neglected and a uniform temperature is assumed. Furthermore, the variation of air temperature with time is also neglected in order to come up with analytic solution. The assumption of uniform temperature for air is not a precise assumption in the initial period of drying. It should be noted that one must distinguish between the temperature of particles and the temperature of air inside the fluidized bed. A uniform particle

temperature inside the bed can be assumed at any time due to high mixing rate of particles. For the air the assumption of uniform temperature is not valid at least for the initial period of drying. This assumption is important from this perspective that in the initial period of drying, the drying rate is usually very high and is close to the maximum drying rate. Any simplification may produce significant error in the results.

Third, in many of the works the diffusion equations are not used in the conservative form but are manipulated to take a simplified form with a constant effective diffusion coefficient. This assumption may have considerable effect on the results, since the diffusion equation plays a fundamental role in the moisture content distribution inside the particle. It is recommended to use the equation in its most general and exact form satisfying the conservative properties of the materials and avoid any simplification for the diffusion coefficient [Patankar, 1980].

Fourth, it is assumed that the fluidized bed is deep enough to assure thermal equilibrium between the particles and the air leaving the bed and also the temperature gradient inside the particles can be neglected. With these assumptions, there is no need for a single particle heat transfer equation and the exit air temperature is taken to be equal to the bed temperature. Although these assumptions may be valid for some particles, it is more accurate to use separate energy equations for each phase, and also consider the variation of temperature in the solid phase.

The above mentioned simplifications are not employed in this work, instead a comprehensive mathematical model is presented which considers the interaction of all important factors inside the bed. Since this model considers the details of heat and mass transfer inside the bed and does not contain any adjustable parameters, it can be used with more confidence and reliability in simulating the drying process in the fluidized bed. The model with a slight change can also be used for fixed bed drying, spouted bed drying and steamed fluidized bed drying.

CHAPTER 3

Equipment, Materials and Procedure

In this chapter the equipment, material and procedure used in conducting the various experiments are described. The experimental setup, used in conducting tests on the swirling induced distributor plate is different from the rest of the work, therefore, it is described separately in the corresponding chapter (chapter 4).

3.1 Experimental Setup

Figure 3.1 shows the schematic of the laboratory scale fluidized bed dryer system designed and constructed to conduct the experimental part of this study. Air is supplied via a root blower and then passed through a 2.5 kW heater. The exit temperature of air from the heater is maintained constant using a PI control system within ±1°C. The air then reaches a precalibrated orifice plate, placed downstream from the heater to measure the air flow rate. The pressure drop across the orifice plate is measured using a differential pressure transducer with the range of 0-10 inch of water (Omega, PX-164-0-10D5V). The air then enters the plenum which is filled with Rasching rings to evenly distribute the air flow before passing through the distributor plate. The distributor plate is constructed from Plexiglas of 6 mm thickness, with 666 holes of 2 mm diameter arranged in a triangular pattern, resulting in 8% free area. The pressure drops across the distributor plate and the bed is measured by another differential pressure transducer (Omega, PX-164-0-10D5V).

The cylindrical bed column is made of Plexiglas with a wall thickness of 7 mm, an internal diameter of 175 mm, and an overall length of 1200 mm. Copper-Constantan (T type) thermocouples are used to measure the temperatures at the inlet and outlet of the bed as well as locations at 20, 40, 65, 105, 145, 185 and 730 mm above the distributor plate. The wall temperature is measured at 50 mm above the distributor plate on the inner side of the column. All thermocouples were the same type and their specifications are given in Table 3.1.

The relative humidity of the exit air is measured by using humidity transducer (Vaisala HMD 20UB), located before the exit. It is calibrated using solutions with different vapor pressures and equilibrium relative humidity. The specifications of humidity transducer are given in Table 3.2.

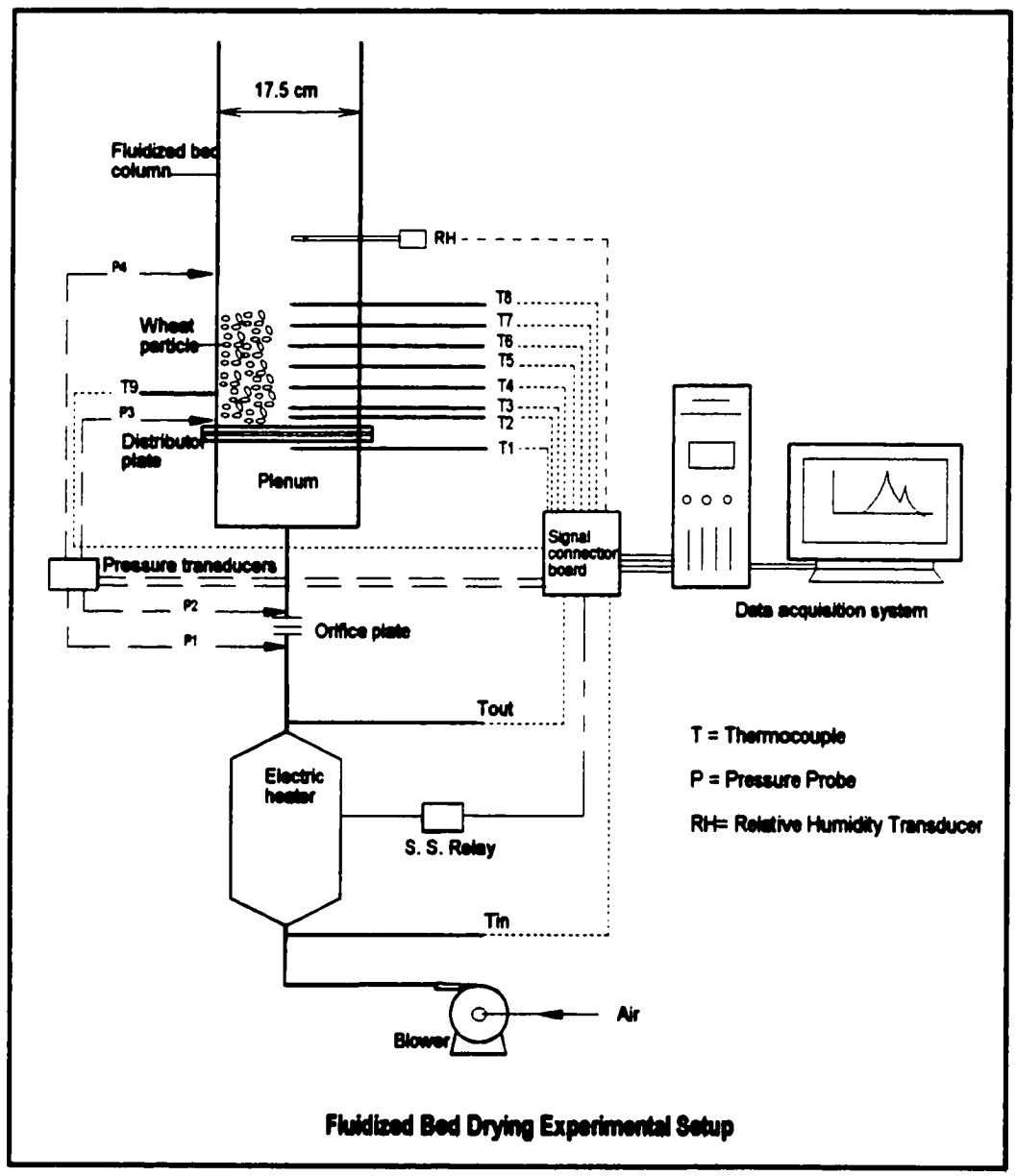

Figure 3.1 Schematic diagram of experimental setup.

Table 3.1 Specifications of thermocouples.

Type	Material	Probe Diameter	Maximum Temp.	Length	Junction Type
T	Copper-Constantan	1/8 inch	204 °C	12 inch	Exposed

Table 3.2 Specifications of humidity transducer.

Type	RH Range	Temp. Range	Accuracy	Sensor	Output Signal
Vaisala, HMB 20UB	0-100%	20-80 °C	±2 RH from 0-90% ±3 RH from 90-100%	HUMICAP® Capacitive thin-film	4-20 mA

3.1.1 The Heater

An electric heater is used to heat the inlet air to the desired temperature. It is made of 5 fin strip heaters, each 500 W, encompassed in an insulated sheet metal frame. Each heater can be controlled separately. One of the heaters is looped through the PI control system to control the heat supply to the air for maintaining a constant air temperature. The inlet air temperature is continuously sampled and compared with the set value temperature, and depending on the comparison, the power supply to the heater is adjusted through a solid state relay.

3.1.2 The Balance

A digital balance, Mettler Hk 160, is used to measure the weight of samples during the experiment runs. The accuracy of the balance is 0.0001 gr. The maximum admissible weight of the balance is 160 gr.

3.1.3 Data Acquisition System

All the signals from the thermocouples, pressure transducers, and humidity transducer are acquired simultaneously every 2 seconds by using the data acquisition board (National

Instrument Corp, Model AT-MIO-64E-3) and LabView software and stored in a desktop computer for subsequent analysis.

3.2 Material Properties

3.2.1 Wheat

Red-spring wheat is used as one of the test materials. The wheat kernel is approximately ellipsoidal in shape with a thread in the direction of longer diameter. In this study, however, for simplicity of the numerical solution the wheat kernel is assumed to be spherical with an average diameter of 3.66 mm and density of 1215 kg/m^3. The moisture diffusion coefficient of wheat is given by Becker [1959],

$$D = \frac{1}{130.5}\exp\left(\frac{-6140}{T_p}\right) \tag{3.1}$$

Thermal conductivity and specific heat of wheat are given in [Kazarian and Hall, 1965],

$$k_t = 0.1167 + 0.1318\left(\frac{M_p}{1+M_p}\right) \tag{3.2}$$

$$C_p = 1398.3 + 4090.2\left(\frac{M_p}{1+M_p}\right) \tag{3.3}$$

Several correlations for the sorption isotherm of wheat have been proposed in the literature. One of the popular correlation is the Henderson [1952] equation. In this study a modified version of Henderson correlation developed by Fortes et al. [1981] is used:

$$RH = \frac{P_v}{P_{sat}} = 1 - \exp\left(-5869 T_p^{-0.775} M_p^{5203 T_p^{-1.363}}\right) \tag{3.4}$$

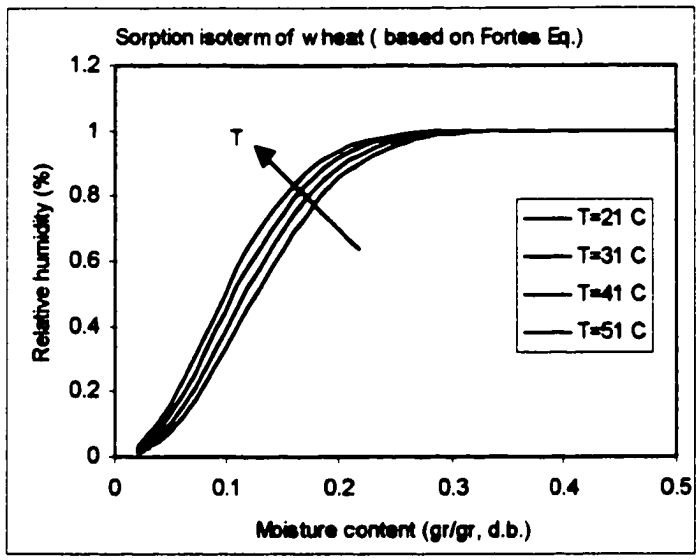

Figure 3.2 Sorption isotherm of wheat particles at different temperatures, based on Fortes et al. (1981) equation.

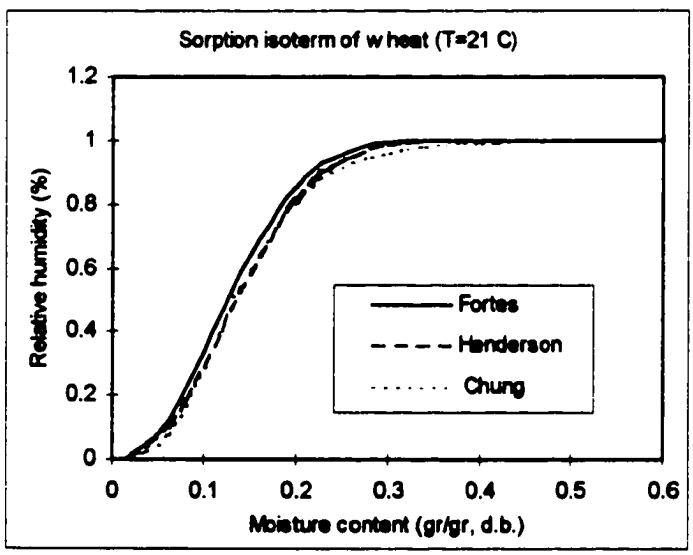

Figure 3.3 Comparison of sorption isotherm curves of different authors.

Figure 3.2 shows the sorption isotherm of wheat particles at different temperatures based on Fortes et al. (1981) equation. Sorption isotherm equations proposed by Chung [ASAE Standard, 1992] and Henderson [ASAE Standard, 1992] for wheat were also tried in the

numerical program and the results did not show a significant difference. Figure 3.3 shows the comparison of sorption isotherm suggested by different authors. The critical moisture content of wheat is between 69% and 85% dry basis based on temperature range of 10 °C to 90 °C [Simmonds, 1953]. In this work, however, the moisture content of wheat particles in all the drying experiments were below the critical moisture content.

3.2.2 Corn

Shelled corn is used as the second material for drying tests. The corn kernel is found to have a shape factor close to the unity with an average diameter of 6.45 mm and the density of 1260 kg/m^3. The moisture diffusion coefficient of corn is given by Chu and Hustrulid [1968],

$$D = 4.203 \times 10^{-2} \exp\left[\left(\frac{-2513}{T_p}\right) + \left(0.045T_p - 5.485\right)M_p\right] \tag{3.5}$$

Thermal conductivity and specific heat of wheat are given from [Kazarian and Hall, 1965],

$$k_t = 0.1409 + 0.1120\left(\frac{M_p}{1+M_p}\right) \tag{3.6}$$

$$C_p = 1465.0 + 3560.0\left(\frac{M_p}{1+M_p}\right) \tag{3.7}$$

The equation for sorption isotherm is given by Pfost et al. [1976],

$$RH = \frac{P_v}{P_{sat}} = 1 - \exp\left[8.6541 \times 10^{-5}\left(100M_p\right)^{1.8634}\left(T_p + 223.4\right)\right] \tag{3.8}$$

3.3 Method of Grain Conditioning

In order to simulate conditions of newly harvested grain, water was added to the material to raise its moisture content. The grain has initially a moisture content of 10-13% on a dry basis and this was raised to 24-41% on a dry basis. The conditioning procedure used in this work, developed by Becker [1960], is carried out by filling a plastic bucket with necessary amount of grain. The calculated amount of water was added to raise the moisture content to the desired value and at the same time the grain was mixed by a mechanical agitator. The grain was stored at room temperature for 48 hours with repeated mixing at periodic intervals. The bucket of grain is then stored in a refrigerator at 5-7 °C, until drying time, to prevent degradation or germination of the grain. Generally, the storage time was between 3-5 days and after that the sample was used in the experiment.

3.4 Moisture Content Determination of Grain

The moisture content of the grain was determined by a standard method developed by the American Society of Agricultural Engineers, ASAE Standard: S352.2. Table 3.3 shows the sample weight and temperature and time of drying.

Table 3.3 ASAE standard for drying of the grains.

Grain	Weight of Sample	Temperature ±1 °C	Drying Time
Wheat	10 gr.	130 °C	19 hours
Corn	15 or 100* gr.	103 °C	72 hours

*Use 100 gr. if moisture exceeds 25%.

Aluminum dishes with tightly fitting covers was used to hold the samples for measurement in the balance and drying in the oven. They were first weighed empty and after taking the samples they were weighed again, before putting in the oven. After drying in the oven they were cooled in the desiccator and then weighed again. All

moisture contents referred to in this work are on a dry basis. The moisture content on a dry basis is calculated by:

$$M_p = \frac{W_B - W_A}{W_A} \tag{3.9}$$

where: W_B = weight of grain before drying

W_A= weight of grain after drying

M = moisture content of grain on a dry basis

The moisture content on a wet basis is given by:

$$M_{pwb} = \frac{M_p}{1 + M_p} \tag{3.10}$$

The air oven is a standard gravity-convection oven, used to dry the particle samples for measuring the moisture content. Its temperature range is 40-200 °C with accuracy ±1 °C.

3.5 Drying Run Procedure

Before each drying run a sample was taken out from the conditioning bucket for determination of the initial moisture content. In order to bring the bed to a uniform working condition, hot air is blown through the bed for about one hour before it is charged with the material (this is not necessarily required for the drying test, since the mathematical model can also predict the nonuniform working condition in the bed). In the meantime, the material to be dried is weighed and recorded. After the bed reached the required temperature and stabilized, the air supply and power to heater was turned off and the material was charged into the bed as quickly as possible. The air supply and heater power were then reinstated and the pressure drop across the distributor and the bed at the corresponding gas velocity were measured. Temperature, pressure, humidity, and

velocity readings are taken continuously every 2 seconds from the bed by the data acquisition system. Since the thermocouples and the humidity transducer were exposed to hot air before the start of the drying process, there might be some experimental errors in the initial reading of them. This is because the transducers cannot rapidly adjust themselves to the new condition in the bed after material was charged into the bed. The material samples are withdrawn from the bed at 0, 1, 2, 4, 7, 10, 15, 20, 25, 30, 35, 45, 55, 65, 75 and 85 minutes to measure the moisture content and the other variables.

CHAPTER 4

Effect of Swirling Induced Distributor Plate on Hydrodynamics of Fluidized Bed

4.1 Introduction

One of the key parameters affecting the successful operation of fluidized beds is the distributor plate. It is known that the efficient and stable operation of fluidized bed is sensitively controlled by the design of the gas distributor [Masters, 1993]. The hydrodynamics of flow in the dense phase, quality of gas dispersion, bubble size and its behaviour, gas-solids contacting, residence time distribution of gas, solid movement and mixing pattern are some of the aspects that are affected by distributor plate design. Among these, gas-solid contacting requires special attention especially in groups B and D particles, where the bubble size may grow up to large diameter and cause slugging in the bed, and consequently poor gas-solid contacting. In fluidized bed drying applications most of the materials belong to groups B and D particles, therefore, the existence of large bubbles in the bed are most likely if the conventional types of distributor plate is used. Bubble size and its frequency have a significant contribution on the performance and characteristics of fluidized bed. Large bubbles may considerably reduce the contact efficiency inside the bed. Therefore, it is very important to prevent coalescence of the small bubbles and formation of large bubbles in the bed. This can be achieved largely by modifying the distributor plate design or its outlet geometry. It is desirable to design a new type of distributor plate or new design for the outlet geometry of the gas from the distributor plate, in order to improve the hydrodynamics of the bed without losing the advantage of high mixing rate in the bed. The aim is to reduce the size of bubbles inside the bed, and consequently the slugging effect, by forcing more gas flow into the emulsion phase. This is important not only in fluidized bed drying systems, but also in other type of fluidized bed application.

A new design for the gas outlet from the distributor, which is called swirling induced distributor plate or swirling outlet geometry, was developed for improving the gas-solid

contact efficiency. Since the effect of this type of gas outlet geometry has not been studied yet, therefore, it is required to investigate the overall effect of this outlet geometry on the hydrodynamics of fluidized bed. This chapter describes the work undertaken to study the effect of distributor-generated swirl flow on the overall bed hydrodynamics.

In spite of the well recognized importance of the distributor plate on the hydrodynamics of the grid zone and the bed, limited information is available on the effect of gas outlet geometry. Most works, Basu [1984], Saxena et al. [1979], considered the effect of hole diameter, open area ratio and pressure drop on the general quality of fluidization. Although, a few investigations about introducing different patterns of swirling flow in fluidized bed are available, the effect of swirling outlet of gas from the distributor plate on the hydrodynamic characteristics of fluidized bed has not been investigated.

Nieh and Yang [1989] developed a vortexing fluidized bed combustor to improve the combustion intensity and turndown capability of conventional FBC boilers. They injected the secondary air tangentially from the freeboard to form a centrifugal flow field. Zayed and Hamdullahpur [1990], and Hamdullahpur et al. [1989] conducted hydrodynamic and combustion experiments using tangential secondary air injection ports in the freeboard. They observed significant reduction in elutriation, NO_X, SO_2 and CO emission and improvement in combustion efficiency as a result of two-staged combustion and swirling flow pattern in the freeboard. Evans et al. [1989] used a spouted bed, suitable for the processing large light particles subject to substantial cohesion or interparticle attraction. They injected secondary air tangentially above the distributor plate to promote rotational motion in bed. Lee et al. [1990] developed a two-stage swirl-flow fluidized bed combustor to improve the combustion efficiency. They investigated the swirling effect on the trapping rate, residence time and combustion rate of fines in the upper stage of the two-stage combustor and reported a 20% enhancement.

In the present study, a new distributor plate is developed to introduce swirling discharge into the bed. Digital signal processing of pressure fluctuations is utilized to analyze the behaviour of the bed. The pressure fluctuations in the bed are related to the bed hydrodynamics and can provide an effective way for on-line diagnosis of the characteristics of fluidized beds. Lirag and Littman [1971] studied the statistical behaviour of pressure fluctuations in the fluidized bed and suggested that they are caused by fluctuations in the bed height resulting from bubble ejection at the bed surface. Fan et al. [1981] used an on-line approach for signal processing of pressure fluctuations to determine the effects of gas velocity, bed height, particle size and distributor design on the major frequency and amplitude of the fluctuations. Sadasivan et al. [1980] proposed correlations for frequency and magnitude of maximum pressure drop fluctuations for group B solids. They also presented a simple equation relating pressure fluctuations to bubble diameter. Recently, Dhodapkar and Klinzing [1993] investigated the effect of gas velocity, tap position and bed height on the frequency of fluctuations using frequency domain analysis.

In the present work, a fast Fourier transform (FFT) and statistical analysis of pressure fluctuations are used to investigate the hydrodynamic behaviour of swirling fluidized bed (SFB). The results obtained are compared with results of the conventional perforated plate.

4.2 Experimental Setup and Materials

Since the experimental setup used in this section is different from the other sections, therefore, it is discussed separately. A schematic of the experimental setup is shown in Fig. 4.1. The fluidized bed includes a bed column, distributor and plenum. The column is cylindrical with 14.5 cm ID and 100 cm length made of Plexiglas to permit visual observation. Two pressure taps (4 mm ID) are placed at 2.5 cm and 6 cm above distributor plate to measure the pressure fluctuations while two others are used for the

overall bed pressure drop measurements. The plenum is filled with wire gauze to assure homogenous distribution of the gas before the distributor.

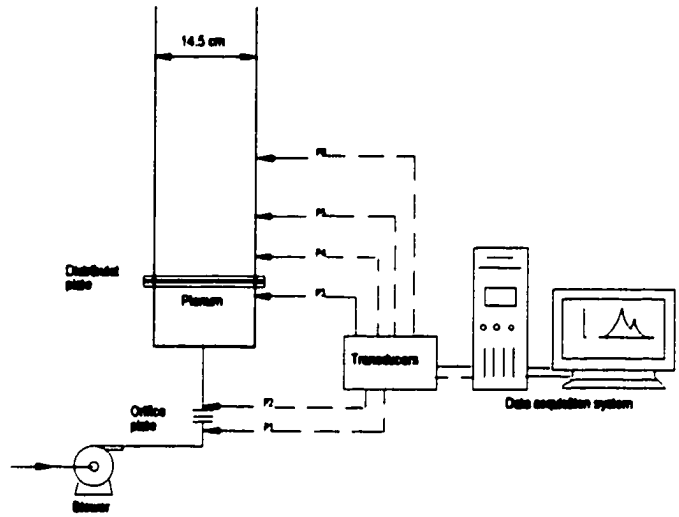

Figure 4.1 Experimental set up for analyzing the pressure fluctuation.

A 10 inch WG pressure transducer (Omega PX-162-010G) is used to measure pressure fluctuations inside the bed. The pressure drop across the distributor plate and orifice plate are recorded using a 27 inch WG (Omega PX-170-027D) and a 10 inch WG (Omega PX-162-010D) differential pressure transducers respectively. The voltage signals from the transducers are simultaneously acquired using a desk top computer with the Labview data acquisition board (Model AT-MIO-64E-3, National Instrument Corp.). To prevent aliasing in data acquisition, a scan rate (sampling frequency per channel) of 1000 Hz was used. The sampling length (number of scan) of 4096 point is found to be a reliable number for data acquisition. A computer code in graphical form is developed by using the Labview software to calculate the power spectral density function, autocorrelation and probability density and distribution functions. The data acquisition for each run is repeated 40 times and their average is considered as a final reading. This allowed approximately 160,000 points to be processed.

4.2.1 Materials

Two different kinds of particles were used in the experiment, wheat and sand (Table 4.1). According to Geldart's classification, wheat and sand belong to group D and B, respectively.

Table 4.1 Specification of particles used in the experiment

	Wheat	Sand
d_p	3.66 mm	0.60 mm
ρ_p	1215 kg/m^3	2610 kg/m^3
ε_{mf}	0.4	0.48
u_{mf}	1.0 m/s	0.302 m/s

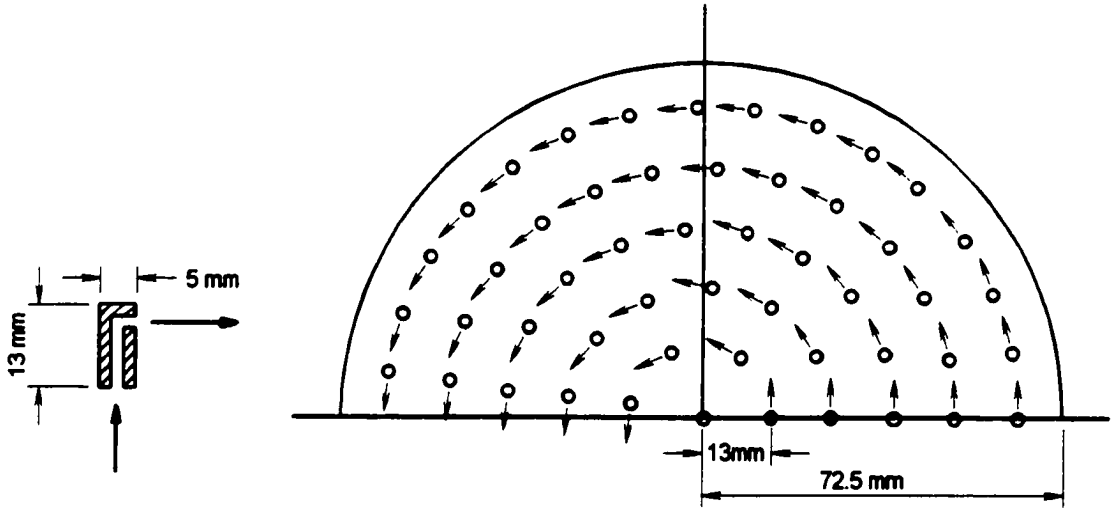

a b

Figure 4.2 (a) Cross section of a tuyere, (b) Half hole layout of the distributor plate and gas outlet direction.

4.3 Distributor Plate Design

The distributor plate was built by placing tuyeres in a circular pitch. Each tuyere (Fig. 4.2a) issues a horizontal jet through a single opening tangential to the circular path as shown in Fig. 4.2b. Arrows show the outlet direction of gas. The tuyeres can also be arranged in rectangular or triangular pitch instead of circular pitch but in any case the opening direction should be perpendicular to the radii to create a swirl pattern. For circular pitch the distance between two tuyeres was obtained by:

$$L = 1.77\frac{d_{or}}{\phi} \tag{4.1}$$

where d_{or} is hole diameter and ϕ is the open area ratio in the plate. To confirm the existence of a vortex motion in the bed a test was run without particles in the bed. Using small tracer particles, the vortex pattern of the gas inside the bed was clearly observed. Following the design methodology given in Kunii and Levenspiel [1991], the total numbers of holes in the distributor were found to be 96 each 3 mm diameter that give an open area ratio of 4.2 in percent. For comparison of the result a straight hole perforated plate distributor was used with the same specification i.e. the same open area and etc.

4.4 Theoretical Background

Pressure fluctuations inside the fluidized bed is a typical random time function which cannot be predicted deterministically. In spite of the irregular and random character, the pressure fluctuation exhibit some degree of statistical regularity, and certain averaging procedures can be applied to establish gross characteristics useful in engineering design. The following statistical concept is used to evaluate and analyze the efficiency and performance of swirling induced distributor plates compare to the ordinary perforated plate distributor.

4.4.1 Probability Distribution

For a continuous stationary random variable x(t), the probability distribution represents the fraction of total time that the variable is less than (more negative than) some specified value, x_1 and can be shown as:

$$\begin{aligned} P(x_1) &= \text{Prob}\left[x(t) \prec x_1\right] \\ &= \lim_{t\to\infty} \frac{1}{t} \sum \Delta t_i \end{aligned} \tag{4.2}$$

Probability density function is the probability of x(t) lying between the value x_1 and $x_1+\Delta x$, and is shown as:

$$p(x) = \lim_{\Delta x \to 0} \frac{P(x+\Delta x) - P(x)}{\Delta x} = \frac{dP(x)}{dx} \tag{4.3}$$

It is evident that p(x) is the slope of the cumulative probability distribution P(x). From the preceding equation, we can also write:

$$P(x_1) = \int_{-\infty}^{x_1} p(x)dx \tag{4.4}$$

The area under the probability density curve, between two value of x represents the probability of the variable being in this interval. Because the probability of x(t) being between $x=\pm\infty$ is certain,

$$P(\infty) = \int_{-\infty}^{+\infty} p(x)dx = 1 \tag{4.5}$$

and the total area under the p(x) curve must be unity.

4.4.2 Correlation

Correlation is a measure of the similarity between two random variables $x_1(t)$ and $x_2(t)$. It is a time-domain analysis useful for detecting hidden periodic signals buried in the apparent random signals. If there are two records, $x_1(t)$ and $x_2(t)$, the correlation between them is computed by multiplying the ordinates of the two records at each time, t, and determining the average value, by dividing the sum of the products by the number of products. It is evident that the correlation so found will be largest when the two records are similar or identical. For dissimilar records, some of the products will be positive and others will be negative, so their sum will be smaller. In the autocorrelation the two signals are the same but shifted by a time τ. If $\tau=0$, there is complete correlation, as τ increases, the correlation decreases. The autocorrelation is defined as:

$$R(\tau) = \lim_{Ts\to\infty} \frac{1}{Ts} \int_{-Ts/2}^{Ts/2} x(t)x(t+\tau)dt \qquad (4.6)$$

4.4.3 Power Spectral Density

The frequency composition of a random variable signal can be described in terms of the spectral density of the mean square value. It is usually desirable to convert the time domain signals to frequency domain to find out its frequency composition. The main objective of this analysis is to find a relationship between the power spectral analysis of the wall static pressure fluctuations with the state of fluidization. The power spectral density function S(f) of a random signal x(t) is the Fourier transform of its autocorrelation function, i.e.,

$$S(f) = \int_{-\infty}^{\infty} R(\tau)e^{-i2\pi f\tau}d\tau \qquad (4.7)$$

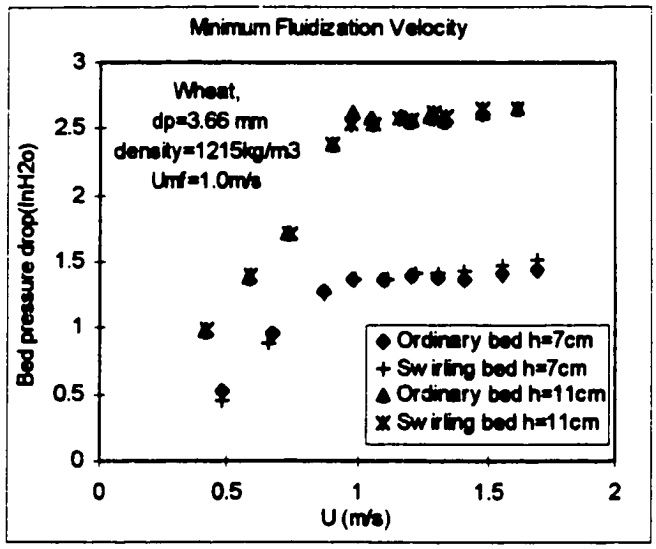

Figure 4.3 Effect of bed height on minimum fluidization velocity of wheat.

4.5 Results for Low Density Materials (Wheat)

4.5.1 Minimum Fluidization Velocity

Figure 4.3, shows the bed pressure drop versus superficial gas velocity in swirling and ordinary beds. Although it is widely accepted that U_{mf} is independent of the bed height, to investigate the effect of bed height on SFB, two different heights was used and U_{mf} was measured the same for both heights. The experimental U_{mf} is in good agreement with the U_{mf} obtained by known correlation (See Eq. 6.10 in chapter 6).

4.5.2 Signal Processing of Pressure Fluctuations

Pressure fluctuations analysis is used to investigate the effect of the tangential gas outlet from the distributor opening. Pressure fluctuations have been used to define an index for the quality of fluidization [Fan et al. 1981]. Within the bubbling and slugging regimes, statistical analysis and correlation of pressure fluctuations have been used to infer bubble and slug properties [Geldart, 1986]. The pressure fluctuations measurement are basically the measurement of the time series of static pressure signals for a given period of time at a specified scan rate. The pressure fluctuations in the bed depend on the internal

dynamics of gas flow. The inhomogeneities in the bed (in the form of bubbles and slugs), which is the result of the dynamic instabilities in the bed near the distributor plate, have a complex relationship with the pressure fluctuation. The nature of these inhomogeneties also affects the heat and mass transfer taking place in the bed. The random passage of the bubbles create fluctuations of the pressure waves which is a function of the bubbles size. The small bubbles create small amplitude fluctuations while large bubbles or slugs are responsible for large amplitude fluctuations. The frequency of fluctuations depends on the number of bubbles passing the probe cross section. The time domain signals is converted to frequency domain using fast Fourier transform (FFT) to evaluate the behaviour of signals meaningfully.

The results obtained from the swirling fluidized bed is compared with those of the ordinary bed that has a perforated plate type distributor. The hole size and open area ratio of both plates are maintained the same, but the pressure drop across them is different. For this reason the effect of pressure drop was also investigated.

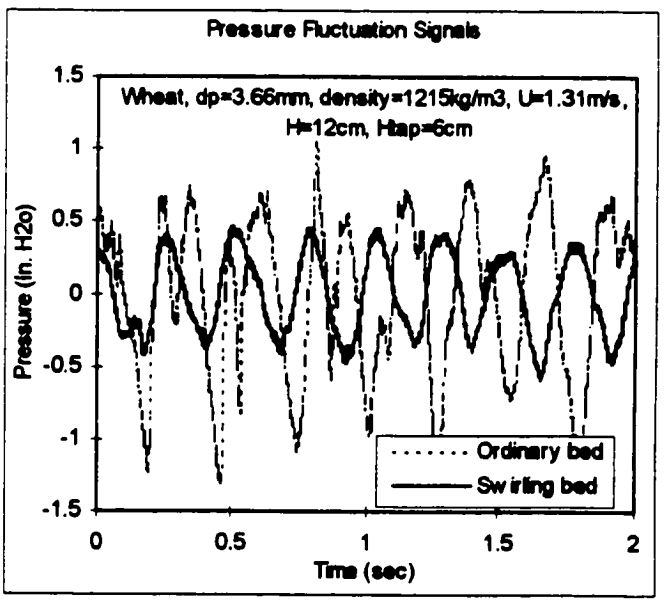

Figure 4.4 Typical pressure fluctuation signal in the bed for wheat particles.

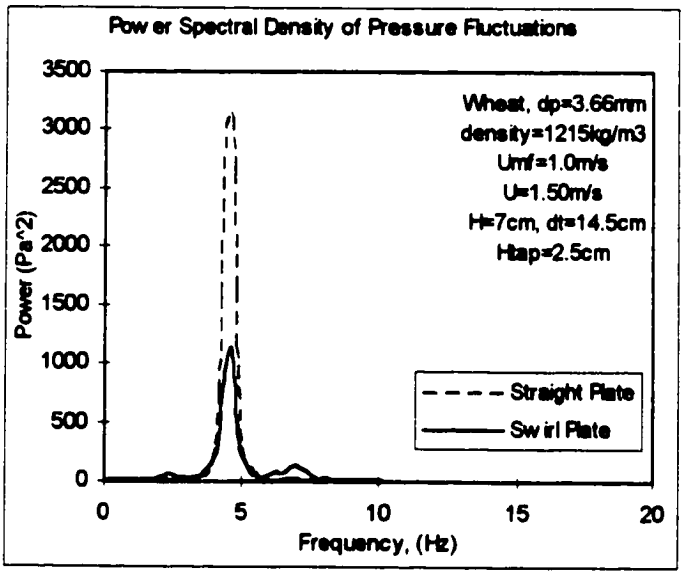

Figure 4.5 Power spectral density function of pressure fluctuations for wheat.

The typical pressure fluctuation, power spectral density function, autocorrelation function, and probability density and distribution function of the pressure fluctuations signals for two types of bed are shown in Figures 4.4 through 4.8 respectively. In these experiments, the static bed height is 7 cm and pressure tap position located at 2.5 cm above the distributor plate. A typical pressure-time curve (Fig. 4.4) shows clearly the difference between amplitude of signals in two beds.

Figure 4.5 shows typical power spectral density of large particle fluidization that consists of a single peak with no major side frequency. As can be seen, even though the main frequency in both beds is the same, the power of fluctuations in SFB is considerably smaller than the ordinary bed. This indicates that the mechanism responsible for generating the fluctuations in the bed is altered, and consequently, the fluctuations are dampened in SFB. Since bubble sizes are proportional to the power of fluctuations, it can be concluded that the size of bubbles in SFB was reduced. This means more gas penetrate into the emulsion phase and better contacting is accomplished.

Figure 4.6, shows the autocorrelation function of fluctuations for two beds. The periodic nature of the curve is an evidence of uniform and smooth fluidization. The difference between the amplitude of the two curves also verify that amplitude of fluctuations in SFB is smaller than it is in the ordinary bed. As expected, the maximum correlation for both cases coincide at zero time lag.

The probability density function (PDF) of fluctuations (Fig. 4.7) always shows a saddle about the mean value of the signal, indicating the presence of periodic component in the signals. Comparison between the two curves in Fig. 4.7, shows that in SFB the density of fluctuations near the zero amplitude is higher than the ordinary bed confirming again the previous finding about the lower value of amplitude in SFB. The same result can be understood from the analysis of probability distribution function shown in Fig. 4.8.

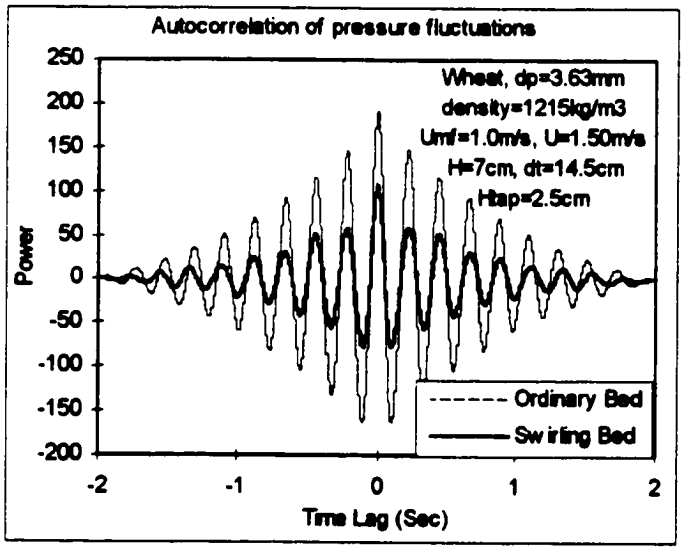

Figure 4.6 Autocorrelation function of pressure fluctuations for wheat.

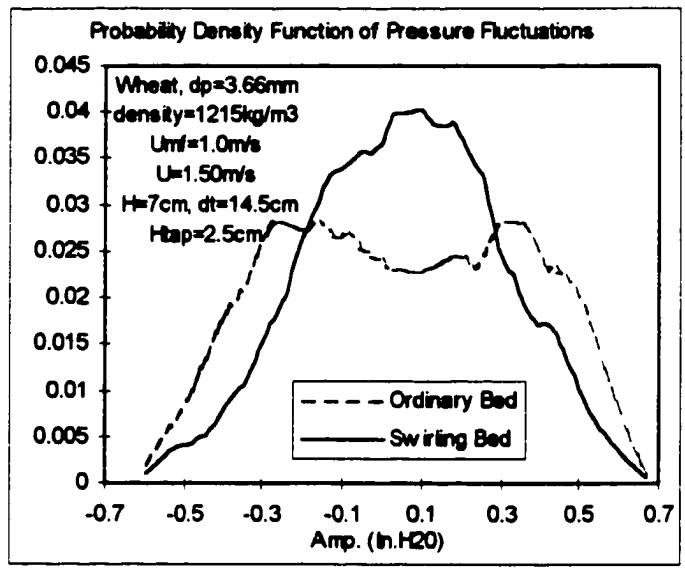

Figure 4.7 PDF of pressure fluctuations for wheat.

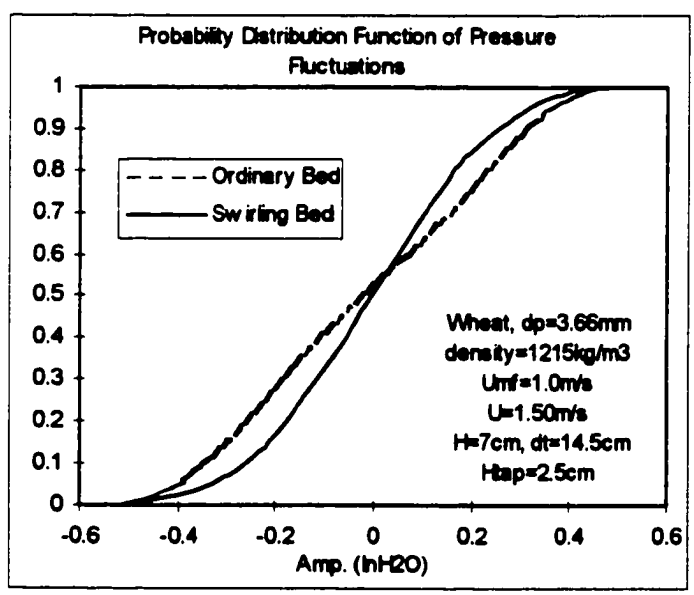

Figure 4.8 Probability distribution of fluctuations for wheat.

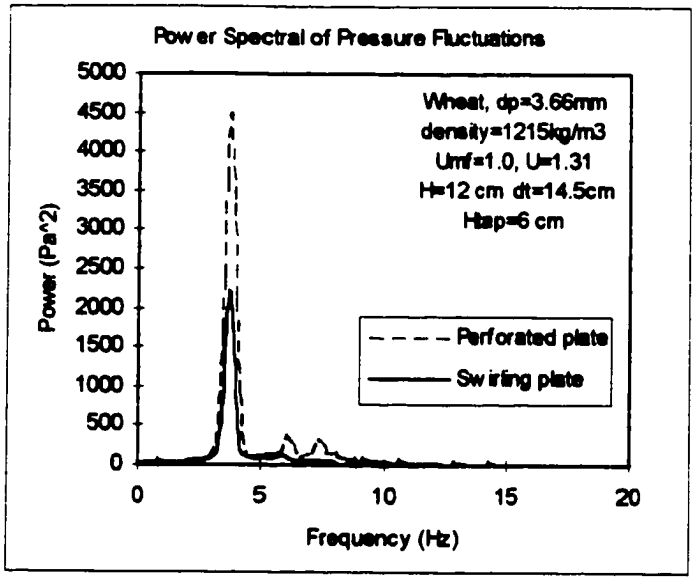

Figure 4.9 Power spectral density of fluctuations for wheat.

4.5.2.1 Effect of Bed Height

To evaluate the effect of bed height on the behaviour of SFB another set of experiments was performed with a second bed height of 12 cm. The pressure tap position was located 6 cm above the distributor plate to be nearly in the middle of the bed. Figures 4.9 and 4.10 show the power spectral density function and autocorrelation function of fluctuations. As seen before, the dominant frequency for both beds do not change but the power of fluctuation in SFB is smaller than it is in ordinary bed.

Comparison of the power spectral results for bed heights of 7 and 12 cm (Figs. 4.5 and 4.9) reveals that the reduction ratio of power is decreased with increasing bed height. This means that the effect of swirling outlet is diminished by increasing the bed height. This behaviour can be expected since by increasing the bed height, the static pressure above the distributor plate is increased and consequently the resistance of particle against gas jet velocity increases and particles rapidly disperse the swirling action above the

distributor plate. There is another difference in the comparison between Figs. 4.4 and 4.9. The main frequency in the Fig. 4.9 is lower than that of in Fig. 4.5, which indicates the frequency of pressure fluctuation decrease as the bed height increase because of bubble coalescence. This is in agreement with the other works [Jirag and Littman, 1971].

4.5.2.2 Effect of Distributor Plate Pressure Drop

As mentioned earlier, the two distributor plates have the same open area ratio but the pressure drop across the swirling plate is higher than the perforated plate. This difference can be attributed to different geometries of these plates. However, this difference may raise a question as to the lower power in SFB maybe the result of higher pressure drop across the plate, not by the swirling effect of the flow. It is, therefore, important to know the effect of distributor plate pressure drop on the amplitude of fluctuations when the open area ratio and opening size are constant. Unfortunately, there is no information in literature in this regard. Fan et al. [1981] investigated the effect of plate pressure drop on the amplitude of fluctuations by changing the hole size and open area ratio. However, it is different situation and the result can not be used here specially when we notice that the effect of the hole diameter is very important in the initial size of bubbles.

To understand the effect of the distributor plate pressure drop on the power spectral density function experiments were performed using the swirling plate and changing the position of tuyeres randomly to different directions. Figure 4.11 compares the power spectrums between random direction plate and swirling (tangential) plate. The dominant power in SFB is again smaller than the random direction plate confirming that the reason for the difference in the power spectrum is not the pressure drop across the plate.

4.6 Results for High Density Materials (Sand)

Experiments were performed for sand particles to investigate the effect of the swirling outlet of gas from the distributor plate. Tests for minimum fluidization velocity showed

that, like wheat particles, there was not any difference at the minimum fluidization velocity between swirling plate and perforated plate.

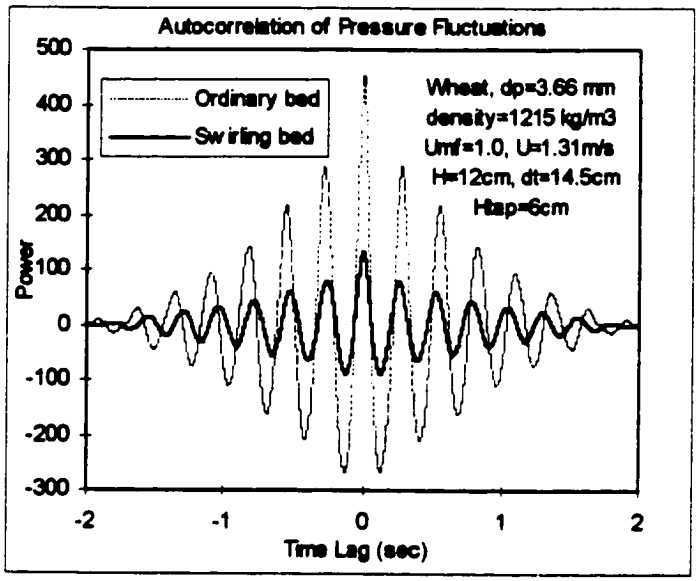

Figure 4.10 Autocorrelation function of fluctuations for wheat.

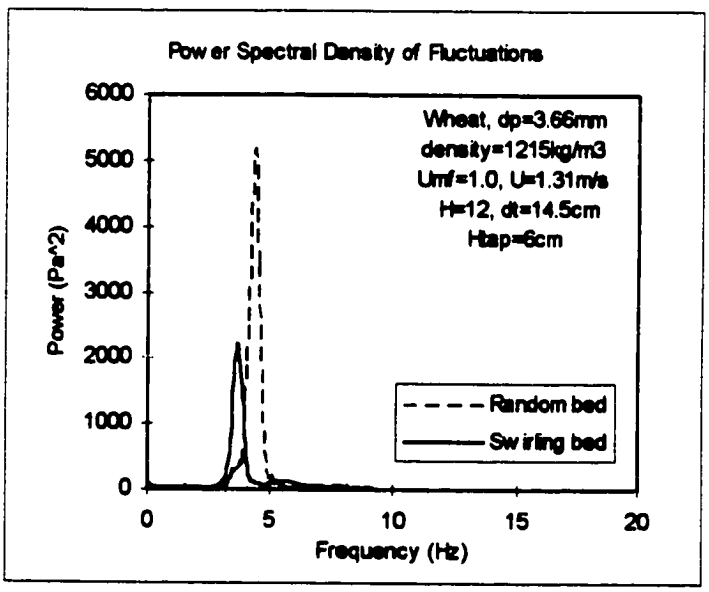

Figure 4.11 Power spectral density function of fluctuations for wheat.

To compare the hydrodynamic characteristics of swirling outlet for this group of particles, the perforated plate was used. Different runs at different bed heights and gas velocities were done for both types of plates to find a common base for comparison. However, it was found that unlike the wheat, these particles are sensitive to pressure drop across distributor plate and a small difference in the pressure drop of plate, significantly affects the quality of fluidization. Since the pressure drops across the two types of plates were different, then the two distributors performed differently at the same superficial gas velocity. When, for example, in the swirling bed the quality of fluidization at a specified velocity was good, for perforated plate jetting and partial channeling was observed. It was, therefore, very difficult to compare the results between perforated plate and swirling plate. Since any attempt to match the pressure drops would result in the change in percentage of open area, the best option for comparison was to use a random direction plate. Since both, random direction and swirl direction plates had the same pressure drop and same open area ratio then the similarity was achieved and the only difference restricted to the outlet geometry of gas. Figures 4.12 through 4.14 show the result of experiments in 5 cm bed height and in Fig. 4.15 the power spectral density function is shown for 10 cm bed height.

The experimental data for this type of particle indicated the basic difference in fluidization of Geldart D and B type material. Unlike the group D particles a significant side frequencies can be seen in this type of particle denoting different bubble sizes at different frequencies passing the cross section of pressure tap. Comparison of results for two types of plates show that like the wheat particles the main frequency of fluctuation does not change but the power of fluctuation in swirling plate is smaller than the random direction plate. Figure 4.15 shows that by increasing the bed height the difference between peak powers diminish.

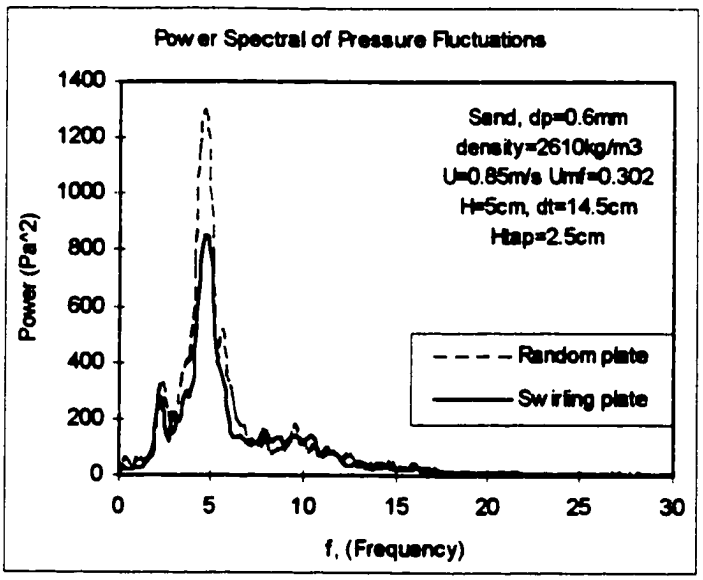

Figure 4.12 Power spectral density function of fluctuations for sand.

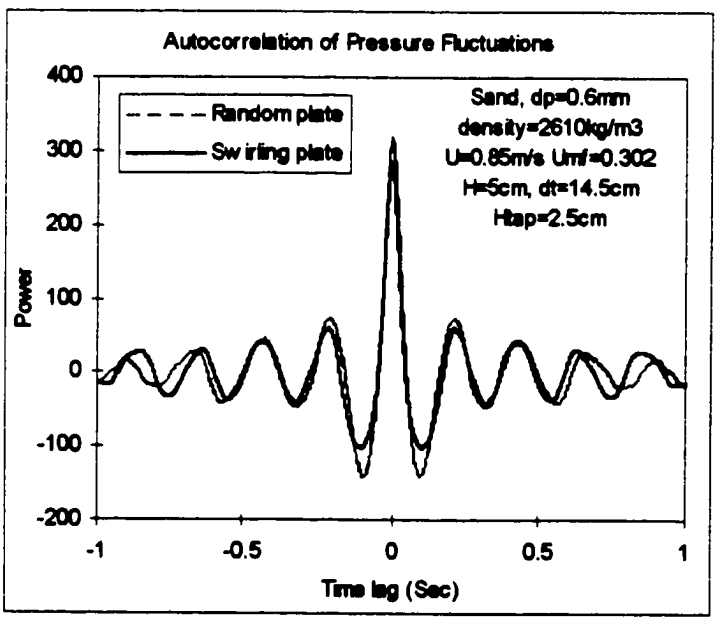

Figure 4.13 Autocorrelation of pressure fluctuations for sand

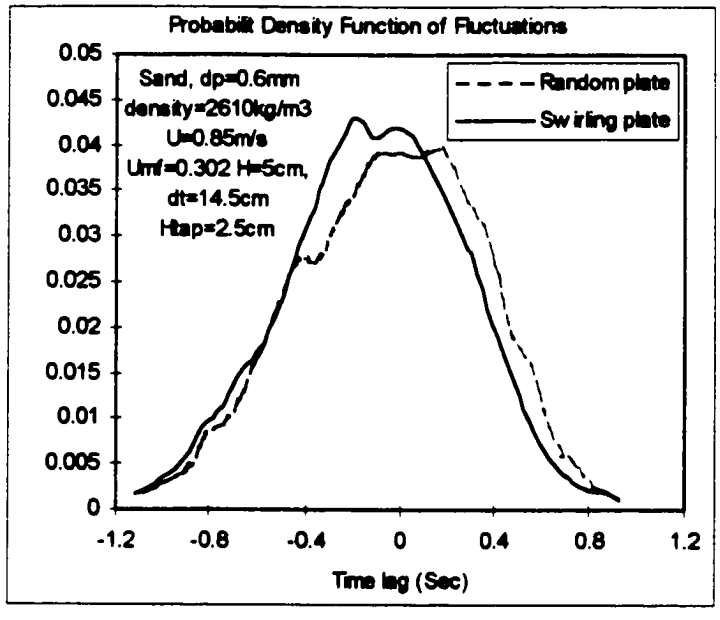

Figure 4.14 PDF of pressure fluctuations for sand.

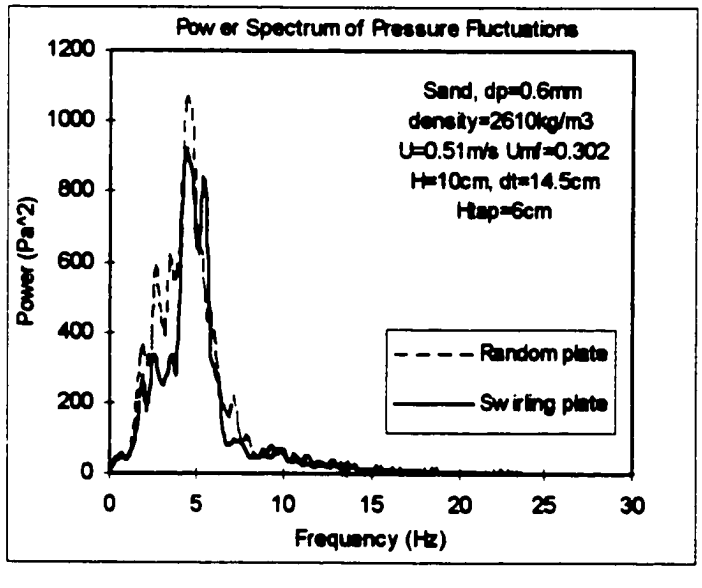

Figure 4.15 Power spectral density of pressure fluctuations for sand.

Analysis of the results between the sand and wheat particles reveals that the rate of power reduction of swirling beds for wheat is higher than it is for sand. This outcome can be anticipated because the density of sand is about twice that of wheat which causes a higher increase in static pressure above the plate which in turn, counterbalances the swirling effect of gas outlet.

4.7 Discussion and Conclusion

The tangential outlet of gas from the distributor plate creates a swirling pattern in the bed which affects the hydrodynamic characteristics of fluidization. The gas-solid contacting is increased through reduced bubble size and its distribution.

Considering the results obtained it can be concluded that for Group D particles such as wheat the effect of the swirling outlet on the bubble size and contact efficiency is noticeable. The swirling outlet causes a reduction in the intensity of pressure fluctuations which is an index of bubble size in the bed, and better contact efficiency is attained. Increasing the bed height cause this effect to decrease due to higher static pressure on particles just above the plate which rapidly disperses the gas flow.

For Group B particles such as sand the effect of swirling outlet on the bubble size and contact efficiency is also significant, especially for shallow beds. Use of the swirling outlet improves the quality of fluidization. Increasing the bed height reduces this effect that is the same trend for group D particles. Comparison of the results for random and circular gas outlet reveals the importance of gas outlet configurations.

It is desirable to investigate the effect of swirling outlet of gas on other characteristics of the fluidized bed such as particle mixing, bubble velocity and coalescence. These also could be studied in other type of fluidized beds such as circulating fluidized beds.

CHAPTER 5

Effect of Moisture Content of Particles on the Hydrodynamics of Fluidized Bed

5.1 Introduction

In the drying process of granular particles, the moisture content of materials is relatively high, and water may constitute an important percent of material weight. The excessive amount of moisture content of particles may affect the "normal" behaviour of particles during the fluidization process. This is largely due to the increased interparticle adhesion force among the particles. The same pattern of behaviour may also be observed when the bed is fluidized with a high relative humidity gas.

Although the effect of bed temperature and pressure change on fluidization are well documented in the literature, limited information is available to understand the effect of the relative humidity of gas, or moisture content of particles on the hydrodynamics of fluidized bed. Increasing the moisture content of particles increases the interparticle adhesive force (due to instantaneous liquid bridge formation) and therefore it becomes necessary to consider the effect of this force in the balance of forces applied on individual particles.

When the particles are relatively dry, the effect of cohesive or adhesive forces between particles is neglected, except for group C particles where the existence of cohesive forces are responsible for difficult or poor fluidization. The existence of adhesive or cohesive forces in the bed has a direct effect on the quality and performance of the bed. Molerus [1982] reported that the difference in the behaviour observed with group A, B, and C powders originates in the increasing relative magnitude of the cohesion force between particles in comparison with the drag force, with decreasing particle size. He derived the limiting conditions where cohesive forces dominate, and ended with a classification of powders somewhat like Geldart's. Massimillia and Donsi [1976] studied the cohesive forces between particles of fluidized bed catalysts. They examined the relative importance

of van der Waals and capillary interparticle forces with respect to particle weight. They calculated unexpectedly high cohesive forces inconsistent with their experiments. They explained this difference by invoking surface asperities, even for apparently perfect microspherical particles. Schubert et al. [1975] studied the behaviour of agglomerates with different bonding mechanism. They developed a model in which agglomerates are held together by liquid bridges which permits the stress-strain behaviour to be predicted. Jaraiz et al. [1992] developed a theory to estimate interparticle cohesive forces from pressure drop versus bed expansion data for very fine particles in a vibrated fluidized bed. Based on this theory they predicted the Geldart C/A transition range.

In the present study, the effect of particle moisture content and relative humidity of fluidizing gas on the fluidization behaviour of two different types of bed material (sand and wheat) are investigated. While the sand particles are characterized as non-hygroscopic material, wheat grain fall into the hygroscopic material category.

5.2 Theoretical Analysis

When a particle is in the minimum fluidization state, a balance between the drag, gravity and buoyancy forces exist. This conventional balance of forces works so long as the particles are dry and large in size, or the humidity of gas is low, thus justifying the neglecting of the interparticle forces. In the case of moist particles, high gas humidity or very fine powders, however, the magnitude of interparticle attractive forces is relatively large, and cannot be neglected in the analysis of forces acting on the particles. Thus, for moist particles in a minimum fluidization state, the balance of forces can be written as follows:

Drag force + Buoyancy force = Gravity force + Adhesive force

$$F_d + F_b = W + F_{At} \tag{5.1}$$

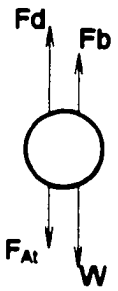

Figure 5.1 Balance of forces on a single particle in the fluidized bed.

To find a correlation for the attractive forces, first of all the nature of these forces should be carefully analyzed. Two important attractive forces between particles are the van der Waals force, and the capillary force formed due to the liquid bridge. In group C particles, where the particles are fine and their surface areas are considerably large, the van der Waals force is the dominant cohesive force. The capillary forces become important if the particles are moist or the gas has high relative humidity. Generally, the contribution of these two forces should be considered in the interparticle force balance, but for all practical purposes, in most cases only one of them is important. Since in this study the group C particles are not under investigation, the effect of van der Waals forces are assumed to be negligible and only the effect of capillary force is taken into account.

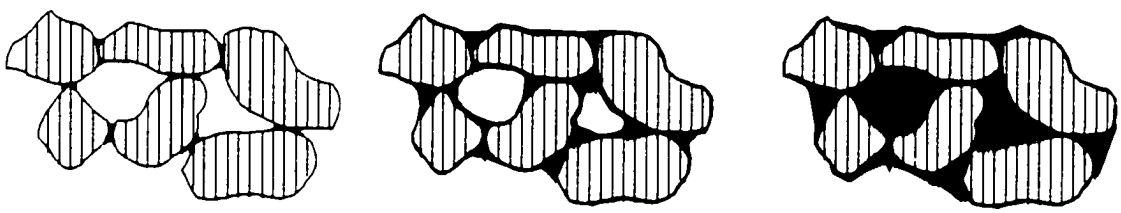

Figure 5.2 State of liquid bonding in a material, (a) pendular state, (b) funicular state, (c) capillary state.

5.2.1 Adhesion Force Due to Capillary Action

When the amount of particles surface moisture is high enough, the attractive capillary forces between particles develop as a consequence of the formation of liquid bridges between contacting bodies. Due to collision and closeness of particles at the contact point, local capillary condensation might occur, even though the vapor partial pressure is smaller than the normal vapor pressure of the liquid. The strength of the liquid bridge force between two contacting particles depends on the structure and geometry of the particles, and the properties of the solid-liquid system such as surface tension of liquid and contact angle. The extent of capillary condensation determines the state of particle saturation. Three states of a moist particle has been described depending on the amount of liquid saturation S_L, which is the relation between the pore volume occupied by the liquid and the total pore volume of particle [Massimila and Donsi, 1976]. (1) A "pendular state" when non-interconnected liquid bridges develop between individual particles, (2) a "funicular state" when liquid bridges coexist with interparticle spaces filled up with liquid due to increased amount of liquid, (3) a "capillary state" when all the interparticle space is filled up with liquid. Figure 5.2 shows the different states of liquid saturation among a group of particles.

It is understood that each state of liquid saturation requires a different treatment. In the drying of moist particles, usually the pendular state exists between particles so we limit our analysis only to the pendular state.

5.2.1.1 Pendular-Bond Strength

If a liquid of low viscosity forms a pendular liquid bridge between two particles, (Fig. 5.3) a force F_A acts between them consisting of two components, the surface tension force F_s exerted by the liquid along the wetted perimeter, and a force F_p due to the difference of the pressure outside and inside the bridge produced by the curvature of the liquid meniscus:

$$F_A = F_s + F_p \tag{5.2}$$

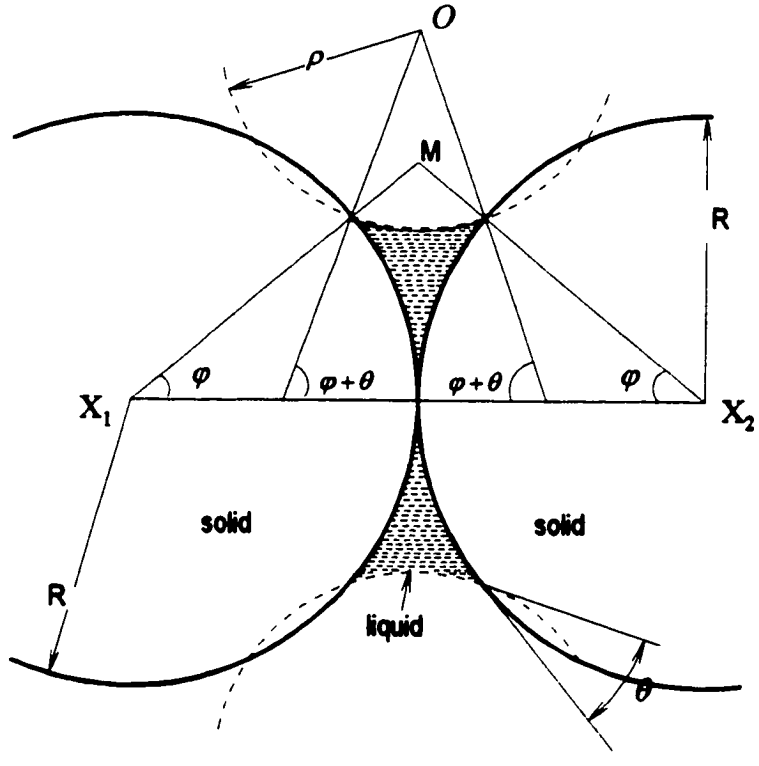

Figure 5.3 Geometrical representation of the pendular liquid bridge between equal-sized spheres.

The force resulting from the surface tension will act on the perimeter where the liquid contacts the particles. The magnitude of this force exerted on each of the particles in the direction X_1X_2 is

$$F_s = \sigma \sin(\varphi + \theta) P_{wp} \tag{5.3}$$

where σ is the vapor-liquid interface tension, φ is bridge angle, θ is contact angle, and P_{wp} is the wetted perimeter given by:

$$P_{wp} = 2\pi R \sin\varphi \tag{5.4}$$

The pressure drop over the liquid surface is given by the well-known Kelvin equation:

$$\Delta P = \frac{-\rho_w R_{cons} T}{M_w} \ln\left(\frac{P_v}{P_{sat}}\right) \tag{5.5}$$

where ρ_w is the water density, R_{cons} is universal gas constant, M_w is molecular weight of water, and T is the absolute temperature. Since the pressure inside the liquid is lower, each of the particles experiences a force of attraction given as:

$$F_p = \Delta P S \tag{5.6}$$

where S is the projected areas of the liquid-solid boundary onto a plane perpendicular to the direction of the force. It is calculated as:

$$S = \pi R^2 \sin^2 \varphi \tag{5.7}$$

Substitution of Eqs. (5.3) through (5.7) in Eq. (5.2) yields an expression for total adhesion force:

$$F_A = 2\pi R\sigma \sin\varphi \sin(\varphi + \theta) + \frac{-\rho_w R_{cons} T}{M_w} \ln\left(\frac{P_v}{P_{sat}}\right) \pi R^2 \sin^2 \varphi \tag{5.8}$$

Equation (5.8) needs a further assumption regarding the geometry of liquid bridge to be able to use for predicting the adhesion force. Schubert [1984] presented a model based on Eq. (5.8) which takes the existence of particle moisture into account. The final form of his correlation assuming complete wetting (θ=0) is:

$$F_A = 8.25R\sqrt{\frac{\rho_s M_p}{\rho_w}}\left[\sigma - \frac{\rho_w R_{cons} T}{2M_w} R\ln\left(\frac{P_v}{P_{sat}}\right)\right] \tag{5.9}$$

Several other authors presented simplified forms of Eq. (5.8) where the effect of gas relative humidity and moisture content of particles are not included in the final correlation due to the simplifications. Israelachvili [1992] presented the adhesion force between two similar spheres as:

$$F_A = 2\pi R\sigma\cos\theta \tag{5.10}$$

Massimilla and Donsi [1976] also used a similar correlation with a different coefficient to estimate the adhesion force due to capillary as:

$$F_A = 8R\sigma \tag{5.11}$$

Since the correlation introduced by Schubert (Eq. 5.9) includes the relative humidity of gas and moisture content of particles, it is considered to be the most accurate model that can be used in a fluidized bed drying application. Therefore, Eq. (5.9) will be used in the further theoretical analysis.

An important parameter that needs to be modified in the capillary force correlations is the radius of particle (R). Massimilia and Donsi [1976] reported that using (R) as the radius of particles gives a high value of the cohesive force which was inconsistent with their experiments. They explained this problem by invoking surface irregulation and asperities. Since the surface of real particles is usually not smooth, their adhesion force is not always given by Eqn. (5.11) [Israelachvili, 1992]. There is an uncertainty in the definition of (R) which depends on the roughness of the particle surface. A value of (R) as low as 0.1 μm is reported in the literature to fit the experimental results [Massimilla and Donsi 1976,

Chaouki, 1985]. In this study, a method has been suggested to calculate the value of (R) for the material used in the experiments.

5.2.2 Minimum Fluidization Velocity

The correlation for the attractive force between two particles at a single point of contact, can be used to derive a correlation for the minimum fluidization velocity of moist particles. Although a large number of correlations for the prediction of minimum fluidization velocity exist in the literature, most of them have neglected the effect of cohesive force between particles. A few which considered the attractive force, only accounted for the van der Waals force. Obviously, it is not plausible to use these correlations in the case of moist particles.

The methodology to obtain a new correlation for minimum fluidization is as follows. The total attractive force between particles in the bed can be expressed as [Jaraiz et al., 1992]:

$$\begin{bmatrix}\text{Total attractive}\\ \text{force in the bed}\end{bmatrix} = \begin{bmatrix}\text{Number of particles}\\ \text{in the bed}\end{bmatrix}\begin{bmatrix}\text{Average number of contact}\\ \text{points per particle}\end{bmatrix}\begin{bmatrix}\text{Attractive force at a}\\ \text{contact pont}\end{bmatrix}$$

or

$$F_{At} = n_p n_c F_A \tag{5.12}$$

where F_{At} is the total attractive force and n_c is coordination number. The number of particles in the bed is:

$$n_p = \frac{A_t H_{mf}(1-\varepsilon_{mf})}{\frac{\pi}{6}d_p^3} \tag{5.13}$$

Substituting Eqns. (5.12) and (5.13) into the Eqn. (5.1) along with corresponding terms for the weight and drag forces in the bed, gives:

$$\Delta P_b A_t = H_{mf} A_t (1-\varepsilon_{mf})(\rho_p - \rho_g)g + \frac{6H_{mf} A_t (1-\varepsilon_{mf}) n_c F_A}{\pi d_p^3} \tag{5.14}$$

The Ergun equation [Ergun, 1952] for pressure drop in a fixed bed is given as:

$$\frac{\Delta P_b}{H} = 150\frac{(1-\varepsilon)^2}{\varepsilon^3}\frac{\mu_g U}{(\varphi_s d_p)^2} + 1.75\frac{(1-\varepsilon)}{\varepsilon^3}\frac{\rho_g U^2}{\varphi_s d_p} \tag{5.15}$$

Combining the above equation and Eqn. (5.14) and considering the bed properties at the onset of fluidization gives:

$$\frac{1.75}{\varepsilon_{mf}^3 \varphi_s}\mathrm{Re}_{mf}^2 + \frac{150(1-\varepsilon_{mf})}{\varepsilon_{mf}^3 \varphi_s^2}\mathrm{Re}_{mf} = \frac{d_p^3 \rho_g (\rho_p - \rho_g) g}{\mu_g^2} + \frac{49.5\rho_g n_c R}{\pi \mu_g^2}\sqrt{\frac{\rho_p M_p}{\rho_w}}\left[\sigma - \frac{\rho_w R_{cons} T}{2M_w} R \ln\left(\frac{P_v}{P_{sat}}\right)\right] \tag{5.16}$$

The first dimensionless term on the right hand side is the Archimides number Ar, and the second term is due to the contribution of adhesion force and can be named as adhesion number, Ad. The final form of equation is:

$$\frac{1.75}{\varepsilon_{mf}^3 \varphi_s}\mathrm{Re}_{mf}^2 + \frac{150(1-\varepsilon_{mf})}{\varepsilon_{mf}^3 \varphi_s^2}\mathrm{Re}_{mf} = Ar + Ad \tag{5.17}$$

The existence of adhesion number Ad on the right hand side of Eq. (5.17) indicates that the minimum fluidization velocity increases for the material considered. The magnitude of

this increase, however, is not very clear mostly because of the difficulty in determining a proper value for (R). The experimental results obtained from the present work for the minimum fluidization velocity are used to estimate a proper value for (R), and are presented below.

5.3 Experimental Results

Two different types of materials were used in the experiment, namely sand and wheat. Sand is a non-hygroscopic material that belongs to group B particles. Because moisture remains mostly on the surface of the sand, and does not penetrate inside the body, the amount of admissible moisture increase of sand is very small. If the moisture increases more than an admissible value, particles stick to each other, and the bed experiences sever channeling, and therefore, fluidization will not take place. On the other hand, wheat is a hygroscopic material that belongs to group D particles. Contrary to sand, wheat can absorb a lot of moisture inside the body so the amount of moisture increase could be very high. These two different materials are used in the experiment to find the effect of moisture content on the fluidization of wide variety of materials. The specification of the materials is shown in Table 5.1.

Table 5.1 Physical properties of various bed materials before and after conditioning.

Wheat (Dry, M_p=0.14)	**Wheat** (Moist, M_p =0.43)	**Sand** (Dry, M_p=0.0)	**Sand** (Moist, M_p =0.0006)
d_p=3.66 mm	d_p=3.89 mm	d_p=0.50 mm	d_p=0.50 mm
ρ_p=1215 kg/m^3	ρ_p=1250 kg/m^3	ρ_p=2610 kg/m^3	ρ_p=2610 kg/m^3
ε_{mf}=0.4	ε_{mf}=0.45	ε_{mf}=0.47	ε_{mf}=0.50
u_{mf}=1.0 m/s	u_{mf}=1.3 m/s	u_{mf}=0.17 m/s	u_{mf}=0.30 m/s

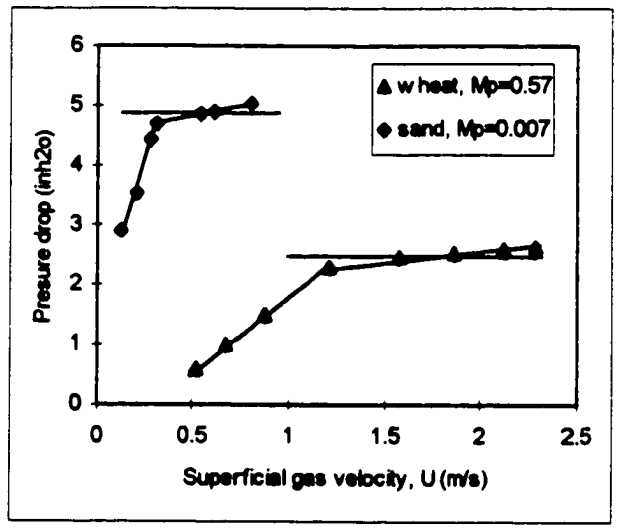

Figure 5.4 General pattern of bed pressure drop for sand and wheat particles with high moisture content. (Horizontal lines show the pressure drop equivalent to weight of bed material)

5.3.1 Pressure Drop versus Gas Velocity

Figure 5.4 shows the general pattern of pressure drop versus gas velocity curves for sand and wheat particles. Each curve consists of two straight lines with different slopes. The intersection point of these two lines is known to be the onset of fluidization in the bed. Unlike dry particle fluidization, the bed pressure drop after the minimum fluidization point is not constant, but gradually increases with increasing gas velocity. This pattern is found to be the most distinctive characteristic of moist particle fluidization induced by the attractive forces between particles. It may be explained that at the start of fluidization, not all particles are fluidized because of the adhesive forces in the bed. Usually, the top layers of bed start fluidizing when the bottom layers are still stationary. Thus, the bed pressure drop is slightly less than the pressure drop equivalent to the weight of bed material. Increasing the gas velocity further, the drag force exerted on the particles increases which can then break apart more contact points between particles, and bring them to the fluidized state. Consequently, the pressure drop increases with increasing the gas velocity as more particles require to be suspended. At a certain velocity, all particles will eventually be suspended and full fluidization will take place. At this point the pressure drop would be

higher than the weight of bed pressure drop because of the effect of the adhesive force. Further increase in the gas velocity may not necessarily cause the pressure drop to increase linearly. It should be noted that during the experiment careful arrangements should be made to prevent changing the moisture content of the particles during their fluidization. This can be done by choosing proper values for air temperature and relative humidity which minimize the change in the moisture of particles.

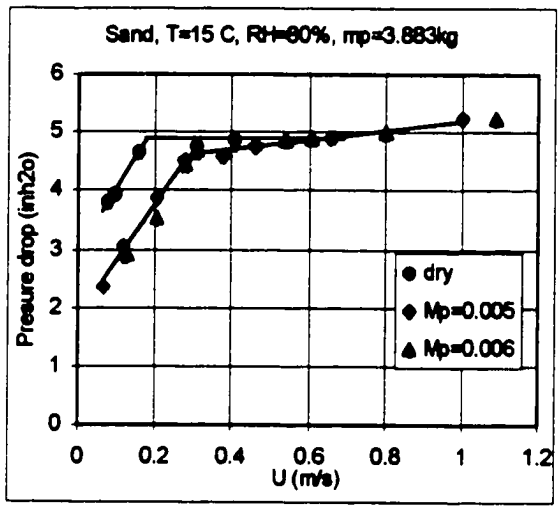

Figure 5.5 Comparison of bed pressure drop for sand with different moisture content.

A similar pattern between the pressure drop and the velocity was observed by Jaraiz et al. [1992] for fluidization of group C particles in a vibrated fluidized bed. For these particles (group C), the van der Waals cohesive forces may be responsible for a gradual increase of bed pressure drop.

5.3.2 Comparison of Bed Pressure Drop for Dry and Moist Particles

Sand:

The results of pressure drop experiments using dry and moist sand are shown in Fig. 5.5. It can be seen that the minimum fluidization velocity increases as the particle moisture

increases. The mean amplitude of pressure fluctuations against the superficial gas velocity was also measured for dry and moist particles. Figure 5.6 shows that the magnitude of the mean pressure fluctuations increases linearly with the superficial gas velocity. The intersection of the inclined line with abscissa can be considered as the minimum fluidization velocity point [Hartman and Svoboda, 1986]. The minimum fluidization velocity results determined by this method is in good agreement with those determined traditionally from the plots of pressure drop across the bed against the superficial gas velocity (Fig. 5.5).

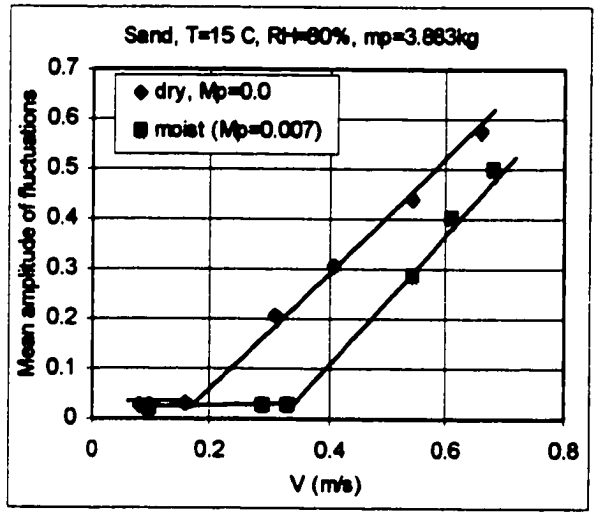

Figure 5.6 Mean amplitude of pressure fluctuation versus superficial gas velocity for sand.

In Fig. 5.5, the pressure drop-velocity variation of the moist particles, during the fixed bed regime, exhibits a peculiar behaviour. The pressure drop of the moist particles was found to be lower than that of dry particles at the same corresponding gas velocity. As a possible justification for this difference, one may suspect a difference in bed voidage at two conditions. However, the bed voidages of dry and moist sand are almost the same because the amount of moisture content of sand is very small, and also because the sand particles are non-hygroscopic and do not swell after conditioning. Moreover, the bed heights for the two cases are identical which is another indication of the same voidage amount at the fixed bed condition. So, what could be the reason for the different bed pressure drop at the fixed

bed condition? It is expected that the pressure drop of the moist particles should be at least equal, if not higher, to that of the dry particles at fixed bed condition.

The reason might be related to the adhesive force in the bed. One possible answer is that the existence of the adhesive force creates a condition in the bed that particles cannot move or slip easily between each other when the local voidage increased by a disturbance. This condition forces the gas to open up some stable low-resistance microchannels extended from the bottom to the top of the bed. Since most of the gas penetrates through these stable low-resistance microchannels, the drag force is not exerted on all the particles in the bed and consequently the bed pressure drop decreases. The adhesion force behaves like an interlocking force and prevents the particles from collapsing into the microchannels. The diameter of these microchannels is usually not large enough to be visible inside the bed, but when they join together, a small size jet may appear on the surface of the bed. In the dry particle case, these stable microchannels are not observed since the particles can freely move and fill any increase in local voidages as soon as they are created and prevent their formation.

This behaviour, actually, is similar to the channeling problem for group C particles. For group C particles the channels, after having developed through the bed, are stable because adhesive forces hold the particles together and prevent them from collapsing into the channels. But in other particle groups such as A, B, and D, and in the absence of adhesive and cohesive forces; the channels are unstable because of the free movement of particles which disconnects them randomly. These disconnected channels, then, manifest themselves as bubbles which pass through the bed and provide smooth fluidization. In beds of group C particles, when the channeling appears, the bed pressure drop decreases because only a small amount of particles located in the channels are suspended and other particles rest on the distributor plate. Hence the bed will never become properly fluidized.

Wheat:

Experiments on wheat showed the same pattern to that of sand particles. Figure 5.7 shows the comparison of bed pressure drop between dry and moist wheat particles while Fig. 5.8 shows the mean amplitude of pressure fluctuation versus superficial gas velocity. The increase in the minimum fluidization velocity is clear in both graphs. Increasing the moisture content from 0.43 to 0.57 does not appear to create a significant difference in minimum fluidization velocity. This is expected since for wheat particles, the equilibrium relative humidity becomes constant (close to 100%) for moisture content values above 0.3 (dry basis). So, as long as the moisture content is limited to the pendular state, the behaviour of the bed does not change considerably.

Wheat particles also show a decrease in the bed pressure drop when they are moist. However, for this type of hygroscopic material, the change in the bed voidage after conditioning, should also be accounted for. Wheat particles swell as their moisture content increase and consequently the bed voidage increases. Therefore, for wheat particles, the decrease in bed pressure drop may be partly because of the increase in bed voidage, and partly because of the existence of microchannels.

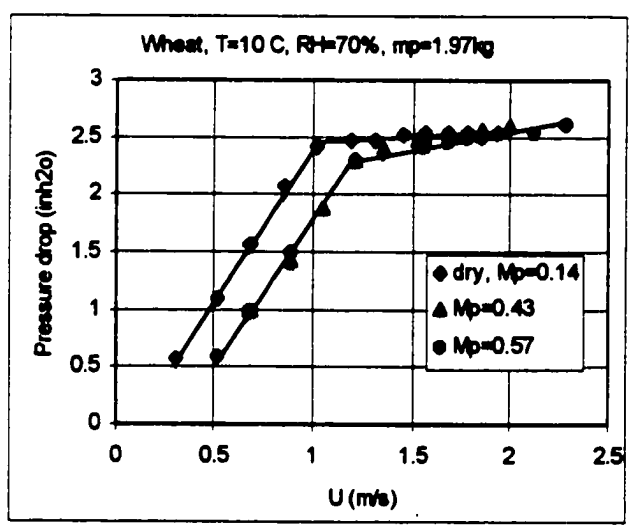

Figure 5.7 Comparison of bed pressure drop for wheat with different moisture content.

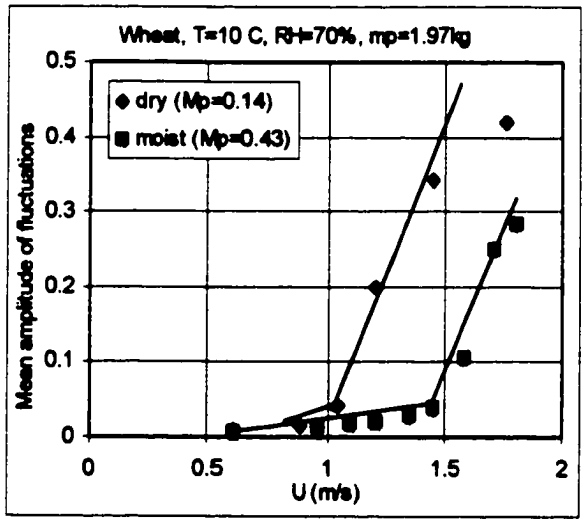

Figure 5.8 Mean amplitude of pressure fluctuation versus gas velocity for wheat.

5.3.3 Effect of Moisture Content of Particles on Minimum Fluidization Velocity

It is already shown that minimum fluidization velocity depends on the moisture content of particles, and that increasing the moisture content, increases the minimum fluidization velocity. Therefore, in the initial stage of drying, one may need to increase the gas velocity in order to fluidize the bed material properly. After the initial stage and when the surface moisture is removed, the gas velocity can be reduced for the rest of the process. It is, therefore, desirable to establish a correlation for the variation of minimum fluidization velocity in terms of moisture content based on the experimental findings.

Figure 5.9 shows the results for sand particles. As already mentioned, sand particle can adsorb a small amount of moisture, and above a specific value, fluidization can hardly take place due to the stickiness of particles, and creation of channeling in the bed. In order to give a correlation for the curve in Fig. 5.9, it is better to divide the curve into two zones. The correlation for each zone can be written as:

$$u_{mf} = 22.105M_p + 0.1784 \qquad (R^2 = 0.9983) \qquad 0 \le M_p \le 0.005 \qquad (5.18)$$

$$u_{mf} = 10.550M_p + 0.2374 \qquad (R^2 = 0.9994) \qquad 0.005 \le M_p \le 0.007 \qquad (5.19)$$

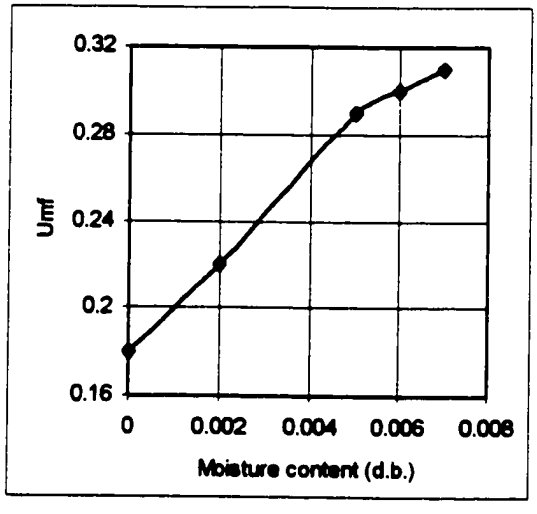

Figure 5.9 Effect of moisture content on u_{mf} for sand particles.

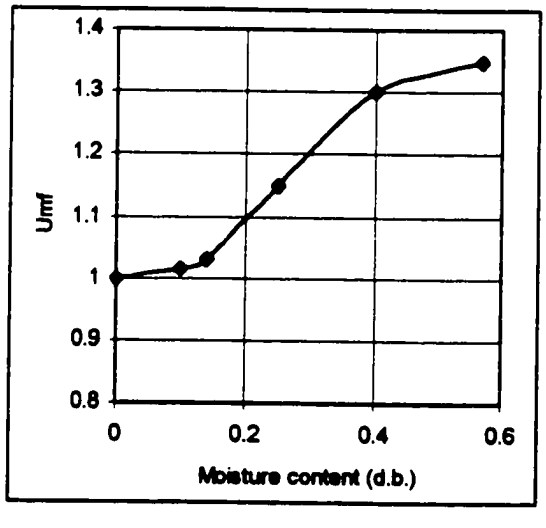

Figure 5.10 Effect of moisture content on u_{mf} for wheat particles.

Figure 5.10 shows the variation of u_{mf} for wheat particles. Three zones can be distinguished in this figure. In the first zone, there is a small slope for variation of u_{mf} with moisture content but in the second zone the variation is relatively high. The third zone

shows again small but a non-linear variation of u_{mf}. These variations can be justified based on the sorption isotherm of wheat grain. For wheat with moisture content above 0.4 (dry basis), the equilibrium relative humidity is almost 100%, which means that water molecules can exist all around the surface and reach to saturation state. So, increasing the moisture content above 0.4 (dry basis) does not have an important effect on the u_{mf}. The correlation for each zone can be written as:

$$u_{mf} = 0.9813M + 0.9054 \qquad (R^2 = 0.9943) \qquad 0.1 \le M \le 0.4 \qquad (5.20)$$

$$u_{mf} = 0.1317Ln(M) + 1.42 \qquad (R^2 = 0.9930) \qquad 0.4 \le M \le 0.6 \qquad (5.21)$$

5.4 Discussion and Conclusions

The data obtained from the experiments for bed pressure drop using moist particles can provide the necessary tool to estimate the magnitude of the adhesive force between individual particles. Using the increased bed pressure drop data and Eqn. (5.12), the total adhesive force F_{At} and the interparticle adhesive force F_A, can be determined. Having determined the interparticle force, F_A, the value of (R) can be calculated from Eqn. (5.9). As was pointed out, there is some uncertainty about the value of (R) due to the surface roughness of material. The value of (R) in Eq. (5.12) is considerably lower than the radius of particle and depends on the structure of the material. Based on the proposed procedure, the values of (R) for sand and wheat are 1.0 μm and 20.0 μm, respectively. Having found the proper value for (R), the Eq. (5.17) can be used to find an estimate value for u_{mf} theoretically. Furthermore, it would be informative to calculate the dimensionless ratio of adhesive force to gravity force, R_f, for an individual particle, which is an indication of quality of fluidization. According to the experimental results, R_f for sand is about 0.035 and for wheat is about 0.08. These small values of R_f mean that despite of the existence of the adhesive force, the bed does not show a behaviour characteristic of group C particles, and fluidization will occur successfully.

Considering the results obtained in the experimental section, the following conclusions can be made. Increasing the moisture content of particles increases the minimum fluidization velocity of particles due to increased adhesive forces inside the bed. This suggests that in predicting the minimum fluidization velocity, the conventional balance of drag with gravity forces is not fully applicable and that the effect of interparticle cohesive forces caused by the liquid bridge of isolated capillaries must be taken into account.

Increasing the moisture content of materials in the fixed bed condition reduces the bed pressure drop along the bed due to creation of low-resistance microchannels in the bed. The existence of low-resistance microchannels may be the responsible factor which reduces the rate of heat and mass transfer in the fixed bed systems. Because these mirochannels reduce the contact efficiency between gas and solids, the overall efficiency is reduced. Therefore, application of fixed bed drying may not be recommended from this perspective.

Another point that needs to be addressed is the applicability of the Ergun equation to predict the pressure drop in a fixed bed with high moisture content. It was shown that for these cases, the bed pressure drop is reduced because of the existence of low-resistance microchannels. Since the Ergun equation does not consider the effect of moisture content of particle, it overestimates the bed pressure drop in the case of moist particles.

CHAPTER 6

Mathematical Modeling of Fluidized Bed Drying

6.1 Introduction

As a preliminary step in hydrodynamic modeling of a fluidized bed, the main features of the bed such as flowrate through the phases, volume fractions, contacting pattern of materials, and other related parameters must be known. Flow pattern and its behaviour is one of the most complicated and unpredictable challenges in fluidization. As a result of the solids movement and the bubbling action, the fluidizing gas passes through the bed in a complex and random manner. In the early days, simple contacting models such as plug flow, mixed flow, dispersion, and tanks in series were tried. Then, following the lead of Toomey and Johnston [1952], two-phase models were proposed. The aim of these models was to account for the observed nonhomogenity of a fluidized bed. Over 30 distinctly different models of this type have appeared in the literature.

The 1960s examined two major advances in the understanding of gas/solid contacting in bubbling fluidized bed. Firstly, Davidson's analysis of the flow of gas within and in the vicinity of rising gas bubbles and, secondly, Rowe's finding that a rising bubble was accompanied by a wake of solids and that this was the main mechanism causing solid circulation in fluidized bed.

These developments led to a new class of fluidized bed models called the hydrodynamic models, in which the bed behaviour was based on the characteristics of these rising bubbles. Over a dozen of these models have been proposed but all to the extreme of very fine particles in which the rising bubbles are surrounded by very thin clouds of circulating gas, mainly because it was often of practical importance in the fluidized bed reactors. That is the reason why most work on fluidized bed drying employed the hydrodynamic model suitable for small size particle (group A) irregardless of the characteristics of particle used for drying. However, with increasing use of large particle beds in different applications,

researchers have developed many hydrodynamic models to predict the behaviour of bubble and dense phase.

6.2 Gas Flow Pattern in Fluidized Bed

Gas flow in fluidized beds is not uniform. This nonuniformity manifests itself as existence of different phases inside the bed. A first attempt to model the bed behaviour was two-phase theory which later on was found to have some shortcomings in modeling all types of fluidization. Discrepancies up to 50% in the value of bubbles flow rate were reported [Geldart, 1986] in using the two-phase theory of fluidization for group D particles analysis. Different theories were proposed for modeling the fluidization process considering its variation with particle type. Here we review the characteristics of different types of fluidization and then choose the appropriate correlation from the literature to use in a drying model. We start with group D particles which have extensive application in drying of agricultural crops.

6.2.1 Group D Particles

Group D represents relatively large diameter particle size. Hydrodynamic of this group show marked deviations from those obtained using the two-phase theory. When these solids are fluidized, the bed does not expand considerably, and bubbles form as soon as the gas velocity exceeds u_{mf}. One sees long lenticular cavities close to the perforated plate distributor. These cavities move slowly upward to transform into nearly spherical bubbles higher up the bed. These bubbles grow rapidly and do not follow any preferred path. Also, note that this nearly spherical bubble shape suggests a very small wake, in contrast to what one finds with small particle system (group A). When the bubble size approaches the bed diameters, flat slugs are observed which slide up the tube and collapse into wall slugs near the surface. For this type of particles, the emulsion gas uses the slow-rising bubbles as a convenient low-resistance shortcut through the bed, providing a mode of gas exchange and by-passing which is different from that observed with group A or B powders. The gas

velocity in the dense phase is high and solid mixing is relatively smaller than the other group but it is good enough to assume uniform distribution of particle properties. Backmixing of the dense phase gas could be neglected. Relatively sticky materials can be fluidized since the high particle momentum and fewer particle-particle contacts minimize agglomeration.

As a bubble rises through the bed, its size, and consequently its velocity increases with the bed height. The increase in the size of bubble is mostly due to the coalescence of small bubbles to larger ones, even though other mechanisms are also proposed for this phenomenon. The varying form of bubble properties during its passage through the bed has not been addressed in the previous works on fluidized bed drying. Instead a constant averaged bubble size was used [Srinivasa Kannan et al., 1994] which may not be a precise representation of bubble behavior in the bed. Figure 6.1 shows various choices which may be used to represent the bubble behaviour in the bed. These are: (a) one mean bubble size; (b) bubbles grow as they rise in the bed but are of the same size at any level in the bed; (c) size distribution of bubbles at any level in the bed but all growing as they rise. For group D particle, choice (b) is used for modeling the bubble behaviour. Implementation of this model, which considers variation of bubble size along the bed, can be done appropriately in this work since the bed is divided into a number of slices in the axial direction.

Voidage of different phases is usually assumed to be constant along the bed (Fig. 6.2a), which is consistent with the constant bubble size assumption. However, for group D particles, the constant bubble size cannot be applied. Since the flowrate through the bubble phase can be considered constant over an average time period, and the velocity of bubble increases as it moves up, the continuity equation requires that the bubble voidage decreases along the bed height (Fig. 6.2b). The solid phase voidage can be assumed to be constant along the bed height. Although this is not true in the freeboard zone, the error associated with this is negligible in drying processes. With the decrease in the bubble

voidage and constant solid phase, the voidage of interstitial gas phase should increase along the bed as shown in Fig. 6.2b.

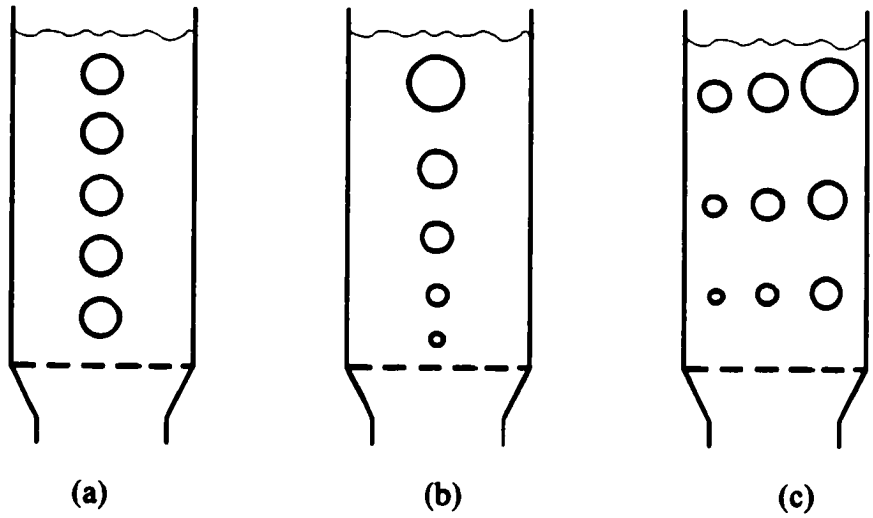

Figure 6.1 Different models for bubble behaviour inside bed: (a) mean bubble size (b) variable bubble size in axial direction (c) variable bubble size in axial and lateral directions.

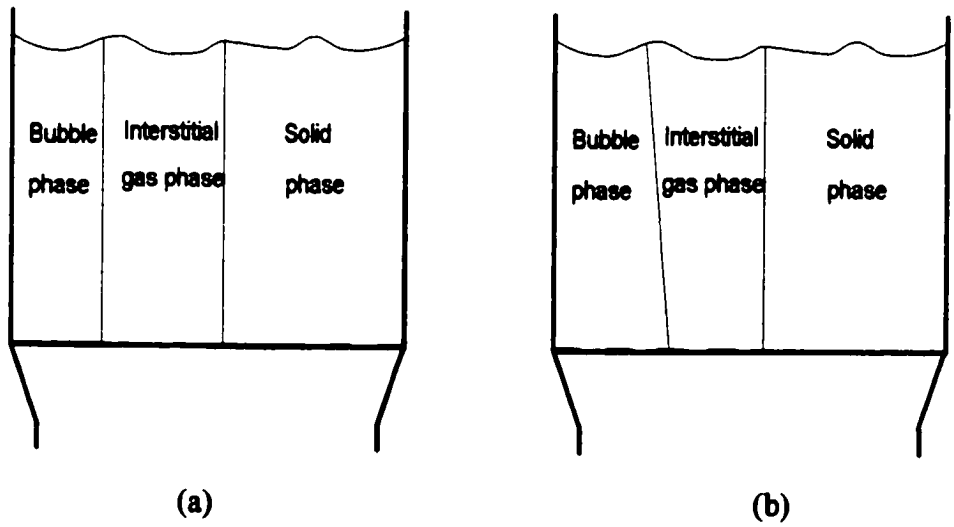

Figure 6.2 Phase distribution inside the bed, (a) constant phase voidage, (b) variable phase voidage.

Based on the above considerations, the flowing correlations are used in modeling the flow pattern. The bubble flowrate is evaluated based on the finding of Hilligardt and Werther [1986]. Their results are shown in a graph which mathematically can be formulated as:

$$Q_b = \psi(u - u_{mf})A_t \tag{6.1}$$

where $\psi = 0.26$ for $H/d_t \le 0.5$

$\psi = \exp[0.464\log(H/d_t) - 1.02]$ for $0.5 \le H/d_t \le 10$

For the bubble size, the correlation proposed by Darton et al. [1977] is used because it considers the variation of bubble size with the bed height,

$$d_{b_j} = 0.54(u - u_{mf})^{0.4}(H_j + 4\sqrt{A_o})^{0.8} g^{-0.2} \tag{6.2}$$

The subscript j indicates the position of bubble in the axial direction of the bed. The bubble rise velocity is predicted using the following correlation,

$$u_{b_j} = (u - u_{mf}) + 0.71(gd_{b_j})^{0.5} \tag{6.3}$$

The bubble voidage is predicted by,

$$\varepsilon_{b_j} = \frac{Q_b}{A_t u_{b_j}} \tag{6.4}$$

The volume fraction of particles is assumed to be constant along the bed. Although it might vary specially close to surface of the bed, it has little effect on the overall performance of the bed.

$$\varepsilon_p = \left(1 - \varepsilon_{b_j}\right)\left(1 - \varepsilon_{e_j}\right) \tag{6.5}$$

The volume fractions and velocity of interstitial gas are given respectively as:

$$\varepsilon_{i_j} = \left(1 - \varepsilon_{b_j} - \varepsilon_p\right) \tag{6.6}$$

$$u_{i_j} = \frac{\left(u - \varepsilon_{b_j} u_{b_j}\right)}{\varepsilon_{b_j}} \tag{6.7}$$

The voidage of the emulsion increases along the bed, and obtained by,

$$\varepsilon_{e_j} = \frac{\varepsilon_{i_j}}{\left(1 - \varepsilon_{b_j}\right)} \tag{6.8}$$

It is assumed that that bed expansion is equal to the average bubble hold-up, so bed height after fluidization is calculated by

$$H_f = \frac{W_b}{\rho_p \varepsilon_p A_t} = \frac{H_{mf}}{1 - \varepsilon_{b_{av}}} \tag{6.9}$$

The general correlation for minimum fluidization velocity, u_{mf} is given by Kunii and Levenspiel [1991]:

$$\frac{1.75}{\varepsilon_{mf}^3 \phi_s} \mathrm{Re}_{mf}^2 + \frac{150\left(1 - \varepsilon_{mf}\right)}{\varepsilon_{mf}^3 \phi_s^2} \mathrm{Re}_{mf} = Ar \tag{6.10}$$

where Re is the Reynolds number and Ar is the Archimedes number defined as:

$$\mathrm{Re}_{mf} = \frac{d_p u_{mf} \rho_g}{\mu_g} \tag{6.11}$$

$$Ar = \frac{d_p^3 \rho_g (\rho_p - \rho_g) g}{\mu_g^2} \tag{6.12}$$

The minimum fluidization velocity for this group is measured experimentally and found to be in good agreement with the Eq. (6.10) in the case of dry particles. For wet particles, the Eq. (6.10) is not valid, and it is recommended to use a correlation based on experimental findings for each type of material like the equation suggested for wheat and sand particles in chapter 5 (Eqs. 5.18-5.21).

6.2.2 Group A Particles

Particles which fall into this group are of relatively small size. Two-phase theory provides a fairly accurate model for this type of material. When these particles are fluidized, the bed expands considerably at velocities between u_{mf} and the velocity at which bubbles appears, U_{mb}. This is as a result of slightly cohesive forces between these particles. Gas bubbles rise more rapidly than the rest of the gas, which percolates through the emulsion. These gas bubbles appear to split and coalesce frequently as they rise through the bed, resulting in a restricted bubble size not far above the distributor, usually less than 10 cm, even in a large bed. So the assumption of average bubble size can reasonably be used for this group (Fig. 6.1a). Since a constant size of bubble can be assumed for this group, the voidage distribution could be assumed constant along the bed height (Fig. 6.2a).

Because the bubble rises much faster than the emulsion gas, according to Davidson's analysis, the rising bubbles are surrounded by thin clouds of recirculating gas. This cloud restricts the heat and mass transfer between bubble gas and interstitial gas. As mentioned earlier, a two-phase model is suitable for this type of particles which assumes that all the gas in excess of u_{mf} flows through the bed as bubbles while the emulsion stays at minimum

fluidizing conditions. So the following correlation from two-phase model can be used. The bubble flowrate is evaluated based on the finding of Hilligardt and Werther [1986] as:

$$Q_b = \psi(u - u_{mf})A_t \tag{6.13}$$

where $\psi = 0.85$

For the bubble size, the correlation proposed by Darton et al [1977] is used.

$$d_b = 0.54(u - u_{mf})^{0.4}\left(H + 4\sqrt{A_o}\right)^{0.8} g^{-0.2} \tag{6.14}$$

The bubble rise velocity is predicted using the following correlation,

$$u_b = (u - u_{mf}) + 0.71(gd_b)^{0.5} \tag{6.15}$$

The bubble voidage is predicted by,

$$\varepsilon_b = \frac{Q_b}{A_t u_b} \tag{6.16}$$

The volume fraction of particle is assumed to be constant along the bed,

$$\varepsilon_p = (1 - \varepsilon_b)(1 - \varepsilon_e) \tag{6.17}$$

The volume fractions and velocity of interstitial gas are given respectively as:

$$\varepsilon_i = (1 - \varepsilon_b - \varepsilon_p) \tag{6.18}$$

$$u_i = \frac{\left(u_o - \varepsilon_b u_b\right)}{\varepsilon_b} \tag{6.19}$$

Voidage of emulsion is constant along the bed and obtained by,

$$\varepsilon_e = \varepsilon_{mf} \tag{6.20}$$

The bed height after fluidization is calculated based on volume fraction of bubbles as,

$$H_f = \frac{W_b}{\rho_p \varepsilon_p A_t} = \frac{H_{mf}}{1-\varepsilon_b} \tag{6.21}$$

For relatively dry particles, the minimum fluidization velocity, u_{mf} is given by Kunii and Levenspiel [1991]:

$$\frac{1.75}{\varepsilon_{mf}^3 \phi_s} \mathrm{Re}_{mf}^2 + \frac{150(1-\varepsilon_{mf})}{\varepsilon_{mf}^3 \phi_s^2} \mathrm{Re}_{mf} = Ar \tag{6.22}$$

where Re is the Reynolds number and Ar is the Archimedes number defined as:

$$\mathrm{Re}_{mf} = \frac{d_p u_{mf} \rho_g}{\mu_g} \tag{6.23}$$

$$Ar = \frac{d_p^3 \rho_g (\rho_p - \rho_g) g}{\mu_g^2} \tag{6.24}$$

For wet particles, it is recommended to use correlation based on experimental finding for each type of materials.

6.2.3 Group B Particles

The group B contains particles in the moderate size range. Sand is the most typical powder in this group. In contrast with Group A powders, interparticle forces are negligible and bubbles start to form in this type of powder at or only slightly above minimum fluidization velocity. Bed expansion is small and the bed collapses very quickly when the gas supply is cut off.

There is little or no powder circulation or mixing in the absence of bubbles and bubbles burst at the surface of the bed as discrete entities. Bubbles rise faster, but not much faster, than the interstitial gas. The bubble size increases roughly linearly with distance above distributor and with the excess gas velocity, $u-u_{mf}$. For this group, variable size bubbles, choice (b) in Fig. 6.1, is used for modeling the bubble behaviour. Since the bubble size changes along the bed height, the voidage distribution of bubble and interstitial gas should be varied for this group (Fig. 6.2b). Backmixing of interstitial gas is relatively low, as is gas exchange between bubbles and the dense phase.

The bubble flowrate is evaluated based on the finding of Hilligardt and Werther [1986]. Their graphical results can be mathematically can be formulated as:

$$Q_b = \psi(u - u_{mf})A_t \tag{6.25}$$

where $\psi = 0.68$ for $H/d_t \le 1.8$

$$\psi = \exp\left[0.483\left(\frac{H}{d_t}\right) - 0.6695\right] \quad \text{for} \quad 1.8 \le H/d_t \le 4$$

For the bubble size, the correlation proposed by Mori and Wen [1975] for group B is used:

$$\frac{d_{bm} - d_{bj}}{d_{bm} - d_{bo}} = e^{-0.3H_j/d_t} \tag{6.26}$$

where d_{bo} is the initial bubble size formed near the bottom of the bed, given by:

$$d_{bo} = \frac{1.30}{g^{0.2}}\left[\frac{A(u-u_{mf})}{N_{or}}\right]^{0.4} \tag{6.27}$$

and d_{bm} is the maximum bubble size in a very deep bed. This is given as:

$$d_{bm} = 0.65\left[A(u-u_{mf})\right]^{0.4} \tag{6.28}$$

The bubble rise velocity is predicted using the following correlation,

$$u_{b_j} = (u-u_{mf}) + 0.71(gd_{b_j})^{0.5} \tag{6.29}$$

The bubble voidage is predicted by,

$$\varepsilon_{b_j} = \frac{Q_b}{A_t u_{b_j}} \tag{6.30}$$

The volume fraction of particle is assumed to be constant along the bed,

$$\varepsilon_p = (1-\varepsilon_{b_j})(1-\varepsilon_{e_j}) \tag{6.31}$$

The volume fractions and velocity of interstitial gas are given respectively as:

$$\varepsilon_{i_j} = (1-\varepsilon_{b_j}-\varepsilon_p) \tag{6.32}$$

$$u_{i_j} = \frac{\left(u - \varepsilon_{b_j} u_{b_j}\right)}{\varepsilon_{b_j}} \tag{6.33}$$

The bed height after fluidization is calculated based on average bubble hold-up as,

$$H_f = \frac{W_b}{\rho_p \varepsilon_p A_t} = \frac{H_{mf}}{1 - \varepsilon_{b_{av}}} \tag{6.34}$$

For relatively dry particles, the minimum fluidization velocity, u_{mf} is given by Kunii and Levenspiel [1991]:

$$\frac{1.75}{\varepsilon_{mf}^3 \phi_s} \mathrm{Re}_{mf}^2 + \frac{150(1-\varepsilon_{mf})}{\varepsilon_{mf}^3 \phi_s^2} \mathrm{Re}_{mf} = Ar \tag{6.35}$$

where Re is the Reynolds number and Ar is the Archimedes number defined as:

$$\mathrm{Re}_{mf} = \frac{d_p u_{mf} \rho_g}{\mu_g} \tag{6.36}$$

$$Ar = \frac{d_p^3 \rho_g (\rho_p - \rho_g) g}{\mu_g^2} \tag{6.37}$$

The minimum fluidization velocity for this group is measured experimentally and found to be in good agreement with the Eq. (6.35). For wet particles, it is recommended to use correlation based on experimental finding for each type of materials.

6.3 The Interstitial Gas Phase

The interstitial gas is in more intimate contact with solid particles than the gas in the bubbles, thus, it has more contribution to the transport phenomena inside the bed. The gas

has interactions with the solid phase, bubble phase and the walls. A plug flow model can be considered for the interstitial gas. The bed is considered to be nonisotermal and also the temperature of interstitial gas phase can change along the bed. For modeling the gas behaviour, it is required to divide the bed into many one-dimensional control volumes. For each control volume, the differential equations can be developed for the mass and energy of the interstitial gas phase. The mass balance for the interstitial gas in the control volume can be written as, Fig. 6.3,

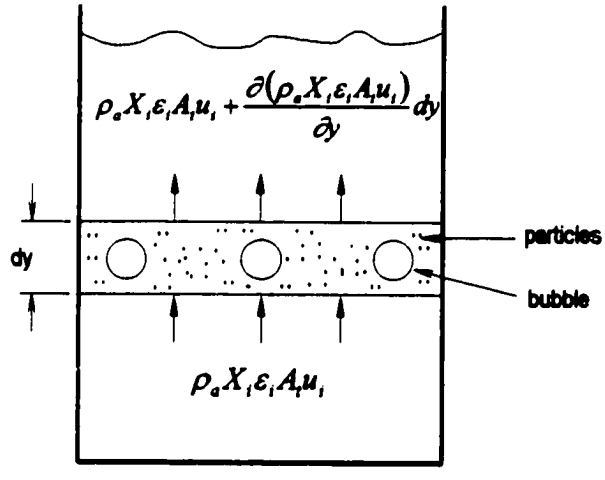

Figure 6.3 One-dimensional control volume for interstitial gas mass transfer analysis.

$$\dot{M}_{in} + \dot{M}_{out} + \dot{M}_g dV = \frac{\partial M}{\partial t} \tag{6.38}$$

where

$$\dot{M}_{in} = \rho_a X_i \varepsilon_i A_t u_i \tag{6.39}$$

$$\dot{M}_{out} = \rho_a X_i \varepsilon_i A_t u_i + \frac{\partial(\rho_a X_i \varepsilon_i A_t u_i)}{\partial y} dy \tag{6.40}$$

Interaction of interstitial gas with solid and bubble phase can be considered in mass generation terms as follow:

$$\dot{M}_g = \dot{M}_{g,particle} + \dot{M}_{g,bubble} \tag{6.41}$$

$$\dot{M}_{g,particle} = \rho_a k_p (X_p - X_i) \frac{A_p}{A_t dy} \tag{6.42}$$

$$\dot{M}_{g,bubble} = \rho_a k_{ib} (X_b - X_i) \frac{A_b}{A_t dy} \tag{6.43}$$

and

$$dV = A_t dy \tag{6.44}$$

Replacing Eqs. (6.40)-(6.45) into Eq. (6.39) results in:

$$\frac{\partial}{\partial t}(\rho_a X_i \varepsilon_i) + \frac{\partial}{\partial y}(\rho_a X_i \varepsilon_i u_i) = \rho_a k_p (X_p - X_i) \frac{A_p}{A_t dy} + \rho_a k_{ib} (X_b - X_i) \frac{A_b}{A_t dy} \tag{6.45}$$

where the ratio of particles and bubbles area per control volume of bed can be written as:

$$\frac{A_p}{A_t dy} = \frac{6\varepsilon_p}{d_p} \tag{6.46}$$

$$\frac{A_b}{A_t dy} = \frac{6\varepsilon_b}{d_b} \tag{6.47}$$

The relation between bubble interchange coefficient K_{ib}, and mass transfer coefficient, k_{ib} is given as:

$$K_{ib} = \frac{A_b}{V_b} k_{ib} = \frac{6k_{ib}}{d_b} \tag{6.48}$$

Substituting Eqs. (6.46) through (6.48) into Eq. (6.45) gives:

$$\frac{\partial}{\partial t}(\rho_a X_i \varepsilon_i) + \frac{\partial}{\partial y}(\rho_a X_i \varepsilon_i u_i) = \rho_a k_p (X_p - X_i)\frac{6\varepsilon_p}{d_p} + \rho_a K_{ib}\varepsilon_b (X_b - X_i) \tag{6.49}$$

The similar approach can be used to develop a differential equation for energy. Figure 6.4 displays the schematic of control volume used for the energy balance. The general equation of energy is:

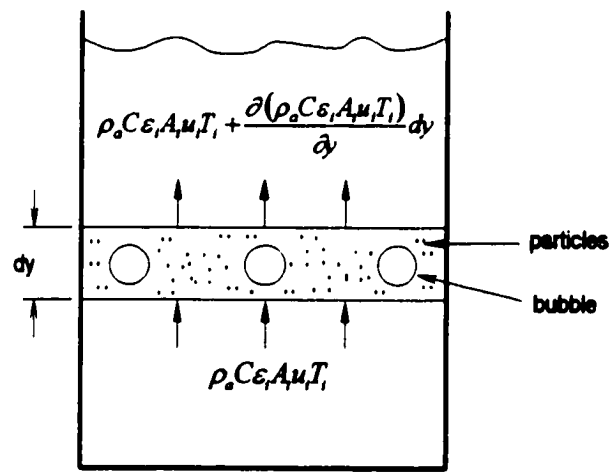

Figure 6.4 One-dimensional control volume for interstitial gas heat transfer analysis.

$$\dot{E}_{in} + \dot{E}_{out} + \dot{E}_g dV = \frac{\partial E}{\partial t} \tag{6.50}$$

where

$$\dot{E}_{in} = \rho_a C\varepsilon_i A_t u_i T_i \tag{6.51}$$

$$\dot{E}_{out} = \rho_a C\varepsilon_i A_t u_i T_i + \frac{\partial(\rho_a C\varepsilon_i A_t u_i T_i)}{\partial y} dy \tag{6.52}$$

Interaction of the interstitial gas with the solid, bubble phase, and surface of the bed wall can be considered in heat generation terms as follow:

$$\dot{E}_g = \dot{E}_{g,particle} + \dot{E}_{g,bubble} + \dot{E}_{g,surface} \tag{6.53}$$

$$\dot{E}_{g,particle} = h_p(T_p - T_i)\frac{A_p}{A_t dy} + \dot{M}_{g,particle} C_v (T_p - T_i) \tag{6.54}$$

$$\dot{E}_{g,bubble} = h_b(T_b - T_i)\frac{A_b}{A_t dy} + \dot{M}_{g,bubble} C_v (T_b - T_i) \tag{6.55}$$

$$\dot{E}_{g,surface} = h_s(T_s - T_i)\frac{A_s}{A_t dy} \tag{6.56}$$

Substituting Eqs. (6.51) through (6.56) into the Eq. (6.50), gives:

$$\frac{\partial}{\partial t}(\rho_a C_i \varepsilon_i T_i) + \frac{\partial}{\partial y}(\rho_a C_i \varepsilon_i u_i T_i) = h_p(T_p - T_i)\frac{A_p}{A_t dy} + \rho_a k_p (X_p - X_i)\frac{A_p}{A_t dy} C_v (T_p - T_i)$$
$$+ h_b(T_b - T_i)\frac{A_b}{A_t dy} + \rho_a k_{ib}(X_b - X_i)\frac{A_b}{A_t dy} C_v (T_b - T_i) + h_s(T_s - T_i)\frac{A_s}{A_t dy} \tag{6.57}$$

Considering Eqs. (6.46) and (6.47) and writing bubble interchange coefficient per volume of bubble, Eq. (6.57) can be written as:

$$\frac{\partial}{\partial t}(\rho_a C_i \varepsilon_i T_i) + \frac{\partial}{\partial y}(\rho_a C_i \varepsilon_i u_i T_i) = h_p(T_p - T_i)\frac{6\varepsilon_p}{d_p} + \rho_a k_p (X_p - X_i)\frac{6\varepsilon_p}{d_p} C_v (T_p - T_i)$$
$$+ H_{ib}\varepsilon_b(T_b - T_i) + \rho_a K_{ib}\varepsilon_b (X_b - X_i) C_v (T_b - T_i) + h_s(T_s - T_i)\frac{(1-\varepsilon_p)}{d_t} \tag{6.58}$$

The interchange coefficients between the solid phase and the interstitial gas are given by Ranz [1952]:

$$h_p = \frac{k_p}{d_p}\left(2 + 1.8\,\mathrm{Re}_p^{1/2}\, Sc^{1/3}\right) \tag{6.59}$$

$$k_p = \frac{D_v}{d_p \phi_m}\left(2 + 1.8 \mathrm{Re}_p^{1/2} Sc^{1/3}\right) \tag{6.60}$$

6.4 The Bubble Phase

The bubbles in a fluidized bed are a source of inhomogenity inside the bed and in many applications, especially those involving fast reaction processes, they are the controlling parameter in determining the overall performance of the bed. In the drying system, there are two modes of drying; constant rate and falling rate. In constant rate drying, where the rate of drying is controlled by external heat and mass transfer coefficients, the role of bubbles are more important than in the falling rate drying, where the rate of drying is controlled by the moisture diffusion inside the particle. However, in any case, for precise modeling of the drying process, it is required to consider the bubble existence and its interaction with the other phases. The characteristics of bubble such as size, velocity, moisture content, temperature, and interchange coefficient usually depend on its axial position in the bed. For the modeling purpose, the bubbles are considered in plug flow and its differential equation can be derived following the procedure applied for the interstitial gas phase. The mass balance equation can be written as:

$$\frac{\partial}{\partial t}(\rho_a X_b \varepsilon_b) + \frac{\partial}{\partial y}(\rho_a X_b \varepsilon_b u_b) = \rho_a K_{ib} \varepsilon_b (X_i - X_b) \tag{6.61}$$

and the energy balance for bubble phase is,

$$\frac{\partial}{\partial t}(\rho_a C_b \varepsilon_b T_b) + \frac{\partial}{\partial y}(\rho_a C_b \varepsilon_b u_b T_b) = H_{ib} \varepsilon_b (T_i - T_b) + \rho_a K_{ib} \varepsilon_b (X_i - X_b) C_v (T_i - T_b) \tag{6.62}$$

For different groups of particles the volumetric mass transfer coefficient between the bubble phase and the interstitial gas phase are not the same. In group A particles the cloud acts as an isolating layer between bubble gas and interstitial gas and decreases the overall

exchange rate coefficient. For this group, the interchange coefficients between the bubble and the cloud can be computed as [Kunii and Levenspiel, 1991]:

$$K_{bc} = 4.5\left(\frac{u_{mf}}{d_b}\right) + 5.85\left(\frac{D_v^{1/2} g^{1/4}}{d_b^{5/4}}\right) \tag{6.63}$$

and between the cloud and the interstitial gas:

$$K_{ci} = 6.77\left(\frac{D_v \varepsilon_{mf} u_{br}}{d_b^3}\right)^{0.5} \tag{6.64}$$

where the relative velocity of bubble to emulsion phase is:

$$u_{br} = 0.71(gd_b)^{0.5} \tag{6.65}$$

The overall interchange coefficient between the bubble and the interstitial gas for group A, is:

$$\frac{1}{K_{ib}} = \frac{1}{K_{bc}} + \frac{1}{K_{ci}} \tag{6.66}$$

The interchange coefficient for the heat transfer between the bubble and the interstitial gas phase can be computed similar to the mass transfer coefficient. The interchange coefficient between bubble and cloud is given as [Kunii and Levenspiel, 1991]:

$$H_{bc} = 4.5\left(\frac{u_{mf}\rho_a C}{d_b}\right) + 5.85\frac{(k_{ga}\rho_a C)^{1/2} g^{1/4}}{d_b^{5/4}} \tag{6.67}$$

and between the cloud and the interstitial gas:

$$H_{cb} = 6.77\left(\frac{\rho_g C k_{ta} \varepsilon_{mf} u_{br}}{d_b^3}\right)^{0.5} \tag{6.68}$$

and the overall interchange coefficient between the bubble and the interstitial gas for group A, is:

$$\frac{1}{H_{ib}} = \frac{1}{H_{bc}} + \frac{1}{H_{ci}} \tag{6.69}$$

For group D and B particles the cloud phase does not appear around the bubble and the gas bubble can directly have heat and mass transfer with the interstitial gas. So, the terms showing the contribution of the cloud phase, K_{ib} and H_{ib}, can be neglected. The overall mass transfer coefficient between the bubble and the interstitial gas can be computed as:

$$K_{ib} = 4.5\left(\frac{u_{mf}}{d_b}\right) + 5.85\left(\frac{D_v^{1/2} g^{1/4}}{d_b^{5/4}}\right) \tag{6.70}$$

and the overall heat transfer coefficient between the bubble and the interstitial gas becomes:

$$H_{ib} = 4.5\left(\frac{u_{mf} \rho_a C}{d_b}\right) + 5.85\frac{\left(k_{ta} \rho_a C\right)^{1/2} g^{1/4}}{d_b^{5/4}} \tag{6.71}$$

6.5 The Solid Phase

Drying of solids can take place in two different modes namely; the constant rate and the falling rate. The existence of each mode depends on the moisture content of the solids and other conditions of solid and drying medium. In the following the governing equations of each mode is discussed separately.

6.5.1 The Falling Rate Drying

The solids experience a set of complex processes in the course of falling rate drying. A variety of mechanisms has been proposed to address the moisture transport in solids [Brooker et al., 1974]. For a complete description of the heat and mass transfer in the solid the coupling effect between the various transport mechanisms should be considered. Luikov [1966] developed a general model for the simultaneous heat and moisture transfer in drying process based on irreversible thermodynamics:

$$\frac{\partial \underset{\sim}{u}}{\partial t} = \nabla^2 K \underset{\sim}{u} \tag{6.72}$$

where $\underset{\sim}{u}$ is a vector as: $\underset{\sim}{u} = \underset{\sim}{u}(r,t) = (M_p, T_p, P_p)^T$ and M_p, T_p and P_p represent the distributions of moisture content, temperature and total pressure within the body of solid. K in the Eq. (6.72) is a 3×3 matrix as:

$$K = \{K_{ij}\}$$

The system of partial differential equations for each variable can be written as:

$$\frac{\partial M_p}{\partial t} = \nabla^2 K_{11} M_p + \nabla^2 K_{12} T_p + \nabla^2 K_{13} P_p \tag{6.73}$$

$$\frac{\partial T_p}{\partial t} = \nabla^2 K_{21} M_p + \nabla^2 K_{22} T_p + \nabla^2 K_{23} P_p \tag{6.74}$$

$$\frac{\partial P_p}{\partial t} = \nabla^2 K_{31} M_p + \nabla^2 K_{32} T_p + \nabla^2 K_{33} P_p \tag{6.75}$$

The elements of matrix K, depend on the physical properties of the product such as mass diffusivity and thermal conductivity. The K_{ii} are phenomenological coefficients while the off-diagonal elements K_{ij}, $i \neq j$, represent coupling between the various transport

mechanism. The difficulty with this formulation is that insufficient data are available for the estimation of all the coupling coefficients in the matrix K. However, under various simplifying assumptions, simplified versions of Eq. (6.71) have been adapted for the description of grain drying. In the drying of cereal grains, the temperature attained by the grain is generally sufficiently small to regard the effect of total pressure gradient within the particle as negligible (Luikov, 1966]. Eq. (6.71) then reduces to a two-equation system involving only grain moisture content and temperature distributions, M_p and T_p respectively.

Moreover, solid particles are assumed to be uniform in size and isotropic, with a sphericity close to the unity. The driving forces which are necessary for mass and heat transfers to take place inside a solid particle are defined as the difference between the vapor pressures and temperatures of solid surface and the interstitial gas. With the relatively large particle size, it becomes necessary to consider the gradient of moisture and temperature inside the solid. For this reason, a diffusion type equation is considered for moisture and temperature distributions with appropriate boundary conditions. It is assumed that moisture inside the particle diffuses in the liquid phase to the surface of particles and the evaporation takes place only at the surface. The general form of diffusion equation in conservative form is written as:

$$\frac{\partial M_p}{\partial t} = \nabla \cdot \left(D \nabla M_p \right) \tag{6.76}$$

In the one-dimensional spherical coordinate system and assuming the moisture gradient to be in the radial direction, equation (6.76) becomes:

$$\frac{\partial M_p}{\partial t} = \frac{1}{r^2} \frac{\partial}{\partial r} \left(r^2 D \frac{\partial M_p}{\partial r} \right) \tag{6.77}$$

with the following initial and boundary conditions:

$$t = 0 \quad 0 \le r \le R \quad M_p = M_{pi}(r) \tag{6.78}$$

$$t > 0 \quad r = 0 \quad \frac{\partial M_p}{\partial t} = 0 \tag{6.79}$$

For the second boundary condition, Eq. (6.77) should be integrated on the surface grid of the solid in a way that would consider the effect of mass transfer between the surface of particle and interstitial gas. The detailed integral is presented in chapter 7, but the general form of equation is:

$$\rho_p \Delta V \frac{\partial M_p}{\partial t} = \dot{m}_{conv.} - \rho_p D A_p \frac{\partial M_p}{\partial r} \tag{6.80}$$

where the mass convection term at the surface of particle can be written as:

$$\dot{m}_{conv.} = \rho_a k_p A_p (X_{sp} - X_i) \tag{6.81}$$

The energy equation is:

$$\frac{\partial(\rho_p C_p T_p)}{\partial t} = \frac{1}{r^2}\frac{\partial}{\partial r}\left(r^2 k_{tp} \frac{\partial T_p}{\partial r}\right) \tag{6.82}$$

and the initial and boundary conditions are:

$$t = 0 \quad 0 \le r \le R \quad T_p = T_{pi}(r) \tag{6.83}$$

$$t > 0 \quad r = 0 \quad \frac{\partial T_p}{\partial t} = 0 \tag{6.84}$$

For the second boundary condition the Eq. (6.82) should be integrated on the surface grid of the solid in a way that would consider the effect of heat transfer at the surface of particle. The detailed integral is presented in chapter 7, but the general form of equation is:

$$\frac{\partial(\rho_p C_p T_p)}{\partial t} = \dot{q}_{evap.} + \dot{q}_{pi} + \dot{q}_{pw} - k_{tp} A_p \frac{\partial T_p}{\partial r} \tag{6.85}$$

The heat transfer of solid with interstitial gas and the wall of bed are $\dot{q}_{pi}$, $\dot{q}_{pw}$, respectively, where $\dot{q}_{evap.}$ is heat transfer due to phase change. For each term we have the following equations:

$$\dot{q}_{evap.} = \dot{m}_{conv.} h_{fg} \tag{6.86}$$

$$\dot{q}_{pi} = h_p A_p (T_i - T_{ps}) \tag{6.87}$$

$$\dot{q}_{pw} = h_{pw} A_{pw} (T_w - T_{ps}) \tag{6.88}$$

and the heat transfer coefficient between the solid and the wall is [Howard, 1989]:

$$h_{pw} = \frac{0.843 Ar^{0.39} k_{ta}}{d_p^{0.5}} \tag{6.89}$$

This model takes into account the simultaneous heat and mass transfer during the drying process as well as internal and external heat and mass transfer resistances. Taking into account the temperature change will improve the fit of predicted drying curve at the beginning of the process. Furthermore, replacing the surface equilibrium moisture content by a convective boundary condition generally gives a better fit at the end of the process.

Diffusion coefficients in the above equations are generally functions of moisture content and temperature of the solid respectively, thus the above equations are coupled and should be solved simultaneously. The boundary conditions for the surface of particles have a great influence on the numerical solution. If the unsteady term in the boundary conditions is neglected, the numerical solution may be unstable and fail to converge. If another type of simplified boundary condition such as moisture equilibrium with the surrounding air is applied, as many researchers have used, the numerical error in the initial step of solution will be quite large. This error in the spherical coordinate system would be very noticeable since the volume of grid at the surface is many times larger than the other grids.

The average moisture content of the wheat at any time can be obtained by integrating over the grain volume,

$$\overline{M}(t) = \frac{4\pi}{V_p}\int_0^R M_p(r,t)r^2 dr \tag{6.90}$$

6.5.2 The Constant Rate Drying

In the constant rate drying, the diffusion type equations for prediction of the temperature and moisture content of solid need not be used because there is enough free moisture in the solid. Usually, it is assumed that the moisture diffusion coefficient is close to infinity, so the diffusion does not control the rate of drying process. To analyze the moisture content and temperature of solid, a lump model differential equation can be used. The mass equation in this case can be written as:

$$\frac{d}{dt}(M_p\rho_p V_p) = \rho_a k_p A_p (X_{sp} - X_t) \tag{6.91}$$

with the initial condition as: $t = 0 \quad M_p = M_{pi}$ (6.92)

The energy equation is:

$$\frac{d}{dt}\left(\rho_p C_p V_p T_p\right) = h_{pi} A_p \left(T_i - T_p\right) - \rho_a k_p A_p \left(X_{sp} - X_i\right) h_{fg} + h_{pw} A_{pw} \left(T_w - T_p\right) \quad (6.93)$$

with the initial condition as: $t = 0 \quad T_p = T_{pi}$ (6.94)

6.6 The Wall Effect

In order to incorporate the effect of wall temperature on the heat transfer interaction inside the bed, a differential equation for the wall region was developed. This equation considers the effect of wall temperature on the interstitial gas and solid phase temperature inside the bed. Similar to the flow field inside the bed, the wall was divided into equal control volumes to be able to consider its longitudinal variation. The effect of ambient air temperature was also considered through convection term with the external boundary of wall. Considering the heat transfer of wall with interstitial gas, particles, and ambient air as q_{wi}, q_{wp}, and q_{wa}, respectively, the energy equation for the wall is:

$$\rho_{wl} C_{wl} \frac{\partial T_{wl}}{\partial t} = k_{wl} \frac{\partial^2 T_{wl}}{\partial y^2} + \dot{q}_{wi} + \dot{q}_{pw} + \dot{q}_{wa} \quad (6.95)$$

where the equations for $\dot{q}_{wi}$ and $\dot{q}_{wa}$ are:

$$\dot{q}_{wi} = h_{wi} A_{wi} \left(T_i - T_{wl}\right) \quad (6.97)$$

$$\dot{q}_{wa} = h_{wa} A_{wa} \left(T_i - T_a\right) \quad (6.98)$$

and heat transfer coefficients are obtained [Howard, 1989]:

$$h_{wi} = \frac{0.86 Ar^{0.15} k_{ta}}{d_p} \tag{6.99}$$

$$h_{pw} = \frac{0.843 Ar^{0.39} k_{ta}}{d_p^{0.5}} \tag{6.100}$$

The heat transfer coefficient between the wall and ambient air depends on the experiment condition and may be different for each case. For the experimental condition conducted in this work, an average heat transfer coefficient for turbulent natural convection flow in vertical wall is used as [Bejan, 1993]:

$$h_{wa} = \frac{k_{ta}}{H}\left[0.825 + 0.325\left(\frac{g\beta(T_w - T_a)H^3}{\alpha\nu}\right)^{\frac{1}{6}}\right] \tag{6.101}$$

CHAPTER 7

Numerical Analysis of Nonlinear Set of Partial Differential Equations

7.1 Discretization of Differential Equations

The next step after derivation of fundamental differential equations, is to use a proper approach for discretization of these equations. The discretization can be derived in many ways, hence one must choose the one which is the most appropriate for the nature of the problem. These include:

1. Taylor series expansion
2. Polynomial fitting
3. Integral method
4. Control-volume approach

Among these approaches, Taylor series expansion and control volume approaches are widely used in the literature for different types of differential equations. Both methods (Taylor series and control-volume) for discretization of equations were examined and applied in the numerical program. It was found that convergence and stability of the control volume approach is better than the Taylor series approach especially at high temperature when the nonlinearity of the process is increased. Thus, the control-volume formulation was chosen to be used in numerical implementation of partial differential equations. The basic idea of the control-volume formulation lends itself to direct physical interpretation. The calculation domain is divided into a number of nonoverlapping control volumes such that there is one control volume surrounding each grid point. The differential equation is integrated over each control volume. Piecewise profiles expressing the variation of dependent variable between the grid points are used to evaluate the required integrals. The discretization equation obtained in this manner expresses the conservation principle for each control volume.

7.1.1 Interstitial Gas Phase

First, let us consider the mass transfer equation for interstitial gas phase. As was mentioned, the mass and energy equations derived for the interstitial gas belong to the hyperbolic type of partial differential equations. Different schemes have been developed to solve the hyperbolic type of equation, for examples, upwind method, Lax-Wendroff method, MacCormack method and so forth. The difference in the quality of solution by using different schemes are generally small except for some specific situations. The most important feature of any scheme is its stability criteria. Since the implicit approach provides a more stable solution than the explicit approach, therefore, this approach is used in the discretization of differential equations under an appropriate scheme.

The interstitial gas equation includes unsteady, convection, and sources terms as:

$$\frac{\partial}{\partial t}(\rho_a X_i \varepsilon_i)+\frac{\partial}{\partial y}(\rho_a X_i \varepsilon_i u_i)=\rho_a k_p (X_p - X_i)\frac{6\varepsilon_p}{d_p}+\rho_a K_{ib}\varepsilon_b (X_b - X_i) \quad (7.1)$$

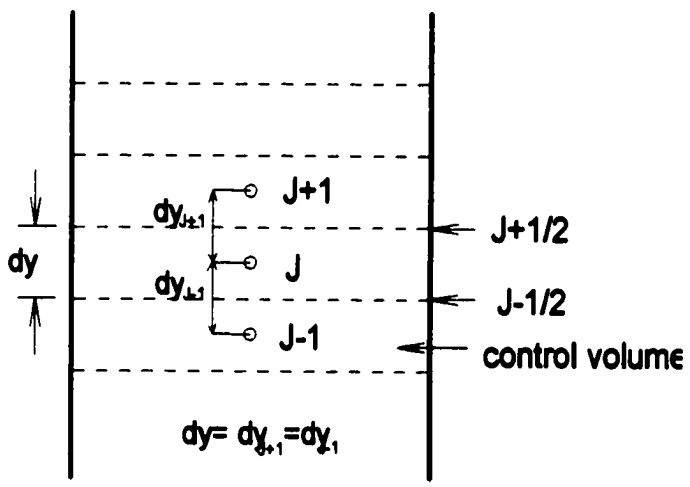

Figure 7.1 Control volumes and grid-point cluster inside the bed.

To derive the discretization equation, the grid-point cluster shown in Fig. 7.1. was employed. The grid point j, which has the grid points j+1 and j-1 as its neighbors was chosen as the focus of attention. The dashed lines show the faces of the control volume. The letters j+1/2 and j-1/2 denote these faces. Integration of Eq. (7.1) over the control volume give:

$$\int_{j-1/2}^{j+1/2}\int_{t}^{t+\Delta t}\frac{\partial(\rho_a X_i \varepsilon_i)}{\partial t}dtdy + \int_{t}^{t+\Delta t}\int_{j-1/2}^{j+1/2}\frac{\partial(\rho_a X_i \varepsilon_i u_i)}{\partial y}dydt = \int_{j-1/2}^{j+1/2}\int_{t}^{t+\Delta t}\rho_a k_p (X_p - X_i)\frac{6\varepsilon_p}{d_p}dtdy$$
$$+ \int_{j-1/2}^{j+1/2}\int_{t}^{t+\Delta t}\rho_a K_{ib}\varepsilon_b (X_b - X_i)dtdy \qquad (7.2)$$

where the order of the integration is chosen according to the nature of the term. For the unsteady term, the first term on the left side of Eq. (7.1), we shall assume that the grid-point value of variables prevails throughout the control volume. Then,

$$\int_{j-1/2}^{j+1/2}\int_{t}^{t+\Delta t}\frac{\partial(\rho_a X_i \varepsilon_i)}{\partial t}dtdy = \left[(\rho_a X_i \varepsilon_i)^{n+1,j} - (\rho_a X_i \varepsilon_i)^{n,j}\right]\Delta y \qquad (7.3)$$

For the convection term the integration yields:

$$\int_{t}^{t+\Delta t}\int_{j-1/2}^{j+1/2}\frac{\partial(\rho_a X_i \varepsilon_i u_i)}{\partial y}dydt = \int_{t}^{t+\Delta t}\left[(\rho_a X_i \varepsilon_i u_i)^{j+1/2} - (\rho_a X_i \varepsilon_i u_i)^{j-1/2}\right]dt \qquad (7.4)$$

At this point a value for the variable at j+1/2 and j-1/2 must be chosen. A simple approach is to use the central difference approach. This means for properties at j+1/2, the average of properties at j and j+1; and for point j-1/2, the average of j and j-1 are used. However, Patankar [1980] found that central difference approach may not lead to a real solution for this type of partial differential equation. Therefore, the upwind scheme is used in this work

for discretization of the convection term. Since it was assumed that the interstitial gas is in plug flow, the velocity of gas always is upward. This means that j+1/2 can be replaced with j and j-1/2 with j-1.

Another assumption is needed since a variable may vary with time from t to t+Δt. Many assumptions are possible but an implicit approach is chosen to preserve the stability. The result can be given as:

$$\int_{t}^{t+\Delta t}\left[(\rho_a X_i \varepsilon_i u_i)^{j+1/2} - (\rho_a X_i \varepsilon_i u_i)^{j-1/2}\right]dt = \left[(\rho_a X_i \varepsilon_i u_i)^{n+1,j} - (\rho_a X_i \varepsilon_i u_i)^{n+1,j-1}\right]\Delta t \qquad (7.5)$$

For the terms at the right side of Eq. (7.1), it was assumed that the grid-point value of variable prevails throughout the control volume and the implicit approach can be used for the variation with time. The final discretization form of the mass balance equation for the interstitial gas is:

$$\left[(\rho_a \varepsilon_i X_i)^{n+1,j} - (\rho_a \varepsilon_i X_i)^{n,j}\right]\Delta y + \left[(\rho_a \varepsilon_i u_i X_i)^{n+1,j} - (\rho_a \varepsilon_i u_i X_i)^{n+1,j-1}\right]\Delta t =$$

$$\left[\rho_a k_p (X_p - X_i)\frac{6\varepsilon_p}{d_p} + \rho_a K_{ib}\varepsilon_b (X_b - X_i)\right]^{n+1,j}\Delta y \Delta t \qquad (7.6)$$

Next, a similar approach for the energy equation in the interstitial gas can be applied since both equation are of the same type. The discretized form of the energy equation is:

$$\left[(\rho_a C_i \varepsilon_i T_i)^{n+1,j} - (\rho_a C_i \varepsilon_i T_i)^{n,j}\right]\Delta y + \left[(\rho_a C_i \varepsilon_i u_i T_i)^{n+1,j} - (\rho_a C_i \varepsilon_i u_i T_i)^{n+1,j-1}\right] =$$

$$\left[h_p (T_p - T_i)\frac{6\varepsilon_p}{d_p} + \rho_a k_p (X_p - X_i)\frac{6\varepsilon_p}{d_p} C_v (T_p - T_i) + H_{ib}\varepsilon_b (T_b - T_i) +\right.$$

$$\rho_a K_{ib}\varepsilon_b(X_b - X_i)C_v(T_b - T_i) + h_s(T_s - T_i)\frac{(1-\varepsilon_p)}{d_{bubble}}\Big]^{n+1,j}\Delta y\Delta t \qquad (7.7)$$

7.1.2 The Bubble Phase

The mass and energy equations for the bubble phase, like the interstitial gas phase, belong to the hyperbolic type of partial differential equations. The basic assumption for the bubble phase is the same as the interstitial gas phase. A similar approach can be used to discretize the mass and energy equations for this phase.

For the mass balance it becomes:

$$\left[(\rho_a\varepsilon_b X_b)^{n+1,j} - (\rho_a\varepsilon_b X_b)^{n,j}\right]\Delta y + \left[(\rho_a\varepsilon_b u_b X_b)^{n+1,j} - (\rho_a\varepsilon_b u_b X_b)^{n,j}\right]\Delta t = \left[\rho_a K_{ib}\varepsilon_b(X_i - X_b)\right]^{n+1,j}\Delta y\Delta t \qquad (7.8)$$

and for the energy balance it is:

$$\left[(\rho_a C_i\varepsilon_b T_b)^{n+1,j} - (\rho_a C_i\varepsilon_b T_b)^{n,j}\right]\Delta y + \left[(\rho_a\varepsilon_b u_b T_b)^{n+1,j} - (\rho_a\varepsilon_b u_b T_b)^{n,j}\right]\Delta t = \left[H_{ib}\varepsilon_b(T_i - T_b) + \rho_a K_{ib}\varepsilon_b(X_i - X_b)C_v(T_i - T_b)\right]^{n+1,j}\Delta y\Delta t \qquad (7.9)$$

7.1.3 The Solid Phase

Contrary to the hyperbolic nature of interstitial gas and bubble phases, the mass and energy equations for the solid phase belong to the parabolic type of partial differential equations. The parabolic system of differential equation has numerous important applications in various branches of science and engineering. Therefore, a lot of different discretization schemes have been developed for this type of equation, among them are: simple method, Crank-Nicolson method, Dufort-Frankel, ADI and ADE methods. Like the approach for the hyperbolic system of equations, an implicit approach is used in the discretization of the solid phase equations.

Another difference between the characteristics of solid phase and gas phase equations is the type of coordinate used in any case. For discretization of gas phase equations, Cartesian coordinates were used, but the solid phase discretization should be expressed in the spherical coordinate because of the spherical shape of particles. These are the two basic differences between the gas phase and the solid phase characteristics. To develop a discretization formula in spherical coordinates, the one-dimensional mass diffusion equation is considered:

$$\frac{\partial M_p}{\partial t} = \frac{1}{r^2}\frac{\partial}{\partial r}\left(r^2 D \frac{\partial M_p}{\partial r}\right) \tag{7.10}$$

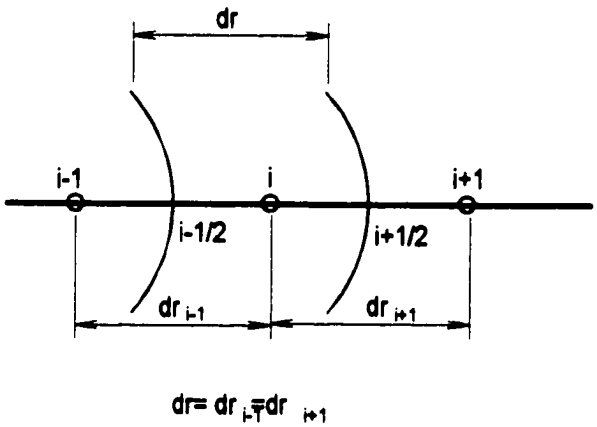

Figure 7.2 Control volumes and grids in spherical coordinates.

The grid and the control volume are shown in Fig. 7.2. To obtain the discretization equation, Eq. (7.10) is multiplied by $4\pi r^2$ and integrated over the control volume and over the time interval from t to $t+\Delta t$ as shown in Fig. 7.2, yielding:

$$\int_{i-1/2}^{i+1/2}\int_{t}^{t+\Delta t} 4\pi r^2 \frac{\partial M_p}{\partial t} dt dr = \int_{t}^{t+\Delta t}\int_{i-1/2}^{i+1/2} 4\pi \frac{\partial}{\partial r}\left(r^2 D \frac{\partial M_p}{\partial r}\right) dr dt \tag{7.11}$$

For the representation of the term $\partial M_p/\partial t$, we shall assume that the grid-point value of M_p prevails throughout the control volume. Then,

$$\int_{i-1/2}^{i+1/2}\int_{t}^{t+\Delta t} 4\pi r^2 \frac{\partial M_p}{\partial t} dt dr = \left(M_{p_i}^{n+1} - M_{p_i}^{n}\right)\Delta V \tag{7.12}$$

Here ΔV is the volume of the control volume. The diffusion term in Eq. (7.11) can be integrated over the control volume yielding:

$$\int_{t}^{t+\Delta t}\int_{i-1/2}^{i+1/2} \frac{\partial}{\partial r}\left(r^2 D \frac{\partial M_p}{\partial r}\right) dr dt = \int_{t}^{t+\Delta t}\left[\frac{r_{i+1/2}^2 D_{i+1/2}\left(M_{p_{i+1}} - M_{p_i}\right)}{\delta r_{i+1}} - \frac{r_{i-1/2}^2 D_{i-1/2}\left(M_{p_i} - M_{p_{i-1}}\right)}{\delta r_{i-1}}\right] 4\pi dt \tag{7.13}$$

Now, an assumption about how M_p varies with time from t to $t+\Delta t$ is needed. Here we express the general form of equation using a weighting factor f which can vary between 0 and 1.

$$\int_{t}^{t+\Delta t}\int_{i-1/2}^{i+1/2} \frac{\partial}{\partial r}\left(r^2 D \frac{\partial M_p}{\partial r}\right) dr dt = f\left[\frac{r_{i+1/2}^2 D_{i+1/2}\left(M_{p_{i+1}}^{n+1} - M_{p_i}^{n+1}\right)}{\delta r_{i+1}} - \frac{r_{i-1/2}^2 D_{i-1/2}\left(M_{p_i}^{n+1} - M_{p_{i-1}}^{n+1}\right)}{\delta r_{i-1}}\right]\Delta t +$$

$$(1-f)\left[\frac{r_{i+1/2}^2 D_{i+1/2}\left(M_{p_{i+1}}^{n} - M_{p_i}^{n}\right)}{\delta r_{i+1}} - \frac{r_{i-1/2}^2 D_{i-1/2}\left(M_{p_i}^{n} - M_{p_{i-1}}^{n}\right)}{\delta r_{i-1}}\right]\Delta t \tag{7.14}$$

The final form of Eq. (7.10) in discretized form is,

$$\left(M_{p_i}^{n+1} - M_{p_i}^{n}\right)\frac{\Delta V}{4\pi\Delta t} = f\left[\frac{r_{i+1/2}^2 D_{i+1/2}\left(M_{p_{i+1}}^{n+1} - M_{p_i}^{n+1}\right)}{\delta r_{i+1}} - \frac{r_{i-1/2}^2 D_{i-1/2}\left(M_{p_i}^{n+1} - M_{p_{i-1}}^{n+1}\right)}{\delta r_{i-1}}\right]\Delta t +$$

$$(1-f)\left[\frac{r_{i+1/2}^2 D_{i+1/2}\left(M_{p_{i+1}}^{\ n}-M_{p_i}^{\ n}\right)}{\delta r_{i+1}}-\frac{r_{i-1/2}^2 D_{i-1/2}\left(M_{p_i}^{\ n}-M_{p_{i-1}}^{\ n}\right)}{\delta r_{i-1}}\right]\Delta t \qquad (7.15)$$

In the numerical program, $f=0.5$ was used which is known as Crank-Nicolson scheme. The interface diffusivities are calculated based on the harmonic mean as,

$$D_{i+1/2}=\frac{2D_iD_{i+1}}{D_i+D_{i+1}} \qquad (7.16)$$

$$D_{i-1/2}=\frac{2D_iD_{i-1}}{D_i+D_{i-1}} \qquad (7.17)$$

For the boundary condition, Eq. (7.10) should be integrated over the surface grid considering the effect of surface mass transfer with the interstitial gas. Figure 7.3 shows the boundary condition of solid phase. In this figure $\dot{m}_{conv}$, is the net mass exchange between the solid and interstitial gas and it could be in either direction depending on the vapor pressure of each phase. So the direction of the arrow in this figure is arbitrary. Integrating along the boundary grid we can write,

$$\int_{i-1/2}^{i}\int_{t}^{t+\Delta t}4\pi r^2\frac{\partial M_p}{\partial t}dtdr=\int_{t}^{t+\Delta t}\int_{i-1/2}^{i}4\pi\frac{\partial}{\partial r}\left(r^2D\frac{\partial M_p}{\partial r}\right)drdt \qquad (7.18)$$

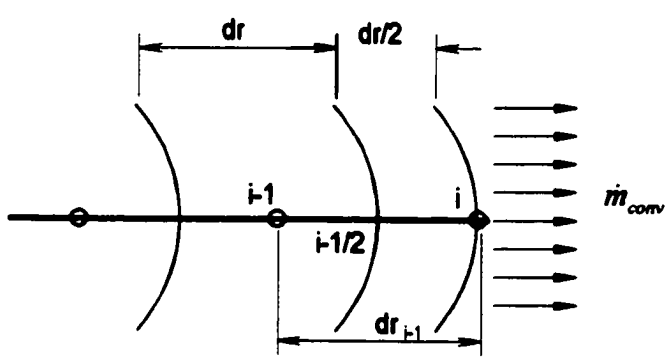

Figure 7.3 Half control volume at boundary condition for mass exchange at the surface.

It should be noticed that the thickness of the boundary grid is one half of the interior grids. The integration results in:

$$\left(M_{p_i}^{n+1} - M_{p_i}^{n}\right)\rho_p \Delta V_i = \int_t^{t+\Delta t}\left[\dot{m}_{conv} - \left(\rho_p A_{i-1/2} D_{i-1/2}\left(\frac{\partial M_p}{\partial r}\right)_{i-1/2}\right)\right]dt \qquad (7.19)$$

Using a weighting factor f to show the variation of variables in term of time and substituting for mass convection from Eq. (6.81), the final form of discretization equation of boundary layer is:

$$\left(M_{p_i}^{n+1} - M_{p_i}^{n}\right)\frac{\Delta V_i}{4\pi\Delta t} = -f\left[A_{i-1/2} D_{i-1/2}\frac{\left(M_{p_i}^{n+1} - M_{p_{i-1}}^{n+1}\right)}{\delta r_{i-1}}\right] - (1-f)\left[A_{i-1/2} D_{i-1/2}\frac{\left(M_{p_i}^{n} - M_{p_{i-1}}^{n}\right)}{\delta r_{i-1}}\right]$$
$$+ f\left[\frac{\rho_a}{\rho_p} k_p A_i \left(X_i^{n+1} - X_{sp}^{n+1}\right)\right] + (1-f)\left[\frac{\rho_a}{\rho_p} k_p A_i \left(X_i^{n} - X_{sp}^{n}\right)\right] \qquad (7.20)$$

The energy equation for the solid phase is:

$$\frac{\partial\left(\rho_p C_p T_p\right)}{\partial t} = \frac{1}{r^2}\frac{\partial}{\partial r}\left(r^2 k_{tp}\frac{\partial T_p}{\partial r}\right) \qquad (7.21)$$

The discretization of the energy equation is the same as the mass balance equation. The final form of discretization equation can be given as:

$$\frac{\left[\left(\rho_p C_p T_p\right)_i^{n+1} - \left(\rho_p C_p T_p\right)_i^{n}\right]\Delta V}{4\pi\Delta t} = f\left[\frac{r_{i+1/2}^2 k_{tp_{i+1/2}}\left(T_{p_{i+1}}^{n+1} - T_{p_i}^{n+1}\right)}{\delta r_{i+1}} - \frac{r_{i-1/2}^2 k_{tp_{i-1/2}}\left(T_{p_i}^{n+1} - T_{p_{i-1}}^{n+1}\right)}{\delta r_{i-1}}\right]\Delta t$$

$$+(1-f)\left[\frac{r_{i+1/2}^2 k_{tp_{i+1/2}}\left(T_{p_{i+1}}^{\ n}-T_{p_i}^{\ n}\right)}{\delta r_{i+1}}-\frac{r_{i-1/2}^2 k_{tp_{i-1/2}}\left(T_{p_i}^{\ n}-T_{p_{i-1}}^{\ n}\right)}{\delta r_{i-1}}\right]\Delta t \qquad (7.22)$$

For the boundary condition, Eq. (7.21) should be integrated on the surface grid of the solid considering the effect of heat transfer with interstitial gas and the wall and also the latent heat due to evaporation. Figure 7.4 shows the contribution of different parameters acting on the surface of a particle. In the figure, $\dot{q}_{evap}$, $\dot{q}_{pi}$, $\dot{q}_{pw}$ represent the heat transfer due to the evaporation of moisture on the particle, between the particle and the interstitial gas, and between the particle and the wall, respectively.

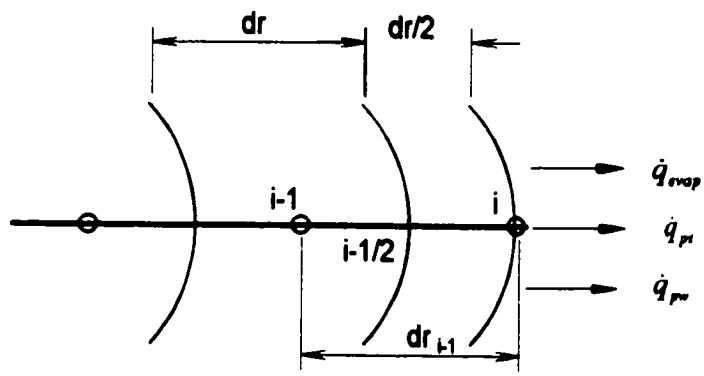

Figure 7.4 Half control volume at boundary condition for heat exchange at the surface.

The final form of discretization equation for boundary grid is:

$$\frac{\left[\left(\rho_p C_p T_p\right)_i^{n+1}-\left(\rho_p C_p T_p\right)_i^{n}\right]\Delta V_i}{4\pi\Delta t}=-f\left[A_{i-1/2}k_{tp_{i-1/2}}\frac{\left(T_{p_i}^{\ n+1}-T_{p_{i-1}}^{\ n+1}\right)}{\delta r_i}\right]-$$

$$(1-f)\left[A_{i-1/2}k_{tp_{i-1/2}}\frac{\left(T_{p_i}^{\ n}-T_{p_{i-1}}^{\ n}\right)}{\delta r_i}\right]+f\left[h_p A_i\left(T_i^{n+1}-T_{p_i}^{\ n+1}\right)\right]+(1-f)\left[h_p A_i\left(T_i^{n}-T_{p_i}^{\ n}\right)\right]$$

$$+f\left[\rho_a k_p A_i\left(X_i^{n+1}-X_{p_i}^{\ n+1}\right)h_{fg}^{n+1}\right]+(1-f)\left[\rho_a k_p A_i\left(X_i^{n}-X_{p_i}^{\ n}\right)h_{fg}^{n}\right]+$$

$$f\left[h_{pw}A_{pw}\left(T_w^{n+1}-T_{p_i}^{\ n+1}\right)\right]+(1-f)\left[h_{pw}A_{pw}\left(T_w^{n}-T_{p_i}^{\ n}\right)\right] \qquad (7.23)$$

7.2 Method of Solution

As was mentioned in the last chapter, the governing partial differential equations in fluidized bed drying are generally of two types. For the gas phases (bubble, interstitial gas) the equations are first-order hyperbolic partial differential equations, while for the solid phase the equations are second-order parabolic partial differential equation. The proper choice of solution method is very important due to dual nature of these equations. Moreover, the system of partial differential equations are coupled and non-linear, which required special attention to reach to the converged solution. Direct methods are not usually employed for nonlinear equations since they are not economical. The alternative, then, is iterative methods for the solution of discretized equations. Iterative methods usually require very small additional storage in the computer, and they are especially attractive for handling nonlinearities.

The gas flow field is divided into a finite number of control volumes after considering the bed expansion to account for the axial change in the gas properties. The solid phase is also divided into finite control volumes to account for variation inside the particles. (Control volumes inside the solid, are called grids to differentiate between the control volumes inside the bed, and prevent confusion).

The solution procedure starts with assuming arbitrary values for all dependent variables in the equations. Next the Gauss-Seidel iterative method is employed to solve the set of equations simultaneously for the first control volume of the bed, which is located at the bottom of the bed attached to the distributor plate. The iteration continues and successive repetition of the algorithm finally leads to a solution that is sufficiently close to the correct solution. After convergence, the moisture and temperature distributions in the solid as well as other parameters related to the gas flow (such as temperature and humidity of the bubble and interstitial gas, and bubble size and velocity) inside the first control volume can be specified. Then, the solution marches into the next control volume and again all the

properties of three phases are calculated for the condition of this control volume. The marching procedure continues until it reaches the last control volume.

In an aggregative fluidization state, the particles in the bed continuously mix due to the movement of bubbles. Since the mixing rate of particles is high, and the time scale of mixing could be as low as the gas residence time in the bed, an average moisture and temperature distribution of all solids in the bed can be assumed. Since the bed is divided into different control volumes and the conditions of the interstitial gas and bubble phases are different in each control volume as they proceed through the bed, therefore, the solids inside each control volume may have different moisture and temperature distribution. The moisture and temperature values of the same grids of solids at different control volume are averaged to obtain an expression for the average moisture and temperature distributions of the solids. This means that the fluidized bed was considered as a fixed bed during the numerical time step and accordingly the distributions of moisture and temperature of solids in each control volume in the bed are calculated and, subsequently averaged to obtain the moisture and temperature distributions of particles at that time step. It should be emphasized that this averaging is only with respect to the bed height (the axial direction of bed). After the averaging there are still moisture and temperature distributions inside the particle, but they are averaged of all the distribution of particles in the control volumes.

In simulation of fixed bed drying (deep bed drying) the averaging step is not required in axial direction since the particle positions are not mixing in the bed, and their positions are fixed. Therefore, there is a gradient of moisture content of solids along the bed for this type of drying which is not desirable.

After the average moisture distribution of solid was determined, the average value of the moisture in the solid at any time is calculated using Eq. (6.90).

7.3 Under-relaxation

In the case of solving nonlinear system of equations, it is often desirable to speed up or slow down the changes in the values of dependent variables from iteration to iteration before convergence to an acceptable level of accuracy is achieved. If the changes in the variable are accelerated, the process is called over-relaxation and if the changes in the variables are decelerated the process is called under-relaxation. The choice of using over-relaxation or under-relaxation is problem-dependent and is mostly determined by the nature and degree of nonlinearity of equations. Over-relaxation is useful when the direction of change in the solution is observed and it is anticipated that the same trend is valid for the following steps. So one may accelerate the solution by making an arbitrary correction to the intermediate values of the unknowns in the direction of change. In this way, less iterations are needed before achieving the final solution. Over-relaxation is usually appropriate for numerical solution to Laplace's equation with Drichlet boundary condition. Under-relaxation appears to be most appropriate when the convergence at a point is taken an oscillatory pattern and tends to "overshoot" the apparent final solution. Under-relaxation is a very useful device for nonlinear problems. It is often employed to avoid divergence or oscillation in the iterative solution of strongly nonlinear equations. In the course of this numerical work, it was found that for the drying equations the under-relaxation approach is necessary and should be used. Without employing under-relaxation approach the solution may not converge to the final point and may oscillate around both sides of the exact solution for a long time. This could be attributed to the highly nonlinear nature of the governing equation specially the sorption isotherm equation. Because of the strong nonlinear behaviour of the sorption isotherm equation, the solution should proceed with a small change to be able to capture the nonlinear pattern of the equation. Otherwise, the solution may overshoot and oscillate continuously with no convergence.

A question may arise here, how can we properly determine a good or even the best value for under-relaxation coefficient (ω)? There are no general rules for choosing the best value of under-relaxation coefficient (ω) but some guidelines can be given.

In the moderate temperature drying the under-relaxation coefficient close to one is adequate for getting the convergence but as the temperature of drying medium rises, the under-relaxation coefficient must decrease. It should be noticed that even though the under-relaxation coefficient helps to converge to the solution, it also increases the time of computation and more iterations are required to reach to final solution. So it is not recommended to use too small a value of ω and in any case it is better to use the maximum acceptable value of ω_{opt} to reduce to the computation time. Usually some numerical experimentation is required to find ω_{opt} for any specific case.

CHAPTER 8

Numerical Solutions and Comparison with Experimental Results

8.1 Introduction

In order to assess the validity of the mathematical model and test its accuracy, the results of numerical solutions are compared with experimental data for wheat and corn grains. Wheat and corn are among the main commodities of agricultural products and have extensive application in drying systems and therefore the accuracy of results for these two products are of primary concern. Furthermore, as the desorption isotherms of these materials are well documented, it is possible to accurately simulate the drying processes. Both wheat and corn are hygroscopic materials with very low diffusivity. However, the nature of the moisture diffusivity and the size of material are very different. Moisture diffusivity of wheat is dependent only on temperature but for corn it is a function of both temperature and moisture content of particles. The other difference is in the size of kernels. The size of the corn kernels is usually many times larger than that of wheat kernels. These differences may cause a different pattern of drying for these particles. Usually, no constant rate period is observed in the course of drying of these materials in the moderate range of initial moisture content, and their drying take place in the falling rate mode. This means that immediately after these particles are exposed to the drying medium, the surface moisture of the material will be removed rapidly due to low external resistance for heat and mass transfer. But later on, the moisture removal will decrease noticeably with time because the inner moisture will face the internal resistance and diffuse gradually to the surface. This scenario suggests that for these types of materials the initial drying rate would be high (due to removal of moisture surface) but then it would diminish rapidly after the removal of the moisture surface.

8.2 Assumptions

In developing the mathematical model, attempts have been made to avoid using simplifying assumptions so that a more accurate and general model can be used to analyze

real industrial drying configurations. Although this approach makes the mathematical model more complex, it provides a powerful model that can be used to evaluate the effect of different parameters without making expensive and repetitive experimentation. Fortunately the development of efficient, accurate and stable numerical techniques, together with the increasing power of modern computing systems readily available at relatively low costs, make it possible to apply this type of complicated model for design and research purposes in drying systems. However, in spite of this effort, there are many areas that still need to use simplifying assumptions. Those are mostly because of the lack of experimental data to use for modeling purposes, or lack of their importance in the drying process. Each of these assumptions can, to a greater or lesser degree, be justified experimentally. The following assumptions were made in the development of the model and numerical solution.

1. All particles within the bed are uniform in size with a sphericity close to unity that can be approximated as a sphere,
2. The particles are isotropic,
3. There is no shrinkage of particles during drying,
4. Moisture movement inside the particle takes place in the liquid phase.

8.3 Comparison of Model and Experimental Results for Wheat Particles

8.3.1 General Agreement

Drying tests were carried out on the wheat particles to obtain complete and reliable experimental results for comparison with the results of mathematical model. Different types of data are collected during each experiment run. These are: temperature at different bed heights, humidity of outlet air, bed pressure drop, air velocity, and moisture content of material at different times. These data compare reasonably well with the results of the mathematical model. In the following, the results are compared for two different

temperatures namely 49.5 °C and 65.0 °C to show the degree of agreement between the model and experimental data. For all practical purposes, the most important aspect of the drying result is the agreement of moisture content between prediction and experimental data. However, other parameters are also very useful for understanding the nature of drying and its physiochemical properties.

8.3.1.1 Comparison of Results at T=49.5 °C

Figures 8.1 presents a comparison of the model prediction for the moisture content evolution with the experimental results for the inlet air temperature of 49.5 °C. As can be seen from the figure, a very good match was observed between the experimental and theoretical results.

Figure 8.2 compares the variation of drying rate versus time for model prediction and experimental results. The drying rate is very high at the initial stage due to rapid evaporation of surface moisture. But it decreases exponentially when all the surface moistures evaporate and the drying front diffuses inside the particle. Usually, surface moisture evaporates very fast due to high heat and mass transfer coefficient in fluidized bed systems. A constant rate drying period is not seen for the given condition.

Figure 8.3 presents the variation of drying rate in terms of moisture content of particles. Model prediction is in good agreement with experimental results except for the initial stage of drying. This can be explained by the fact that the high drying rate at the initial stage is very short lived and its detection by experimental devices is difficult.

Figure 8.4 compares relative humidity of air at the exit of the bed. As seen in the figure, after the initial stage of drying, the variation of exit humidity is very small. At the initial stage of drying, a difference between experimental and numerical results is obvious. This may be attributed to the initial response time of humidity transducer. Before the start of the test, the value of humidity is very low (equal to the inlet relative humidity) it then

undergoes through a fast change, so the transducer may not have enough time to respond quickly to these changes. Furthermore, the existence of a filter on the transducer probe which prevents from contacting particles with the tip of the probe, makes the response time even longer.

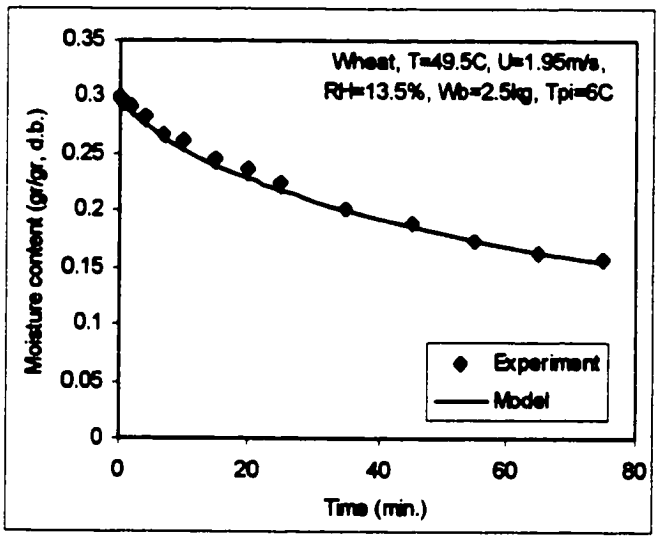

Figure 8.1 Comparison between experimental data and model predictions for moisture content vs. time.

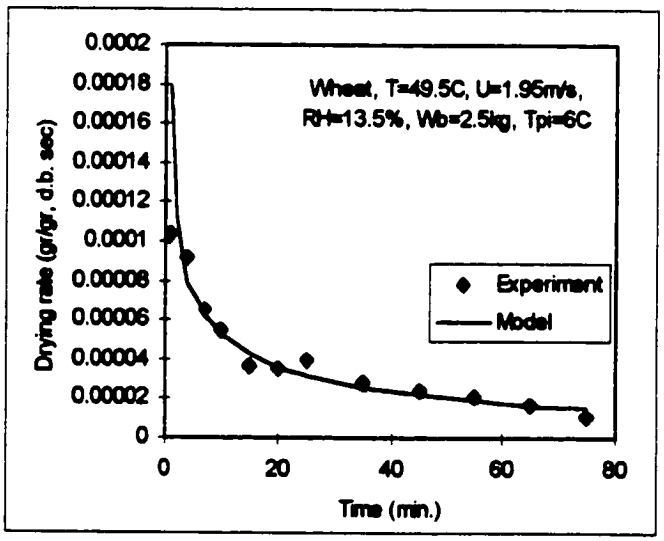

Figure 8.2 Comparison between experimental data and model predictions for drying rate vs. time

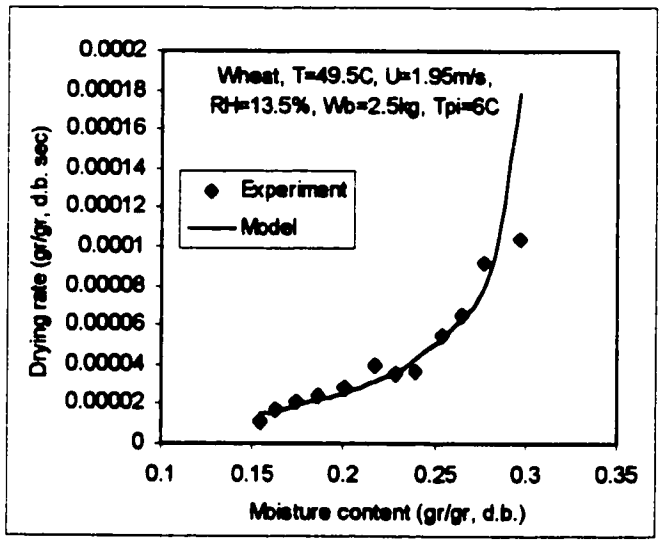

Figure 8.3 Comparison between experimental data and model predictions for drying rate vs. moisture content.

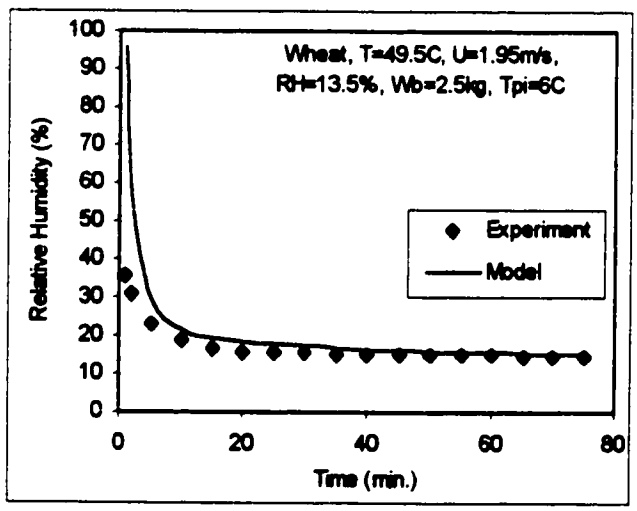

Figure 8.4 Comparison between experimental data and model predictions for relative humidity of exit air vs. time.

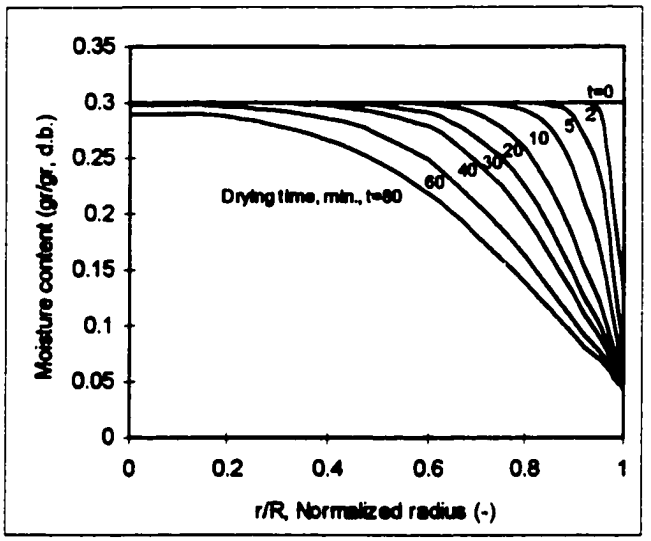

Figure 8.5 Predicted moisture distribution profiles inside the wheat kernel.

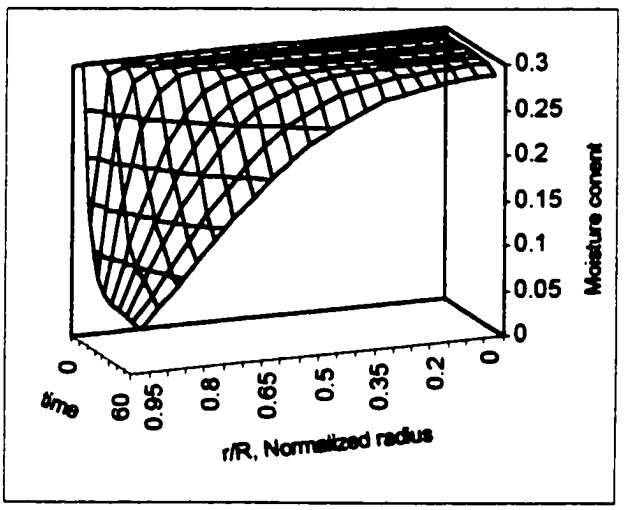

Figure 8.6 Predicted moisture distribution profiles inside a wheat kernel vs. time.

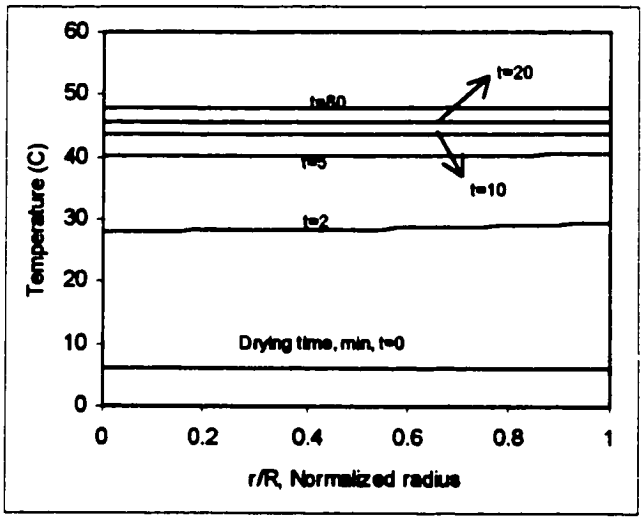

Figure 8.7 Predicted temperature distribution profiles inside the wheat kernel.

Figures 8.5 shows the model prediction of average moisture content distribution of particles inside the bed. The moisture content shows a significant concentration gradient inside the particle which is an indication of high mass transfer Biot number for the wheat. This also means that the limiting mechanism of heat and mass transfer is primarily of an internal nature.

Figure 8.6 presents the moisture distribution inside the particle at different times of drying. This graph helps to better understand the gradient of moisture distribution as time elapses. As it is clear in the graph, the moisture at the surface of particle initially decreases very fast and then undergoes a more gradual variation.

Figures 8.7 shows the model prediction of average temperature distribution of particles inside the bed. Contrary to the moisture distribution, the temperature profile is quite flat which is an indication of low heat transfer Biot number for the wheat. No attempt was made to measure these distributions experimentally since the result would not be reliable

due to the interaction of the measuring device on the wheat properties during the measurement.

Figures 8.8 shows the temperature-time profile at a bed height of 2 cm (H=2cm). Initially, the temperature gradient is very high, but as time passes its variation becomes very small. The experimental results show good agreement with the numerical results. This agreement is very important since, as it will be shown later, the temperature has a significant effect on the drying rate and any important discrepancy in temperature comparison between model and experiment may indirectly indicate an error in the moisture content prediction. Figure 8.9 shows the temperature-time profile at the exit of bed and also on the surface of the particles. The agreement between model prediction and experimental results is clear. The air temperature at the exit is very close to the particle surface temperature. Figure 8.10, shows temperature distribution inside the bed at different times. At the beginning of drying, the gradient of temperature is important, and after a while the temperature distribution in the bed becomes nearly uniform. Since in the initial stage the drying rate is very high, it is important to take into account the temperature gradient inside the bed for accurate modeling of the drying process.

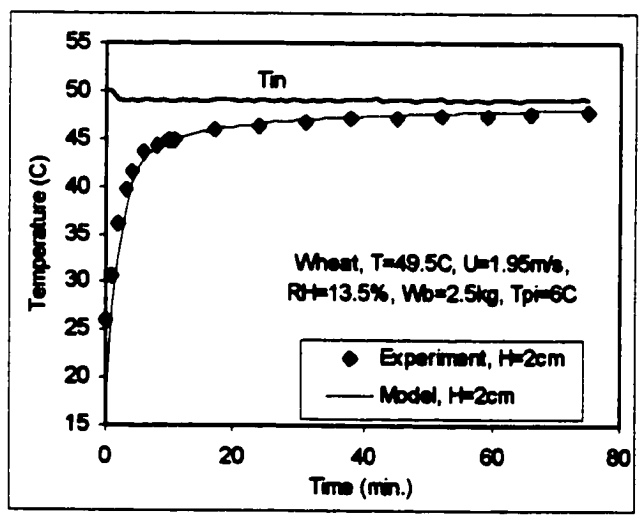

Figure 8.8 Comparison between experimental data and model prediction for gas temperature at H= 2 cm.

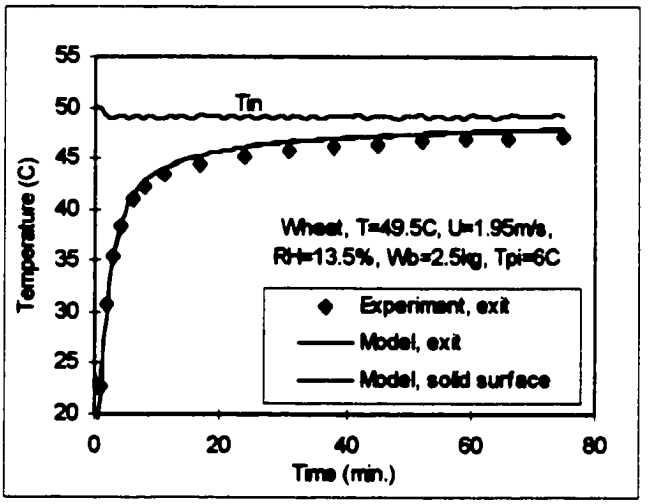

Figure 8.9 Comparison between experimental data and model predictions of exit gas temperature.

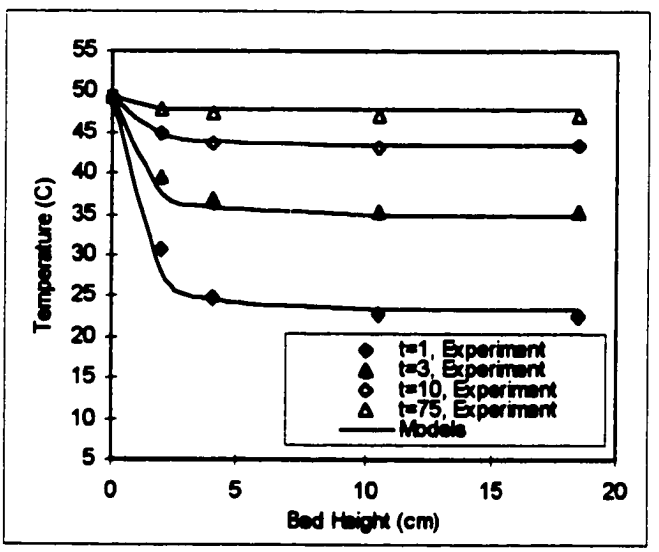

Figure 8.10 Comparison between model predictions and experimental data for gas temperatures as a function of bed height at different times.

8.3.1.2 Comparison of Results at T=65 °C

The comparison of data are shown for an inlet air temperature at 65.0 °C. This temperature is somewhat higher than the last run (49.5 °C) and can evaluate the reliability of model prediction in a more critical environment. Temperature has an important effect on the drying rate of any type of material and therefore any deficiency of the mathematical model can be better evaluated at higher temperature tests. However, there is some restriction on the limit of temperature for drying of grains due to possible damage to the quality of grain and its physical properties. It is generally accepted that a grain temperatures higher than 65 °C leads to considerable damage on the germination capacity and quality of grain (Giner and Calvelo, 1987). Also, other effects like drying-induced stress and cracking may deteriorate the physical quality of grain.

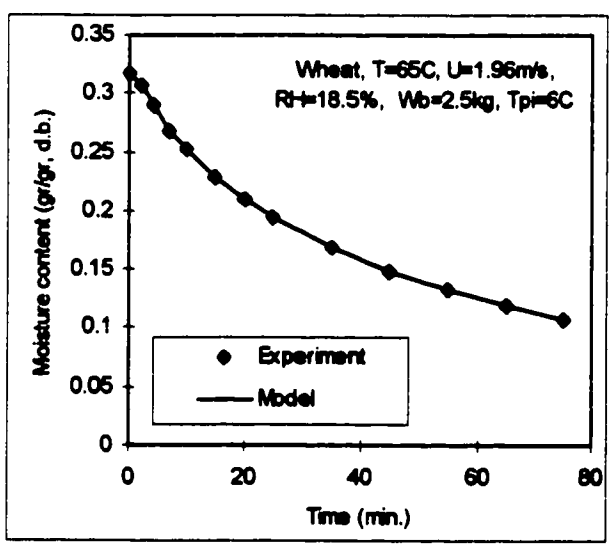

Figure 8.11 Comparison between experimental data and model predictions for moisture content vs. time.

The general trends of data for the test at T=65.0 °C are the same as test at T=49.5 °C, except that for the former, the drying rate is higher and drying time is considerably shorter. A comparison of model predictions and experimental results in the following figures

shows that the agreement is very good and the mathematical model can predict the behaviour of the drying process successfully.

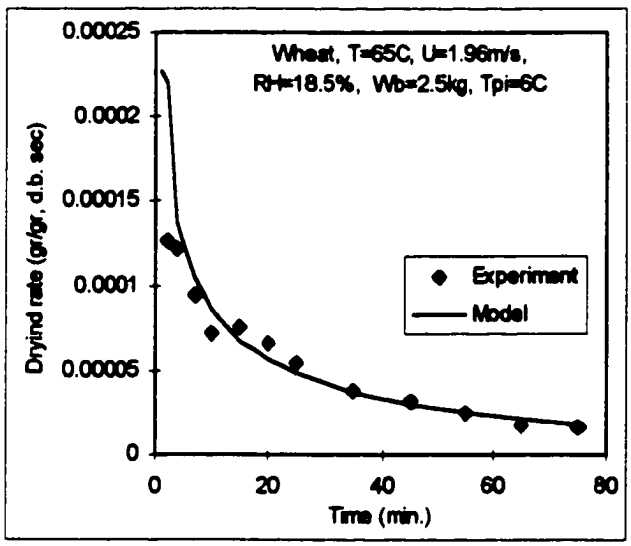

Figure 8.12 Comparison between experimental data and model predictions for drying rate vs. time.

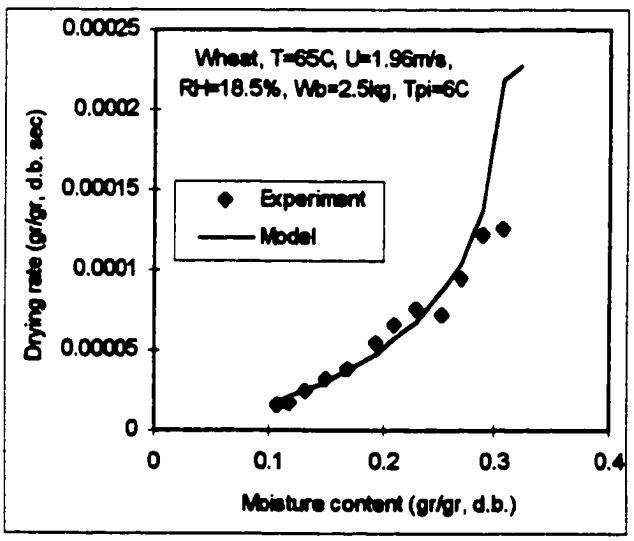

Figure 8.13 Comparison between experiment and model predictions for drying rate vs. moisture content.

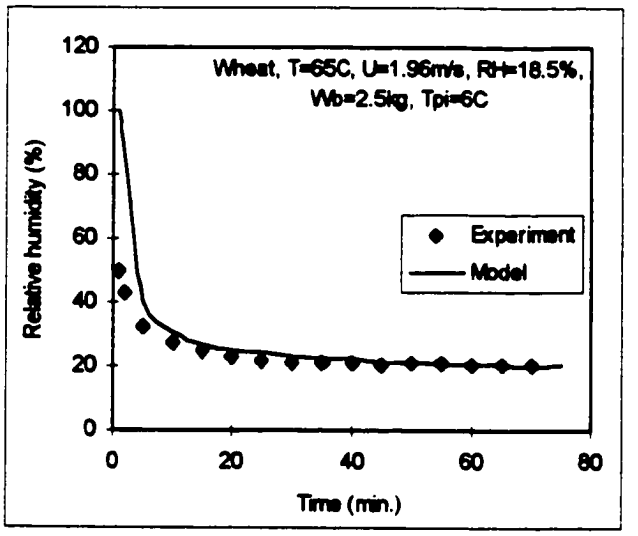

Figure 8. 14 Comparison between experiment and model predictions for relative humidity of exit air vs. time.

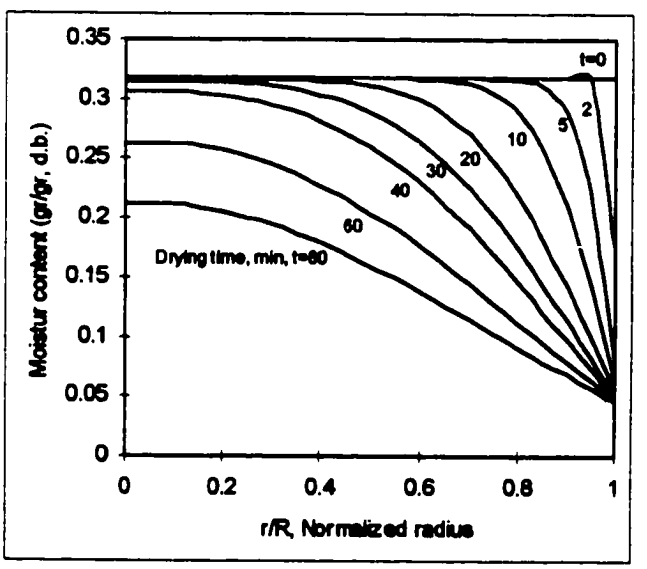

Figure 8.15 Predicted moisture distribution profiles inside the wheat kernel.

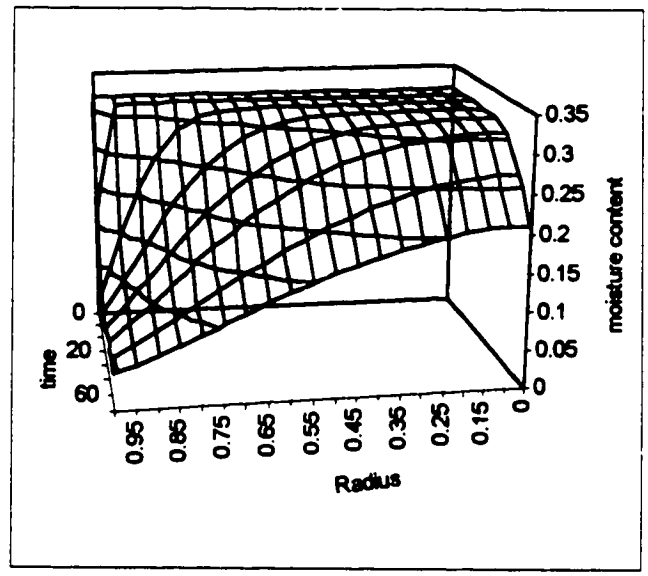

Figure 8.16 Predicted moisture distribution profiles inside the wheat kernel vs. time.

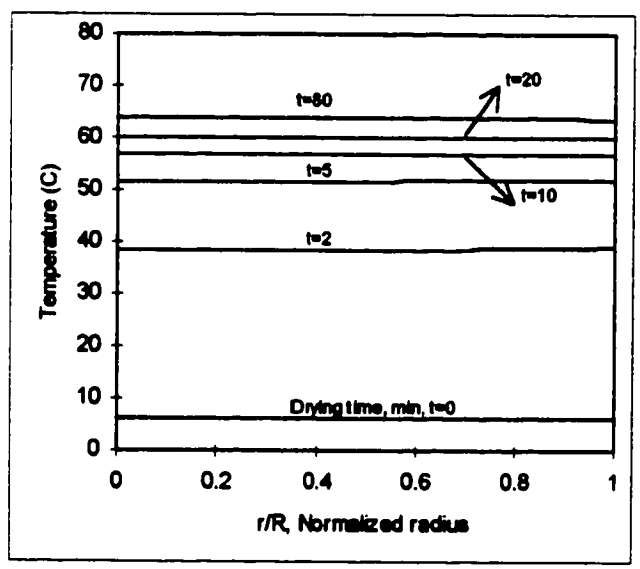

Figure 8.17 Predicted temperature distribution profiles inside the wheat kernel.

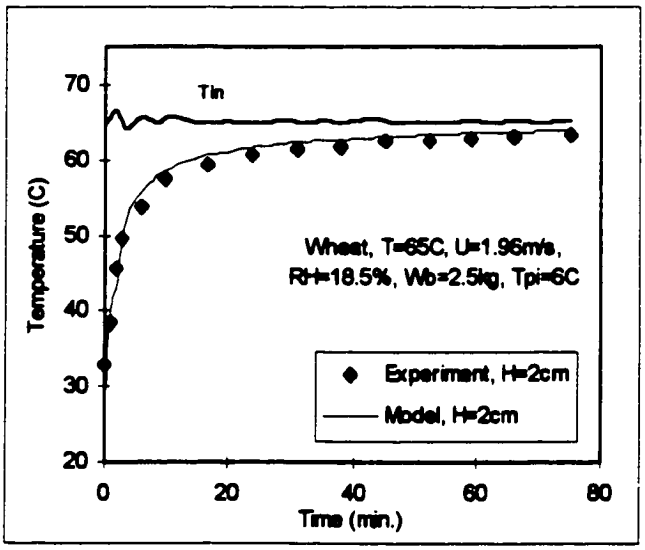

Figure 8.18 Comparison between experimental data and model prediction for gas temperature at H=2 cm.

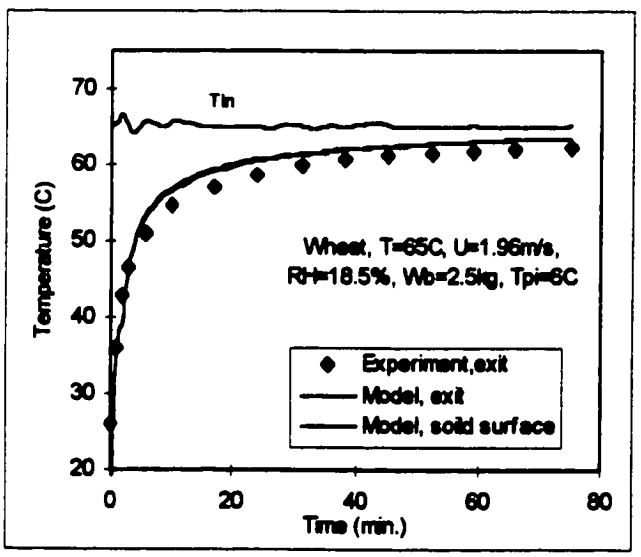

Figure 8.19 Comparison between experimental data and model predictions for gas temperature at exit.

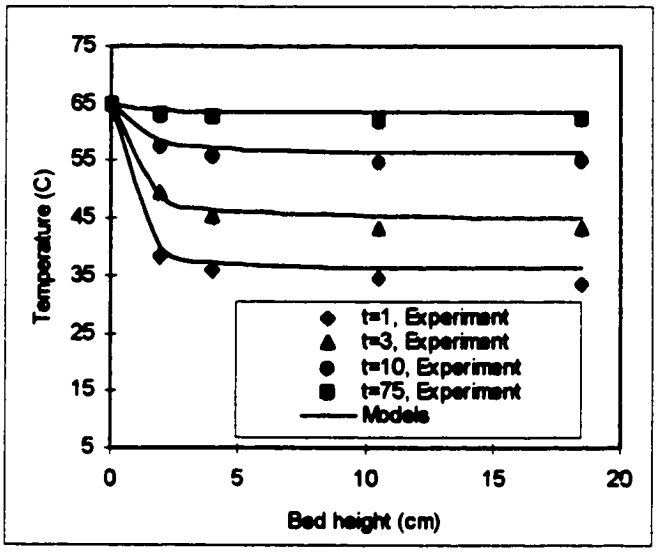

Figure 8.20 Comparison between model predictions and experimental data for gas temperature as a function of bed height at different time.

8.3.2 Effect of Temperature

In order to compare and analyze the effect of independent variables on the drying rate and also to evaluate the degree of accuracy of model prediction at different conditions, tests were performed with changing one variable and keeping the other variables constant. Figure 8.21 presents the effect of air temperatures on the moisture content of particles versus time. Since the initial moisture contents of particles are different, the normalized moisture content can provide a more meaningful way for comparison of the results. Therefore, it is used for analyzing the data. Conditions of inlet air and particles for each test are given in Table 8.1. It can be seen from Fig. 8.21, that the temperature of the drying medium (air) significantly influences the drying curve of particles. Increasing the temperature, effectively reduces the moisture content of particles for the same period of drying time. Figure 8.22 shows the variation of drying rates in terms of time for different temperatures. A clear difference is observed between the drying rate curves at different

temperatures. These differences at the initial stage of drying are higher than at the final stage. Figure 8.23 shows the variation of drying rate in terms of normalized moisture content. Since the initial moisture content of grain used in the tests at different air conditions are different (Table 8.1) comparison of drying rate in terms of absolute moisture content may be misleading. The results clearly display the differences between drying rates and the extent of temperature on the drying rate.

Table 8.1 Experimental conditions for investigating the effect of temperature.

	T (°C)	M_{pi} (d.b.)	W_b (kg)	RH (%)	U (m/sec)	T_a (°C)	T_{pi} (°C)
Run 8	40.5	0.326	2.50	21.1	1.95	22.0	7.0
Run 6	49.5	0.300	2.50	13.5	1.95	18.0	6.0
Run 11	65.0	0.317	2.50	18.5	1.96	22.0	6.0

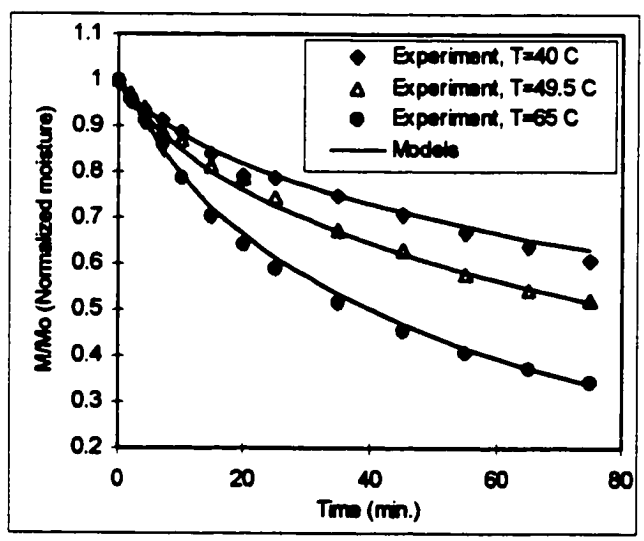

Figure 8.21 Effect of inlet air temperature on drying and comparison between experimental and numerical results for wheat.

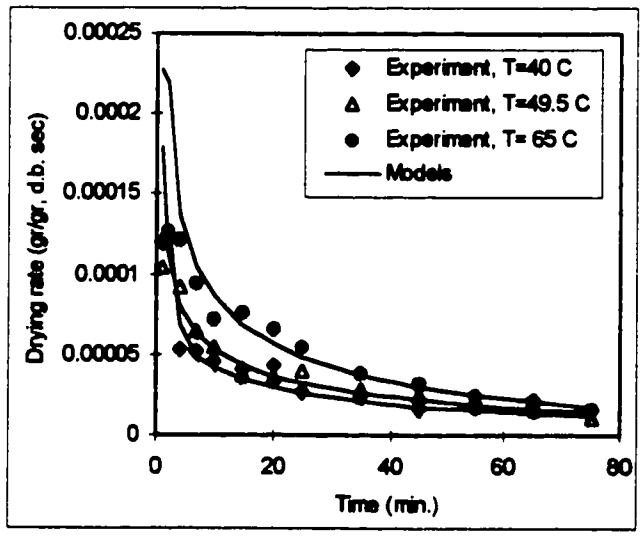

Figure 8.22 Effect of inlet air temperature on drying rate and comparison between experimental and numerical results for wheat.

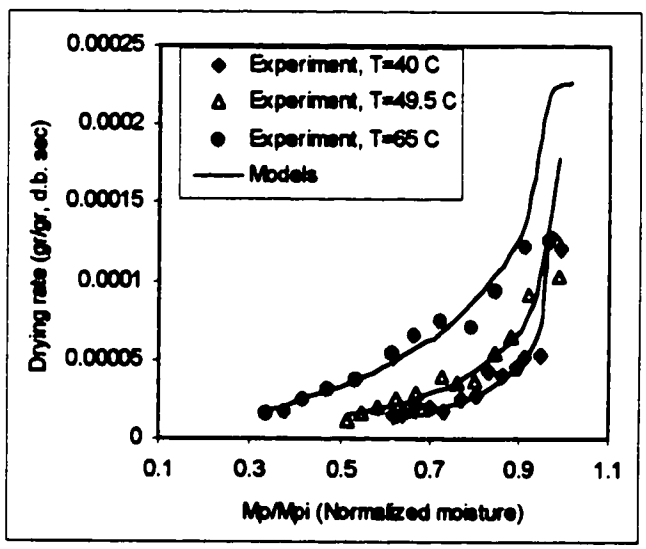

Figure 8.23 Effect of inlet air temperature on drying rate and comparison between experimental and numerical results for wheat.

8.3.3 Effect of Bed Hold up

Figures 8.24 and 8.25 show the effect of bed hold up on the variation of moisture content of particles, and the drying rate, respectively. The test conditions are given in Table 8.2. As can be seen, although the content of bed material increased by a factor of two, its effect on drying rate is seen to be relatively small. The drying rate of particles increase slightly as the bed hold up decreased. This means that one can use as much material as possible in the bed for drying without a significant reduction in the drying rate. However, there are practical restrictions for the amount of maximum bed material due to the slugging phenomenon in the fluidized bed. When the hold up of bed increases, the bed height also increases and for an aspect ratio more than one the bed behaviour gradually change from the bubbling mode to the slugging mode. This is the case for group "D" particles, but for other groups the bed can reach a higher value of aspect ratio without showing any slugging effect. DiMattia [1992] found that slugging has little effect on the drying rate of group "D" particles so one still can use this mode of fluidization in the drying if other side effects of this phenomenon could be neglected.

Figure 8.26 shows the variation of drying rate in terms of moisture content of particles. Since the initial moisture contents of particles are close to each others (Table 8.2), the absolute moisture content is used for presenting the results in this figure. This figure also shows the effect of bed hold up on the drying rate of wheat particles is negligible.

Table 8.2 Experimental conditions for investigating on the effect of bed hold up.

	T (°C)	M_{pi} (d.b.)	W_b (kg)	RH (%)	U (m/sec)	T_a (°C)	T_{pi} (°C)
Run 6	49.5	0.300	2.50	13.5	1.95	18.0	6.0
Run 13	49.5	0.311	1.25	17.3	2.00	19.5	6.0

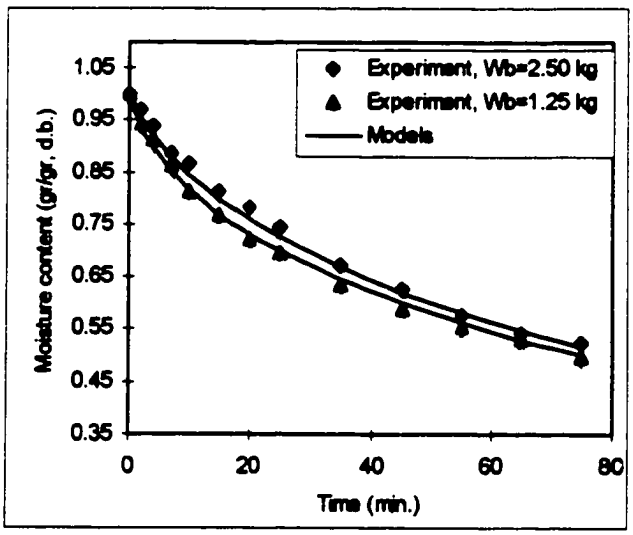

Figure 8.24 Effect of bed hold up on drying and comparison between experimental and numerical results for wheat.

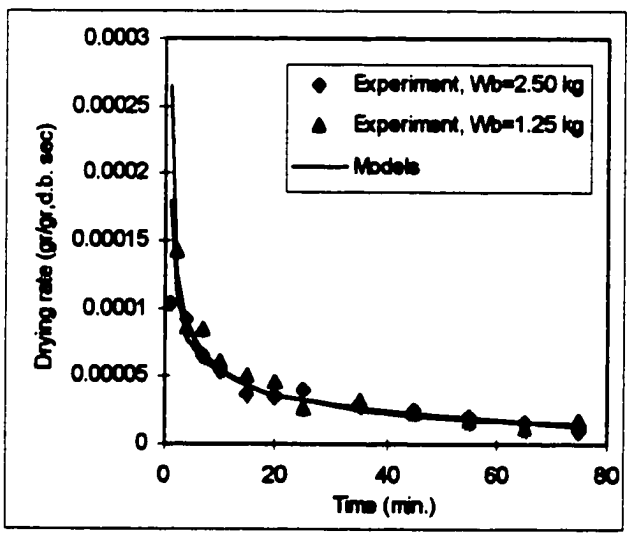

Figure 8.25 Effect of bed hold up on drying rate and comparison between experimental and numerical results for wheat.

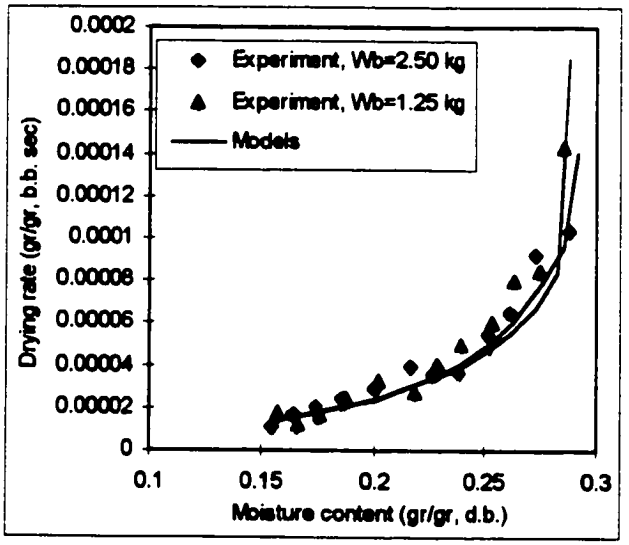

Figure 8.26 Effect of bed hold up on drying rate and comparison between experimental and numerical results for wheat.

8.3.4 Effect of Gas Velocity

Figures 8.27 through 8.29 show the effect of gas velocity on the drying process, and compare the experimental results with model predictions. The test conditions are listed in the Table 8.3. For a reduction of about 15% in the air velocity, the changes in the drying properties are hardly distinguishable. The most significant effect take place at the very initial stage of drying, when the surface moisture content is being removed from the grains. After that, the effect of velocity is not important. The reason for the narrow difference in velocities between the two tests conditions can be related to the problem with fluidization of wet particles in the initial stage of drying. Since wet particles fluidization needs higher gas velocity, it was not possible to reduce the velocity very much.

Table 8.3 Experimental conditions for investigating the effect of velocity.

	T (°C)	M_{pi} (d.b.)	W_b (kg)	RH (%)	U(m/sec)	T_a (°C)	T_{pi} (°C)
Run 6	49.5	0.300	2.50	13.5	1.95	18.0	6.0
Run 12	50.0	0.323	2.50	15.7	1.63	23.0	6.0

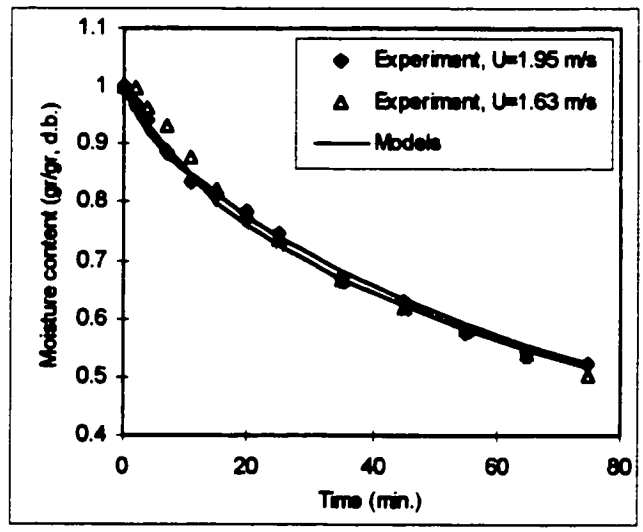

Figure 27 Effect of gas velocity on drying and comparison between experimental and numerical results for wheat.

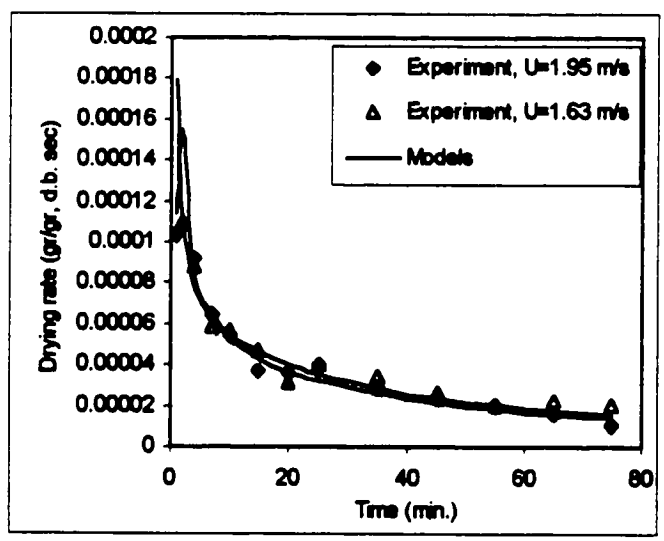

Figure 8.28 Effect of gas velocity on drying rate and comparison between experimental and numerical results for wheat.

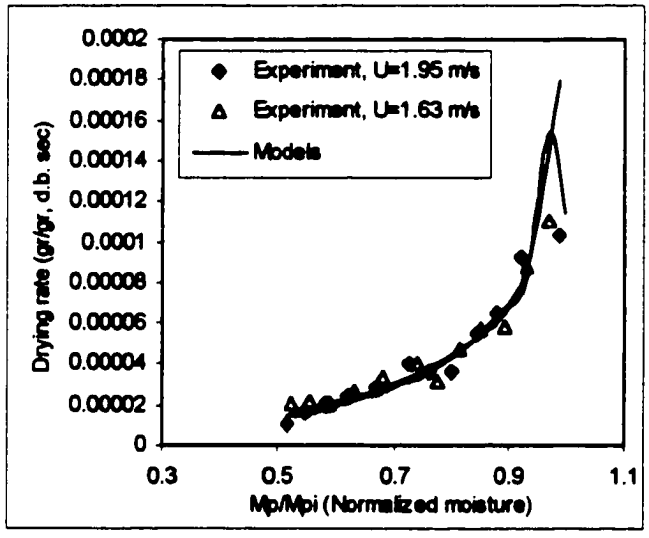

Figure 8.29 Effect of gas velocity on drying rate and comparison between experimental and numerical results for wheat.

8.3.5 Effect of Initial Moisture Content

Figures 8.30 shows the effect of initial moisture content on the drying curve and compare the experimental results with model predictions. In order to show the different trends of drying, both normalized and absolute moisture content curves are presented in the graph. The test conditions are listed in the Table 8.4. The figure shows that although the absolute moisture content curves are apart from each other, the normalized moisture content does not show any significant difference between two curves. One possible reason could be the lack of dependence of diffusion coefficient on moisture content for wheat particles. Figure 8.31 shows the effect of initial moisture content on the drying rate. Increasing the moisture content cause a time lag on the maximum drying rate in the initial stage of drying. Therefore, the start up period and initial rising of the drying rate can be seen in the graph. Absolute drying rate shows higher value for particles with high moisture content which is mostly due to the time lag of drying rate. Figures 8.32 and 8.33 show the

variation of drying rate versus moisture content in two forms, first absolute moisture content, and secondly normalized moisture content. As it is clear from comparison of two curves, in the absolute form the drying rate for low moisture content seems to be higher, but in the normalized form the trend is converse and drying rate is higher for particles with higher moisture content. This difference indicate that if the initial moisture content of particles are different, the best way for comparison is using the normalized moisture content.

Table 8.4 Experimental conditions for investigating the effect of initial moisture content.

	T (°C)	M_{pi} (d.b.)	W_b (kg)	RH (%)	U (m/sec)	T_a (°C)	T_{pi} (°C)
Run 2	54.5	0.409	2.54	17.0	1.91	20.5	7.0
Run 4	54.0	0.307	2.48	14.7	1.93	20.0	7.0

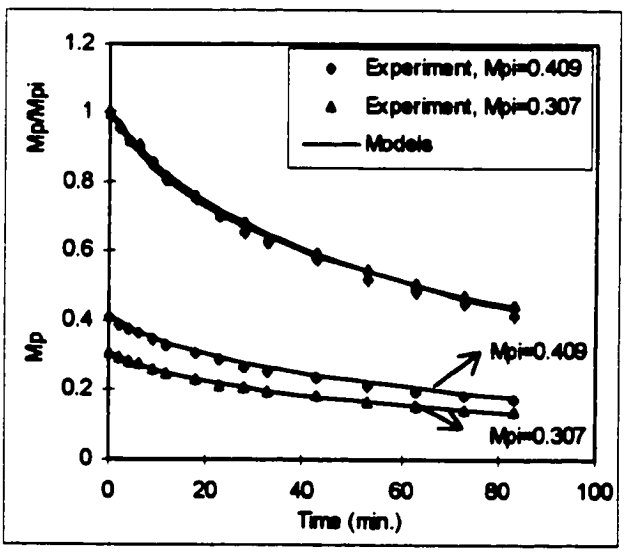

Figure 8.30 Effect of initial moisture content on drying and comparison between experimental and numerical results for wheat (top curves are normalized and bottom curves are actual moisture content)

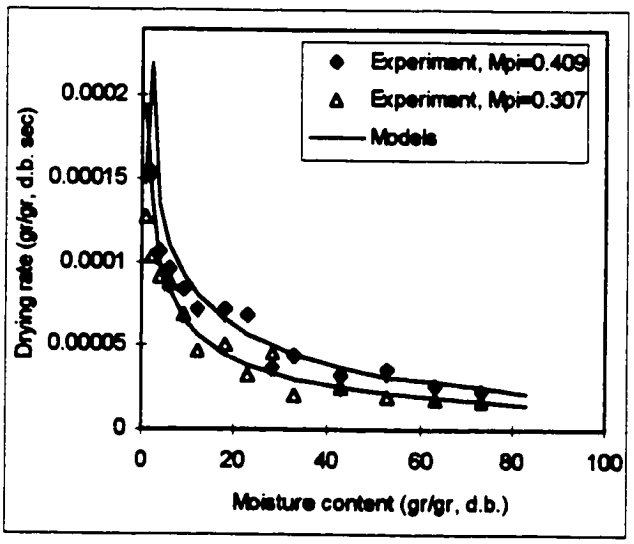

Figure 8.31 Effect of initial moisture content on drying rate and comparison between experimental and numerical results for wheat.

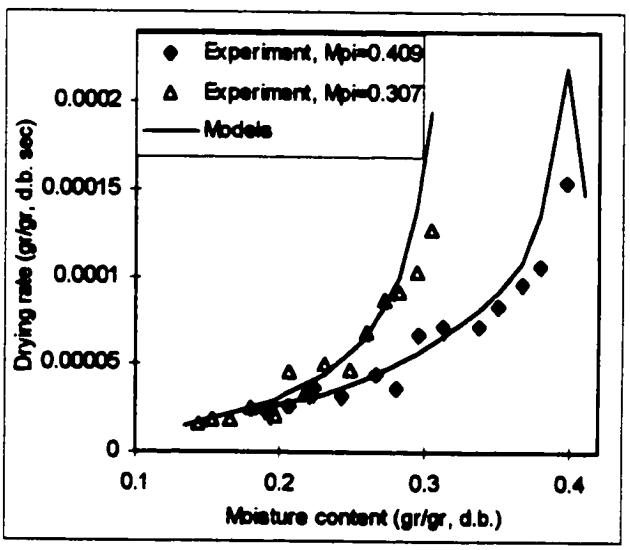

Figure 8.32 Effect of initial moisture content on drying rate and comparison between experimental and numerical results for wheat.

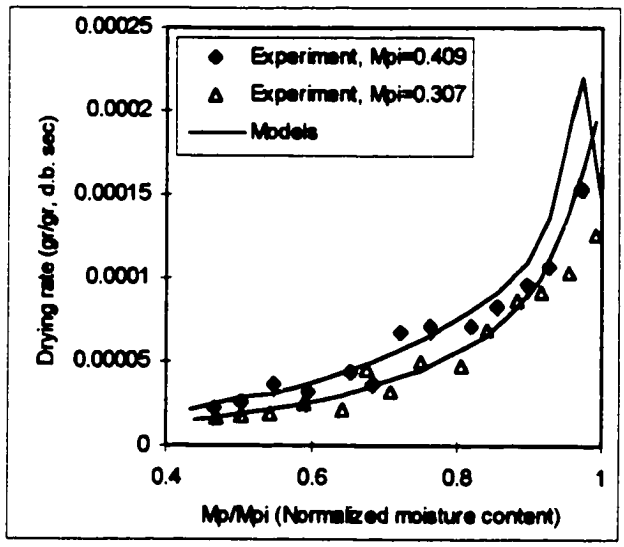

Figure 8.33 Effect of initial moisture content on drying rate and comparison between experimental and numerical results for wheat.

8.4 Comparison of Model and Experimental Results for Corn Particles

8.4.1 General Agreement

As a second particle, corn was used to compare the model predictions with the experimental results and evaluate the accuracy of the model. Corn grains are usually many times bigger than wheat grains and their mass diffusivity, unlike the wheat particles, depends on moisture content. Since the mass diffusion is controlling the rate of drying process, it is possible that corn will have a different pattern in the drying process. Another change, that is required in the numerical implementation of the model for corn particles, is about the number of grids. Because the diameter of corn grains is larger, the number of grids used in the solution must be larger than that of the case for wheat particles. The number of grids used for corn particles is 40 compared to 20 for wheat particles.

In the following, model and experimental results are presented for the inlet temperature of air at 50.0 °C to display the degree of agreement between them. Figure 8.34 indicates the variation of the average moisture content versus time. The predicted moisture content and experimental data are in good agreement. Similar to the results obtained for wheat particles, the constant drying rate is not realized in the drying curve. This could be better observed from Fig. 8.35, which shows the variation of drying rate. It can be seen that at the initial stage, the drying rate is very high due to fast evaporation of surface moisture, but then it decreases exponentially when the surface moistures evaporates and drying front diffuses inside the kernel. This trend can also be seen in Fig. 8.36, which presents the variation of drying rate in terms of moisture content of particles. Figures 8.37 through 8.43 show different experimental results versus model predictions. Examination of these results shows that reasonable agreement between model predictions and experimental results is obtained.

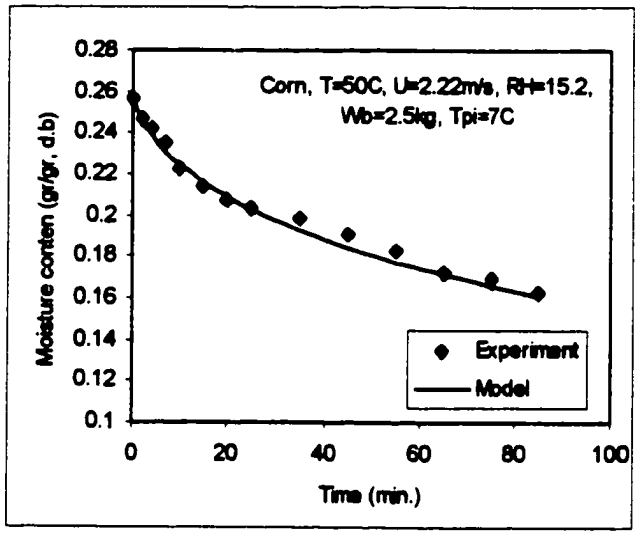

Figure 8.34 Comparison between experimental data and model predictions for moisture content vs. time.

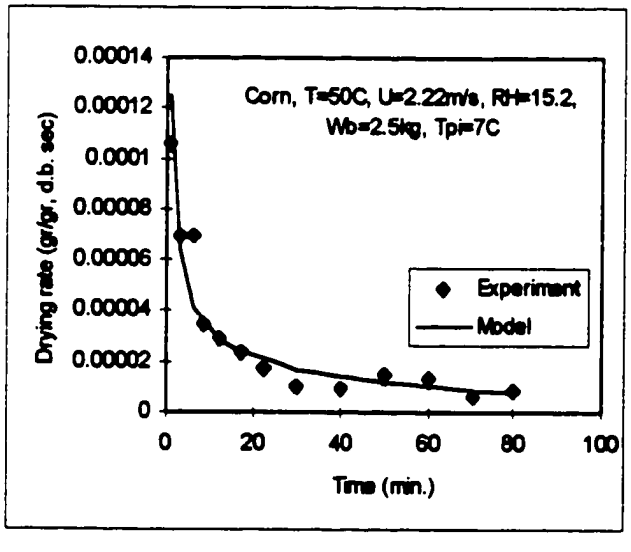

Figure 8.35 Comparison between experimental data and model predictions for moisture content vs. time

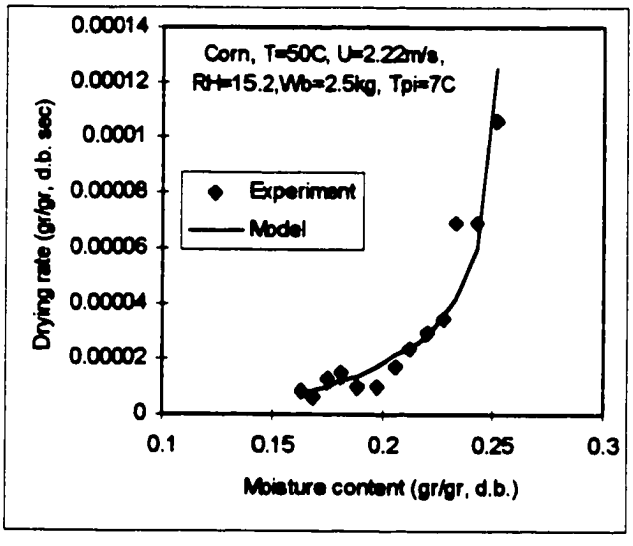

Figure 8.36 Comparison between experimental data and model predictions for drying rate vs. moisture content.

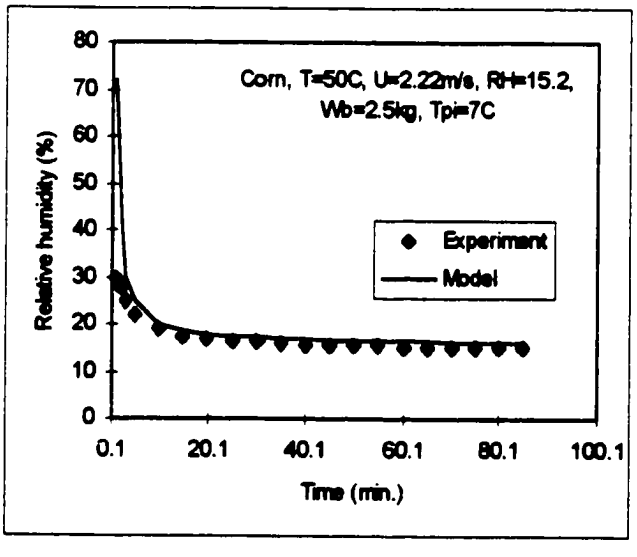

Figure 8.37 Comparison between experimental data and model predictions for relative humidity of exit air vs. time.

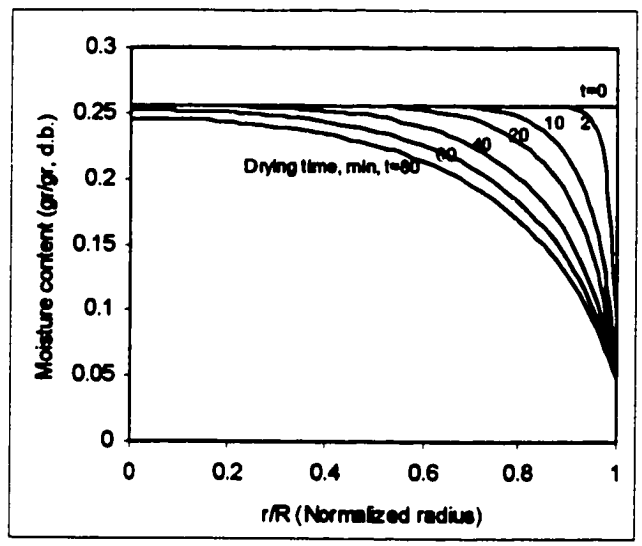

Figure 8.38 Predicted moisture distribution profiles inside the corn kernel.

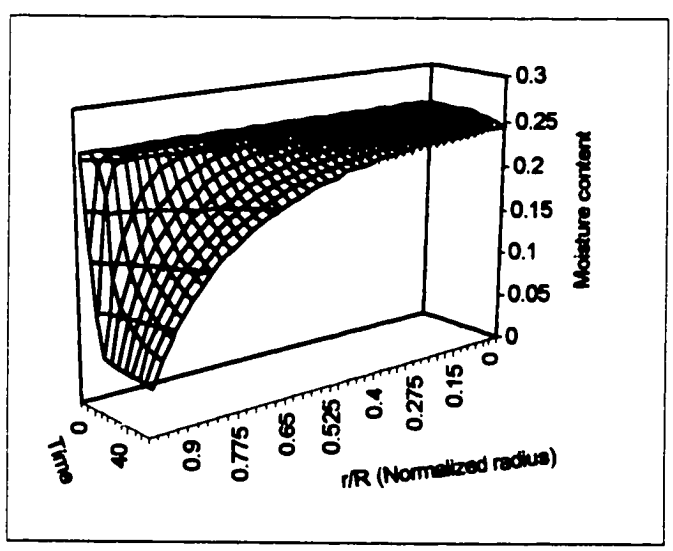

Figure 8.39 Predicted moisture distribution profiles inside the corn kernel vs. time.

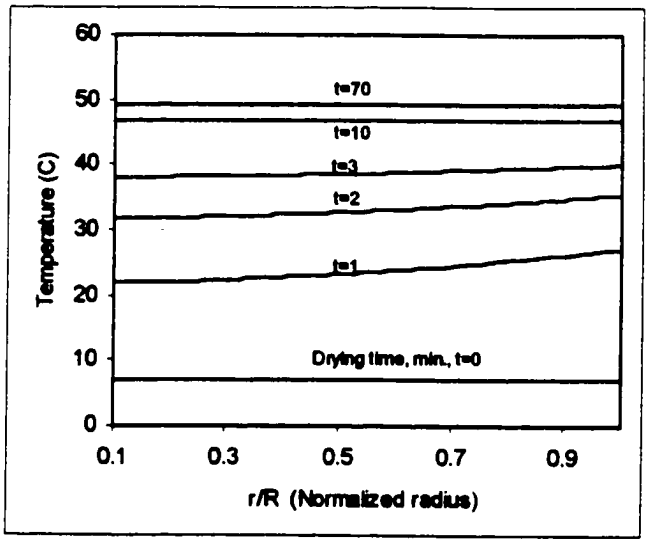

Figure 8.40 Predicted temperature distribution profiles inside the wheat kernel.

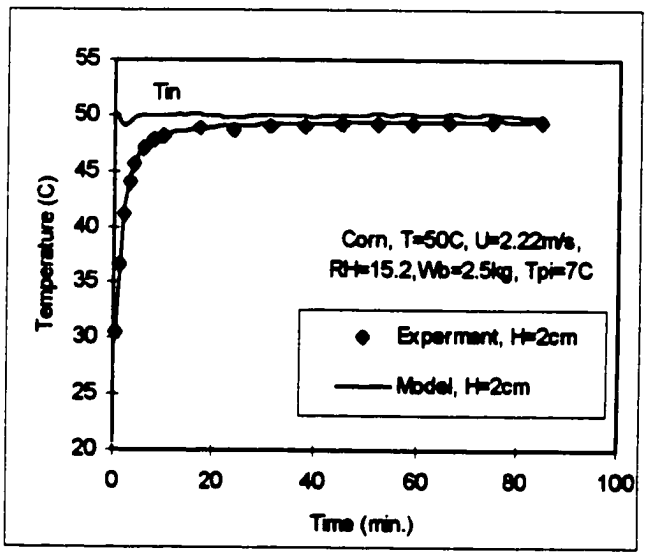

Figure 8.41 Comparison between experimental data and model prediction for gas temperature at H=2 cm.

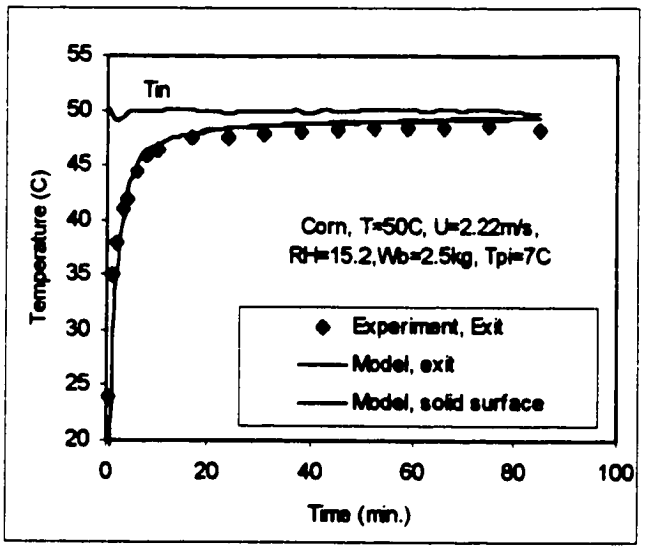

Figure 8.42 Comparison between experimental data and model predictions of exit gas temperature.

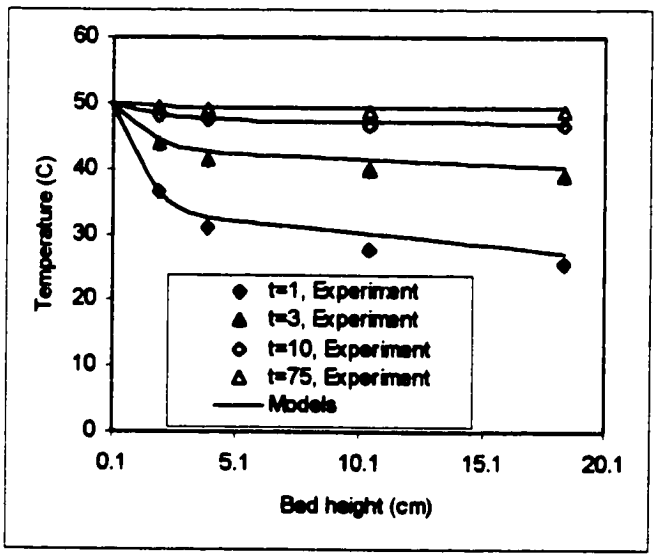

Figure 8.43 Comparison between model predictions and experimental data for gas temperature s a function of bed height at different time.

Table 8.5 Experimental conditions for investigating the effect of temperature.

	T (°C)	M_{pi} (d.b.)	W_b (kg)	RH (%)	U (m/sec)	T_a (°C)	T_{pi} (°C)
Run C1	50.0	0.256	2.50	15.2	2.22	17.0	7.0
Run C3	63.0	0.246	2.5	17.5	2.24	17.5	7.0

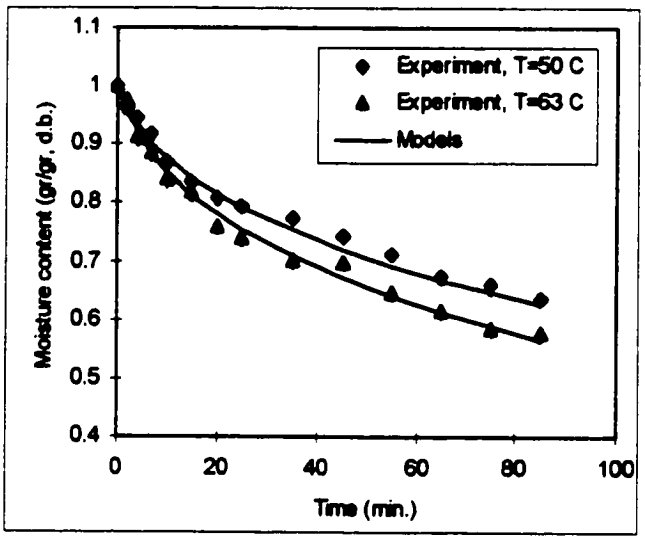

Figure 8.44 Effect of inlet air temperature on drying and comparison between experimental and numerical results for corn.

8.4.2 Effect of Temperature

Figures 8.44 through 8.46 show the effect of temperature on the drying characteristics of corn grains, and compare experimental results with model predictions. The test conditions are listed in Table 8.5. It can be seen that temperature has an important effect on the drying time. These figures clearly indicate that increasing the air temperature decreases the moisture content considerably and the time required to reach a specific moisture content reduces substantially. Also, for high temperature tests the drying rate at the initial stage is higher than the low temperature test, but the difference between the two curves decreases quickly as the moisture content of particles decreases and surface moisture is removed.

The only problem for using very high temperature drying is its side effect on the quality of grain. Fast drying of grain may create thermal stresses and damage to the physical properties of grain.

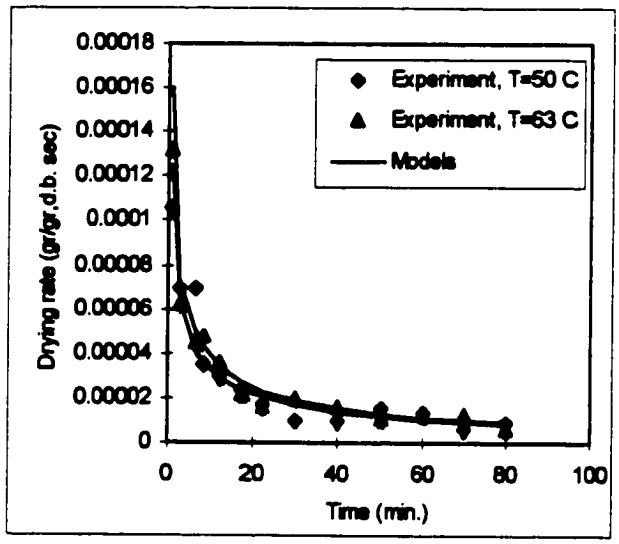

Figure 8.45 Effect of inlet air temperature on drying rate and comparison between experimental and numerical results for corn.

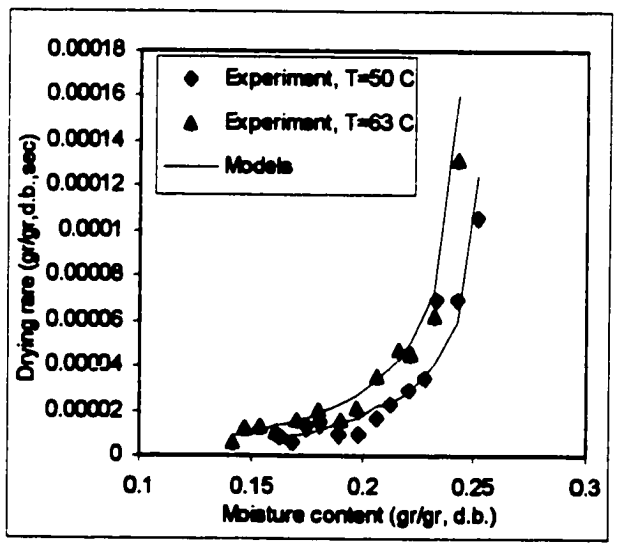

Figure 8.46 Effect of inlet air temperature on drying rate and comparison between experimental and numerical results for corn.

8.4.3 Effect of Bed Hold Up

Figures 8.47 through 8.49 show the effect of bed hold up on the drying process and compare the experimental results with model predictions. The test conditions are listed in Table 8.6. The bed hold up shows little effect on the drying process for corn particles which was also observed for the wheat particle. This means that one can use as much as material in the bed for drying and increase the efficiency of process. However, the restricting parameter in increasing the bed material is the slugging phenomenon which already was discussed for the wheat particle case.

Table 8.6 Experimental conditions for investigating the effect of bed hold up.

	T (°C)	M_{pi} (d.b.)	W_b (kg)	RH (%)	U (m/sec)	T_a (°C)	T_{pi} (°C)
Run C1	50.0	0.256	2.50	15.2	2.22	17.0	7.0
Run C2	50.0	0.240	1.25	15.4	2.23	17.0	7.0

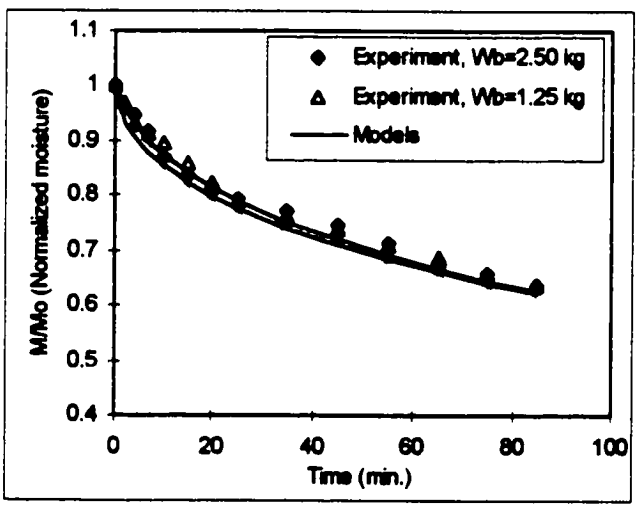

Figure 8.47 Effect of bed hold up on drying and comparison between experimental and numerical results for corn.

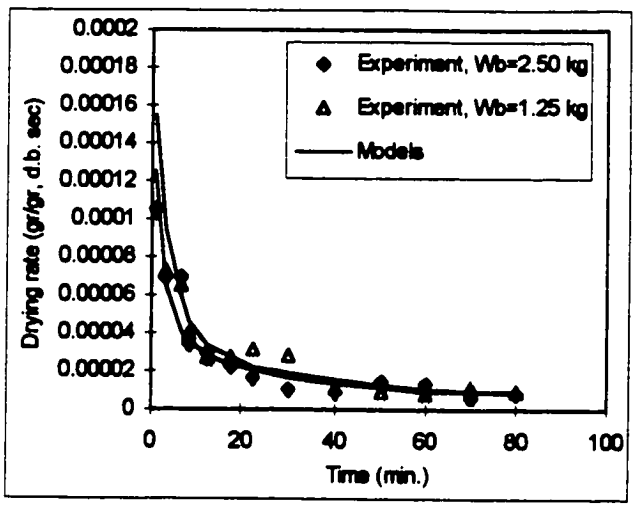

Figure 8.48 Effect of bed hold up on drying rate and comparison between experimental and numerical results for corn.

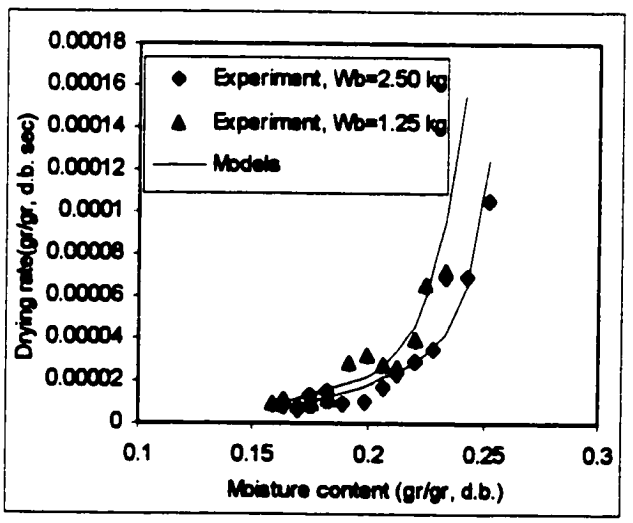

Figure 8.49 Effect of bed hold up on drying rate and comparison between experimental and numerical results for corn.

8.4.4 Effect of Gas Velocity

Figures 8.50 through 8.52 show the effect of gas velocity on the drying process and compare the experimental results with model predictions. The test conditions are listed in Table 8.7. For the air velocity reduction about 15%, the change in the drying process is hardly noticeable. The most noticeable variation takes place at the very initial stage of drying, when the surface moisture content is removed from the grains. After that, the effect of velocity becomes unimportant. The reason for choosing a narrow difference in velocities between two tests conditions was with the problem of fluidization of wet particles at the initial stage of drying. Since wet particles need higher gas velocity for fluidization, it was not possible to reduce the velocity to a lower value.

Table 8.7 Experimental conditions for investigating the effect of velocity.

	T (°C)	M_{pi} (d.b.)	W_b (kg)	RH (%)	U (m/sec)	T_a (°C)	T_{pi} (°C)
Run C1	50.0	0.256	2.50	15.2	2.22	17.0	7.0
Run C4	50.0	0.257	2.50	17.5	1.88	17.6	7.0

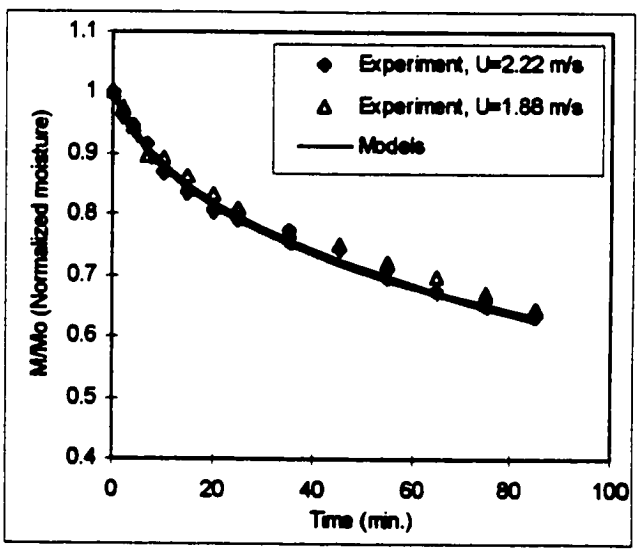

Figure 8.50 Effect of gas velocity on drying and comparison between experimental and numerical results for corn.

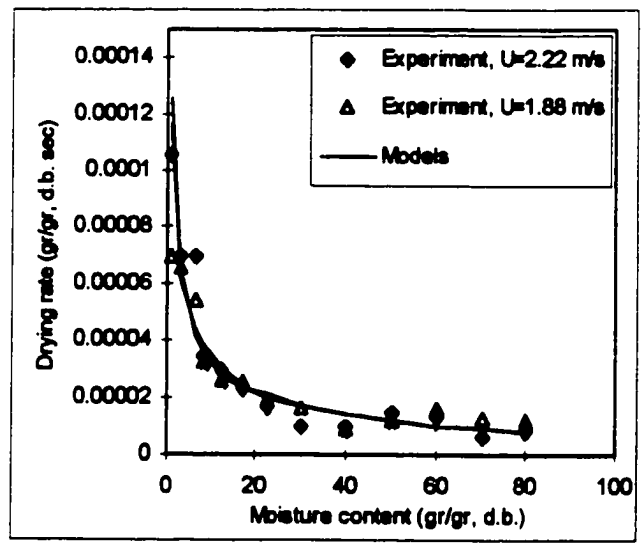

Figure 8.51 Effect of gas velocity on drying rate and comparison between experimental and numerical results for corn.

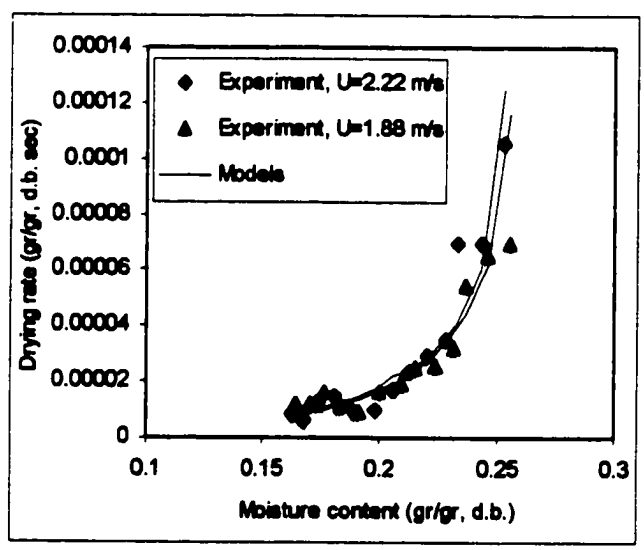

Figure 8.52 Effect of gas velocity on drying rate and comparison between experimental and numerical results for corn.

8.4.5 Effect of Initial Moisture Content

Figures 8.53 through 8.56 show the effect of initial moisture content of grains on the drying process and compare the experimental results with model predictions. The test conditions are listed in Table 8.8. As it can be seen, corn particles with a higher moisture content dry faster than those with a lower moisture content. This trend for the corn particles is different from the one for wheat particles. The mass diffusion coefficient of corn, unlike wheat, is a function of moisture content. Therefore, increasing the moisture content helps faster migration of moisture to the surface of the corn. Drying rate versus time also shows a higher value for the corn which has a higher initial moisture content.

Table 8.8 Experimental conditions for investigating the effect of initial moisture content.

	T (°C)	M_{pi} (d.b.)	W_b (kg)	RH (%)	U (m/sec)	T_a (°C)	T_{pi} (°C)
Run C1	50.0	0.256	2.50	15.2	2.22	17.0	7.0
Run C5	50.0	0.324	2.5	17.0	2.21	18.2	6.0

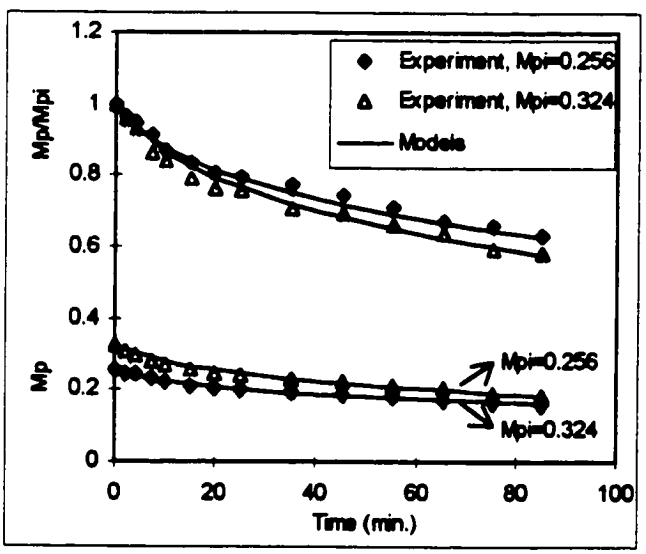

Figure 8.53 Effect of initial moisture content on drying and comparison between experimental and numerical results for corn (top curves are normalized and bottom curves are actual moisture content)

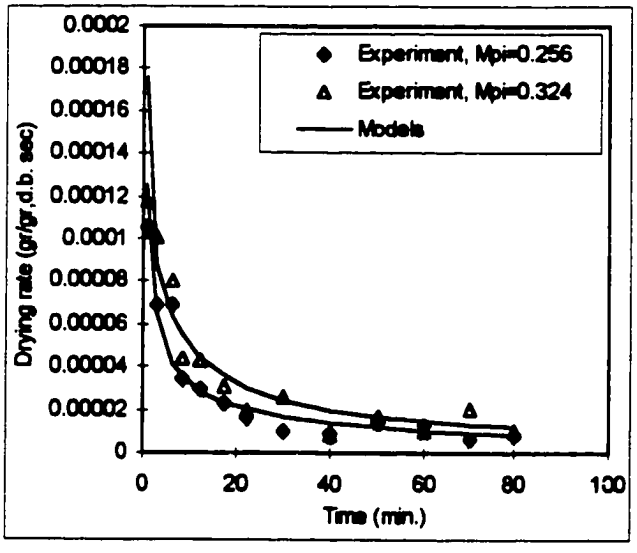

Figure 8.54 Effect of initial moisture content on drying rate and comparison between experimental and numerical results for corn.

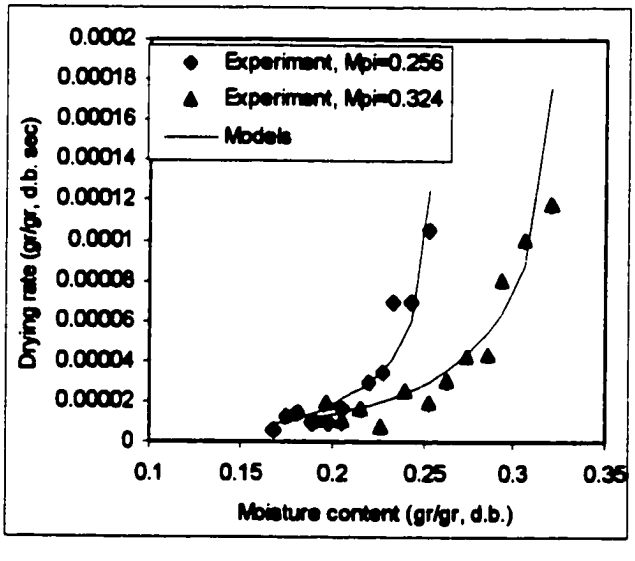

Figure 8.55 Effect of initial moisture content on drying rate and comparison between experimental and numerical results for corn.

Figure 8.55 shows the drying rate versus absolute moisture content which is not a good approach for comparison of results. Because the moisture content of particles are different, the best approach is comparison of drying rate versus normalized moisture content which is shown in Fig. 8.56. The high drying rate for corn with a higher initial moisture is clearly shown in this figure. At the initial stage, the difference in the drying rate is more than the rest which again could be attributed to the dependency of diffusion coefficient to the moisture content.

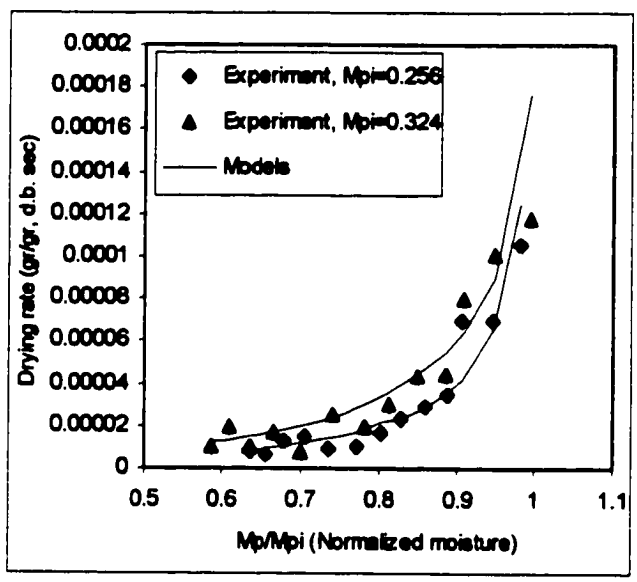

Figure 8.56 Effect of initial moisture content on drying rate and comparison between experimental and numerical results for corn.

8.5 Effect of Hydrodynamic Modeling on Drying Characteristics

It has already been mentioned that most models in the literature used the two-phase theory of fluidization in the hydrodynamic analysis of fluidized bed drying, regardless of the type of material which was used in the drying process. In this work, however, we have accounted different models for different types of materials. It may be interesting and

instructive to find out how much the result of model predictions can change if we use only the two-phase theory of fluidization instead of a more exact model in the hydrodynamic analysis of bed.

Figures 8.57 and 8.58 compare the results of drying curves under two different types of hydrodynamic models for wheat particles. The first model is the model which was used for group D particles (and already discussed in chapter 6) and the second model is the two-phase theory of fluidization. The figures show that there are considerable differences in the results of drying assuming the two different models, even in the falling rate mode of drying. As it can be seen, two-phase theory of fluidization underestimates the drying rate of particles in the bed. This underestimation could be justified since this model underestimates the amount of flow rate through the interstitial gas phase and predicts much of air goes through the bubble phase. Since the contribution of bubble phase in mass and heat transfer is less than the interstitial gas phase, therefore, the drying rate inside the bed decreases. Also, the figures show that the difference in drying rate is more important in the initial stage of drying.

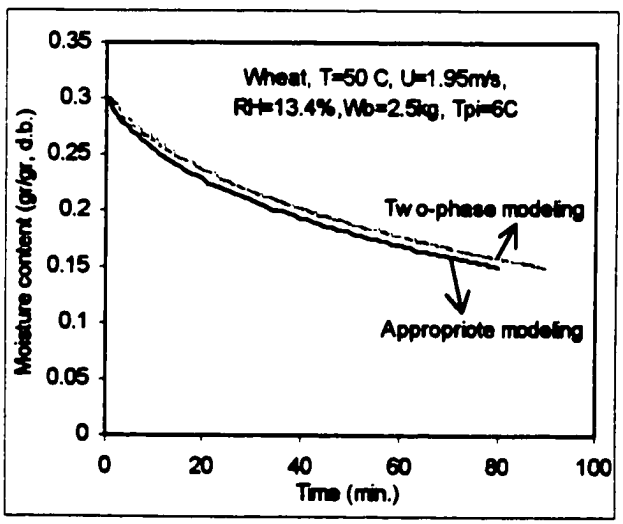

Figure 8.57 Effect of hydrodynamics modeling on the drying curve of wheat.

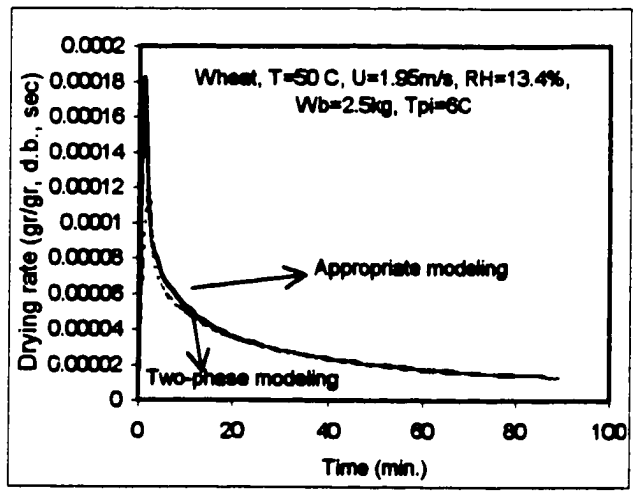

Figure 8.58 Effect of hydrodynamics modeling on the drying rate of wheat.

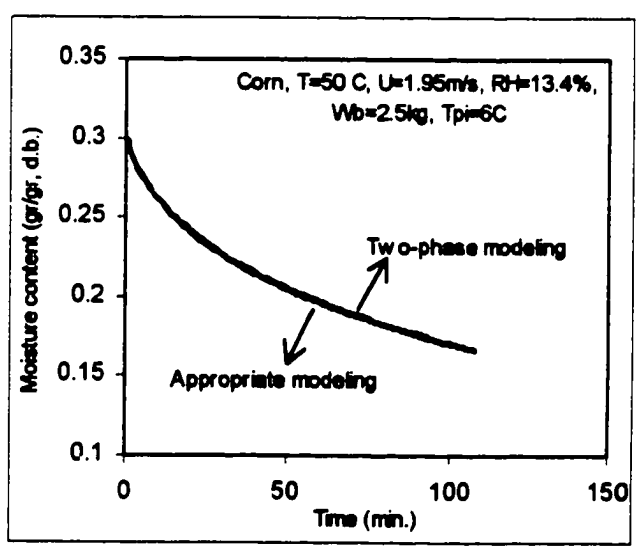

Figure 8.59 Effect of hydrodynamics modeling on the drying curve of corn.

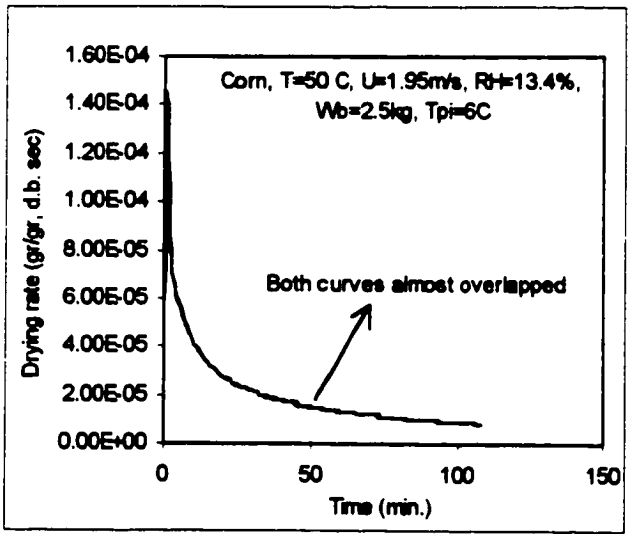

Figure 8.60 Effect of hydrodynamics modeling on the drying rate of corn.

Figures 8.59 and 8.60 compare the drying characteristics of corn particles under the same hydrodynamic models used for wheat particles. As it can be seen, the results do not show much difference between two different hydrodynamic models compare to the wheat particles. This could be attributed to the physical properties of corn particles especially diffusion coefficient which is lower than the wheat particles. Also, the other important factor is the difference in the surface area of two types of materials. Because the diameter of corn particles is almost twice as much as the wheat particles, the total surface area of corn is much lower than that of wheat. Therefore, the effect of external parameters become more negligible for corn particles.

8.6 Discussion and Conclusions:

A comprehensive mathematical model has been developed to simulate the drying of particles in fluidized beds. The model uses physical and thermal properties of different material available in the literature without using any adjustable parameters to fit the experimental data. Two different materials (wheat and corn) were used in the drying

experiments to obtain the complete experimental data for comparison with the model predictions. The model exhibits very good agreement with various experimental results. Error analysis between experimental results and model predictions of moisture content of particles showed that the maximum relative error for wheat is less than 6% and for corn is less than 5%. The mean relative error for wheat is less than 3% and for corn is less than 2%, which demonstrates the extent of reliability and accuracy of the model. The model has no restriction for the ranges of operational conditions of fluidized bed, and any range of air temperature or relative humidity could be used for prediction. From the experimental and numerical data the following observation are made. The drying rate of biological material is significantly influenced by air temperature. The effect of temperature is more critical than other parameter and could reduce the drying time substantially. No significant effect of bed hold-up, and gas velocity were observed on the drying rate in the falling rate period. Particles with higher initial moisture content can present different patterns of drying depending on their physical properties. For wheat particles where the diffusion is only a function of the temperature, the effect of initial moisture content is not discernable. For corn particles, where the diffusion coefficient depends on temperature and moisture content, increasing the initial moisture content increases the drying rate and reduces drying time. During drying, the moisture profile inside the particle shows the existence of relatively large concentration gradients, while the temperature profile shows negligible gradients. It was found that gas temperature gradient along the bed is initially important when the moisture on the surface of particles is removed, and after that period the temperature profile has a small gradient in the bed.

Observation of exhaust air humidity results shows that after rapidly increasing of gas humidity at the initial stage, the humidity of gas is not changed very much for the rest of drying period. The high humidity of gas at initial stage can be attributed to the fast removal of surface moisture at the beginning of drying. After the removal of the surface moisture, the rest of internal moisture cannot be removed easily because of low moisture

diffusivity coefficient of material, causing a rapid decrease in the relative humidity of the exhaust air. The low humidity of the exit gas can be considered as a good justification for applying the recycling method. Since this exit gas has high enthalpy and low humidity, it can be reused in drying process to reduce the amount of heating to the bed and consequently increase the thermal efficiency of the drying process.

Hydrodynamic modeling of fluidized bed drying may be able to play an important role on the drying process of particles even in the falling rate. Its importance depends on the physical properties of particle and conditions of drying medium. Using two-phase theory of fluidization for group B and D particles, underestimates the drying rate of particles in the bed, therefore, it is not recommended to use in the modeling of these particle groups. Instead, an appropriate model for each group of particles should be used to minimize the contribution of hydrodynamic error in the final results.

CHAPTER 9

Methods for Increasing Thermal Efficiency of Fluidized Bed Drying

9.1 Thermal Efficiency

Fluidized bed drying, like other types of conventional convective drying processes, is one of the most energy-intensive processes in industry. The efficiency of conventional drying systems is usually low and it could be as low as 10% depending on the gas temperature and other conditions. It is, therefore, desirable to improve the thermal efficiency of the drying process to reduce the overall consumption of energy. The thermal efficiency of drying process can be defined as [Giner and Calvelo, 1987]:

$$\eta_{th} = \frac{\text{Energy transmitted to the solid}}{\text{Energy introduced to the bed by gas}}$$

which can be expressed as:

$$\eta_{th} = \frac{W_b\left[h_{fg}\left(M_{pi} - M_{pf}\right) + C_p\left(T_{pf} - T_{pi}\right)\right]}{\rho_g u C_a \left(T - T_a\right)\Delta t} \qquad (10.1)$$

In the light of numerical modeling and experimental results one could implement different methods to increase the thermal efficiency of fluidized bed. Selection of specific type depends mostly on the experimental conditions of drying. Two methods, which generally are recommended for this purpose, are:

(1) recycling the exhaust air, and

(2) intermittency.

In the following, the results of implementation of these two methods on the drying system are discussed.

9.2 Recycling of Exhaust Gas:

As was found in the numerical predictions and experimental data, the relative humidity of exit gas rapidly decreased after removal of surface moisture content of the grain, which takes only few minutes after the onset of drying. This means that the exhaust gas, which has enough enthalpy, can be recycled and reused for drying purposes. This recycling can considerably reduce the amount of energy consumption in the drying system. Although this method was already recognized and recommended in drying processes little information is available in the literature regarding the details of its effect on the drying performance. When the exit gas is introduced into the bed again, the inlet condition of gas will change continuously because the exit gas temperature is continuously changing and the drying process is in an unsteady state condition. So, it is important that the model could handle variable inlet condition in the process of numerical simulation.

Usually total recycling of exit air is out of question since the air undergoes through a closed loop cycle and humidity will reach to 100% which will terminate the drying process. So for using the recycling method, one usually can recycle part of the exit gas into the bed which is called partial drying. The other question that may arise is the starting time of recycling. Should partial recycling start from initial stage of drying (simultaneous recycling) or should it start later (lagged recycling)? This question is important from this prospect that in the initial stage of drying the thermal efficiency and the humidity of exit gases are high so recycling them may not necessarily increase the overall efficiency. To investigate the effect of start time on the overall efficiency several runs with different time lags have been performed. Numerical modeling showed that the result for lagged recycling is not very much different from the simultaneous recycling because the humidity of gas is decreased rapidly after a few minutes and practically this time is very small compare to the total drying time. So, in the following, only the results of simultaneous recycling are discussed.

Figure 9.1 show the effect of recycling gas on the variation of moisture content of material. The drying conditions for all runs are constant and only a percentage of recycled gas was changed. Also, in order to find a common base for the comparison of different recycling scenarios, it is considered that the initial moisture content of the particles to be 0.3 d.b. and the final moisture content to be 0.15 d.b. for all the runs. So, the drying time is defined as the time required to bring the moisture content of material from 0.3 d.b. to 0.15 d.b. (dry basis).

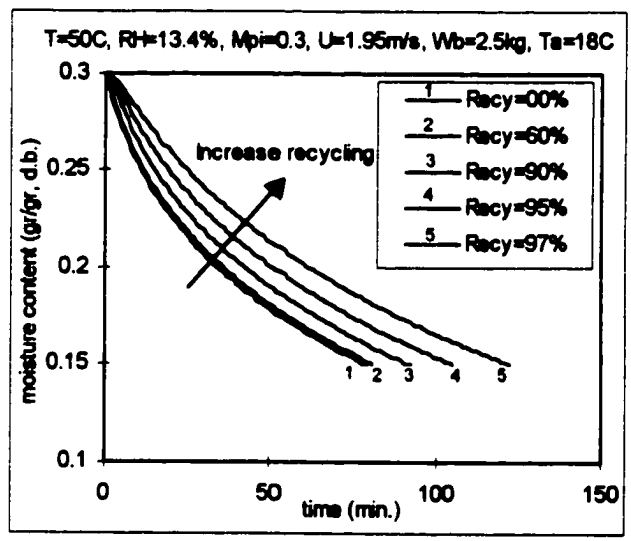

Figure 9.1 Effect of percentage of air recycled on the moisture content of particles.

As is evident in the Fig 9.1, increasing the percentage of recycled gas up to 60% of total inlet gas does not change the drying time considerably (the increase time is about 3 %) but the thermal efficiency increases considerably from about 13.3 % to 28.5 % (see Fig. 9.2). Recycling a greater percentage of outlet gas will increase the drying time faster than before but also increases the overall efficiency of the system.

Figure 9.2 shows the rate of increase in the thermal efficiency versus the percentage of recycling gas. Increasing the recycling gas increases the efficiency of drying because much of the outlet gas enthalpy can be reused. The trend of increase, however, is not linear but close to exponential

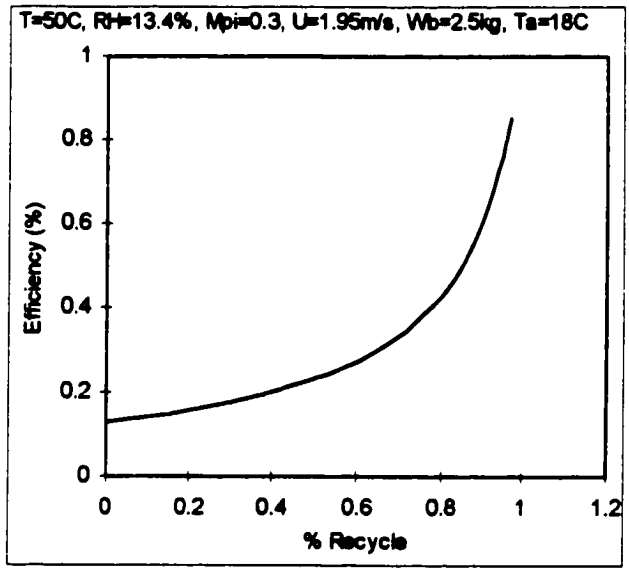

Figure 9.2 Effect of percentage of air recycled on the efficiency of drying.

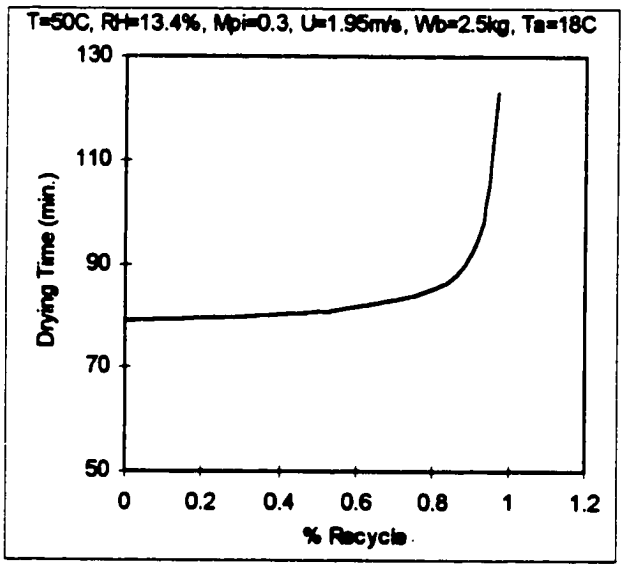

Figure 9.3 Effect of percentage of air recycled on the drying time.

Figure 9.3 shows the effect of recycling on the drying time. Up to about 60% recycling, the drying time does not increase considerably, but later on, the drying time will increase rapidly. Comparison of Fig. 9.2 and Fig. 9.3 shows that up to 60%, the slope of curve in Fig. 9.2 is much higher than the one in Fig. 9.3. This suggests the advantage of using the recycled gas in increasing the efficiency without increasing the drying time considerably. This scenario can be better understood from Fig. 9.4 which presents the efficiency versus drying time. As it is clear in the graph, the slope of the curve is much steeper at the low recycling percentage. This means that initially, with a small increase of drying time due to recycling, the increase in efficiency is much higher, but later on with increasing the drying time (which corresponds to more recycling percentage) the rate of efficiency increase is reduced.

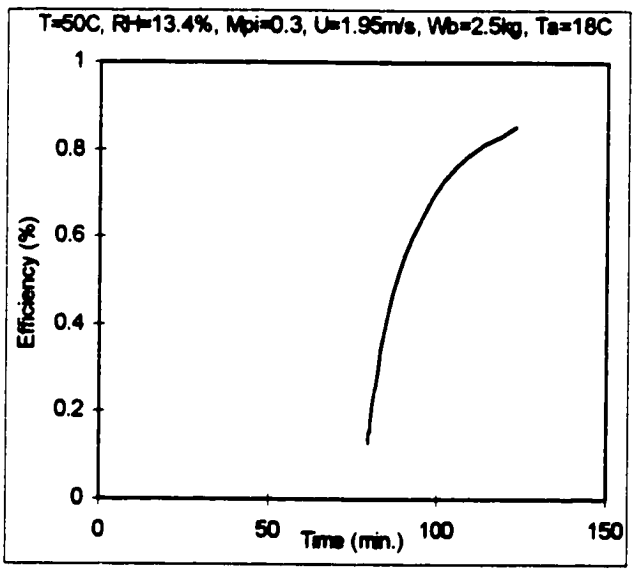

Figure 9.4 Variation of time vs. efficiency when the percentage of air recycled increases

Figure 9.5 shows the effect of recycling gas on the relative humidity of the outlet gas. The relative humidity at the initial stage is high due to the removal of moisture in the surface layers, and it decreases sharply as the internal moisture diffusion controls the rate

of drying. Clearly, the trend of variation in different recycling percentages changes considerably.

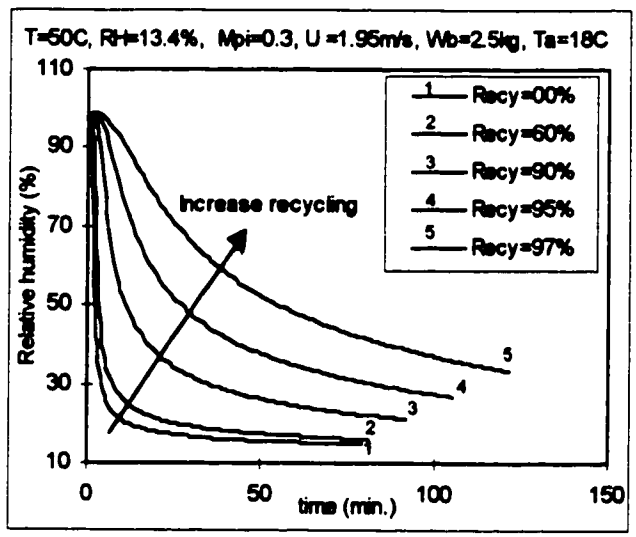

Figure 9.5 Effect of percentage of air recycled on the exit relative humidity of gas.

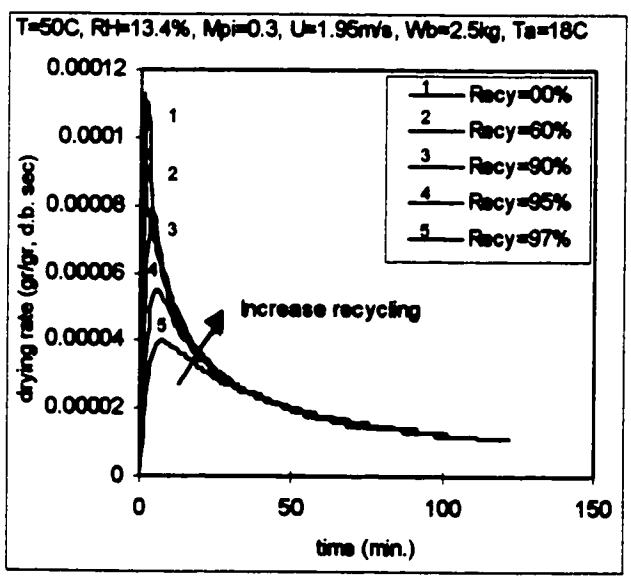

Figure 9.6 Effect of percentage of air recycled on the drying rate of process.

Figure 9.6 shows the effect of recycling gas on the drying rate. Initially, the drying rates are very high, but they decrease rapidly with time. The most important differences between the schemes are observed to be in the initial stage of drying. When there is no recycling (Recy=0.0), the drying rate, initially, is very high, it, however, rapidly changes and falls in a logarithmic fashion. With the introduction of the recycling air, the initial drying rate is significantly reduced but the effect of recycling air on the rest of the drying rate is negligible. This can be justified by the fact that in the beginning of drying the effect of external parameters (like the humidity of air) are relatively important, but later on this become ineffective. This is compatible with the fact that at the initial stage of drying, moisture at the outer layer of particle is removed first and that the external heat and mass transfer parameters are predominant. However, when the drying front progresses inside the particle, the effect of the external parameters diminish.

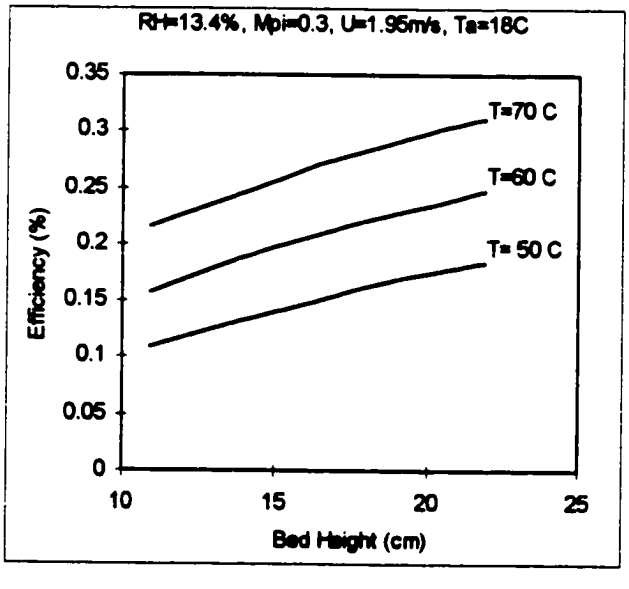

Figure 9.7 Thermal efficiency as a function of inlet air temperature and bed height.

Figure 9.7 shows the effect of bed height (which for a fixed diameter corresponds to bed hold up) on the thermal efficiency at different temperatures. Increasing the bed height increases the thermal efficiency almost linearly. Also, increasing the temperature has an important effect on the improvement of thermal efficiency.

9.3 Intermittency

The basic idea for operating the bed intermittently can be demonstrated by using the variation of moisture content distribution versus nondimensional radius graph, as shown in Fig. 9.8.

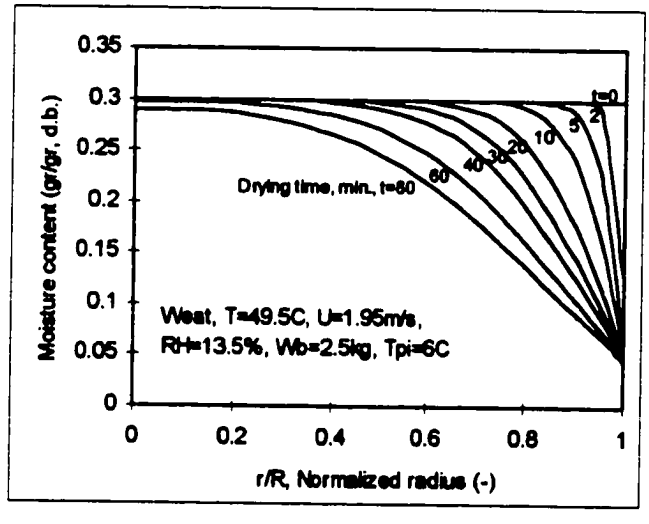

Figure 9.8 Typical variation of moisture inside the wheat grain during the drying.

As it seen in Fig. 9.8, there is a strong moisture gradient inside the particle during the drying process. This is due to the low moisture diffusion coefficient of the grain. The existence of this gradient suggests that the moisture should migrate naturally from the inner layer to the outer layer of particle and flatten the moisture distribution even if hot air is not introduced into the bed anymore. Although a high temperature would accelerate

this migration, it can also take place at low temperatures at a lower rate. This migration is useful for drying purposes since it aids the drying process by bringing more moisture close to the surface layer where it can be removed easier. To take advantage of the moisture gradient it is required to stop the hot gas flow into the bed and let the particles inside the bed undergo a rest period (tempering period). In the tempering period, the moisture can move from the interior to the exterior where it is readily available for evaporation. The purpose of the tempering process is to allow the moisture within the kernel to be redistributed to eliminate the gradient. When this is accomplished, some of the stresses in the exterior layers of the kernel caused by the rapid high temperature drying process are relieved. This technique which is called intermittent drying reduces some of the energy consumption and increases the thermal efficiency of the process. Furthermore, the material can be protected against drying-induced stresses, shrinkage, and cracking during the drying processes

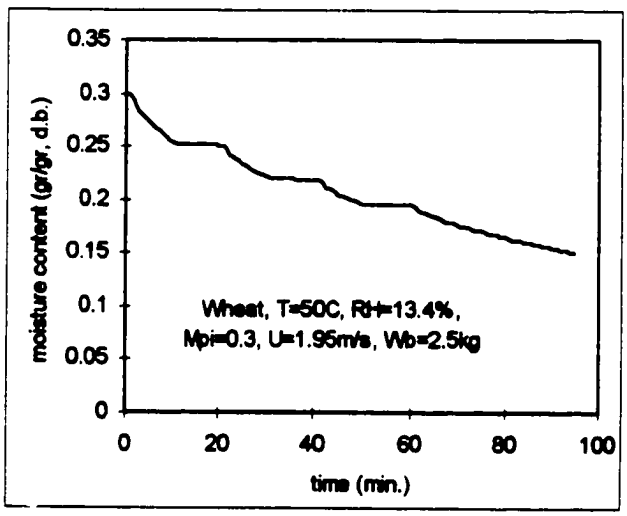

Figure 9.9 Prediction of drying curve in the intermittent scheme.

Figure 9.9 shows the moisture content versus time for intermittent drying of a wheat particle. In this figure intermittency is 0.5, which means hot gas was introduced during the "on" period (10 min.) and stopped during "off" periods (10 min.). As can be seen

from the figure, during the "off" period moisture content is constant and then during the "on" period it starts with high drying rate. This behaviour can be seen clearly in Fig. 9.10, which shows the variation of drying rate versus time. During the "off" period (tempering period) the drying rate is zero and after introducing the air, drying rate has initially a high rise and then a rapid fall. This initial rise in the drying rate is the result of migration of moisture and its accumulation close to the outer layers during the off periods. Practically the drying rate may be less than what is predicted if the particles during the off period do not seal properly.

The increase in the moisture content of outer layers of particles is shown in the Figure 9.11. The solid lines are moisture distribution at the end of the "on" period where the dashed lines are the moisture distribution at the end of "off" period. It is shown that intermittent drying allow gradual moisture redistribution inside the particle which tends to level the moisture gradient by migration of moisture toward outer layer of particle.
Figure 9.12 presents the result of numerical prediction of outlet humidity for intermittent drying. During the "off" period the humidity is constant since there is no drying and the airflow is discontinued. In the "on" period the relative humidity starts with a very high value and then rapidly drops down. This pattern is in accordance with drying rate pattern.

Figure 9.13 shows the results of the simulation of the air temperature (at H=2 cm) and the temperature of particle surface during drying. Particle temperature stays constant during the "off" period since it is assumed that there is no heat transfer interaction. Moreover, it is shown in this graph that both air and particle experience a sudden temperature drop at the initial stage of "on" period. This can be justified by the fact that high drying rate at this time require more heat for vaporization of moisture which is supplied by the air, causing a temperature drop in the system. Like the drying rate, this phenomenon is very short lived and after that the temperature increase rapidly to its normal value.

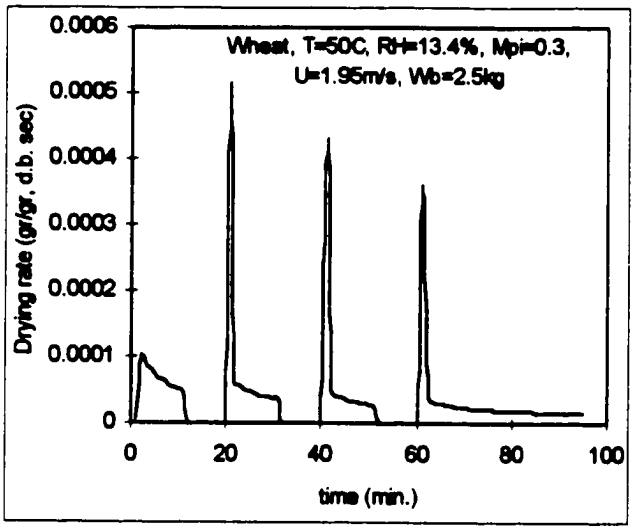

Figure 9.10 Drying rate vs. time in the intermittent scheme.

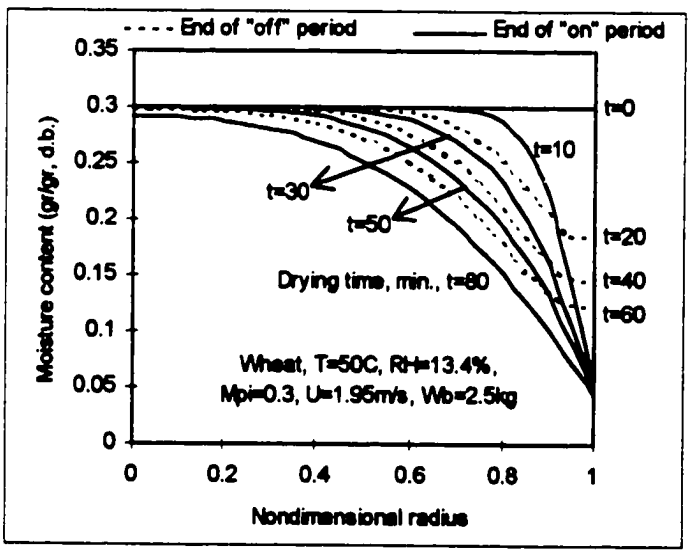

Figure 9.11 Predicted moisture distributions for intermittent scheme (solid lines are at the end of "on" period and dashed lines are at the end of "off" period).

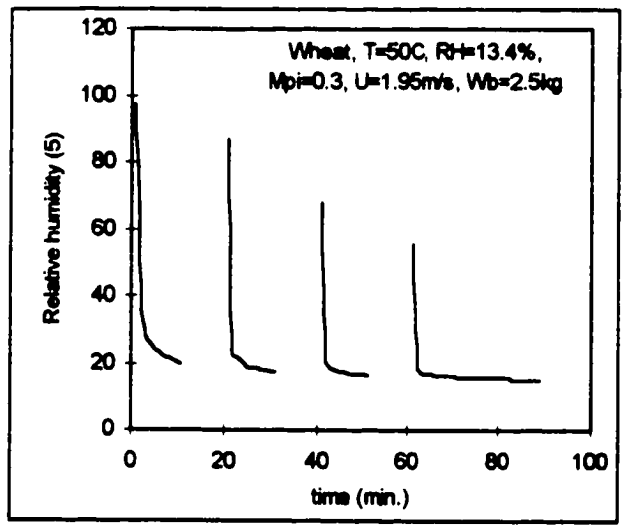

Figure 9.12 Predicted relative humidity vs. time in the intermittent scheme.

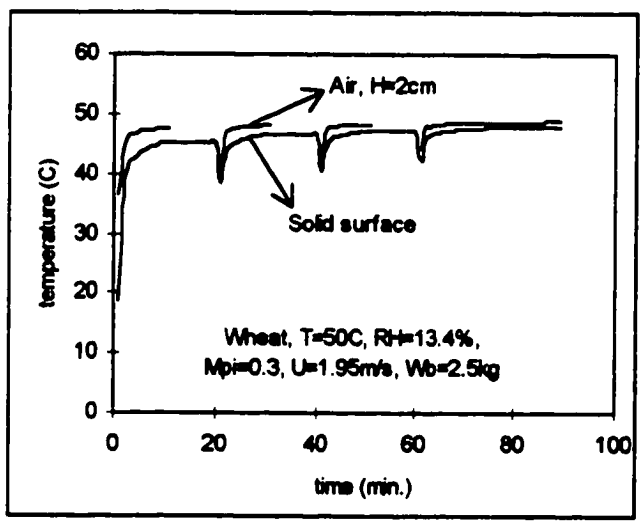

Figure 9.13 Predicted temperature of grain and air at H=2 cm, vs. time in the intermittent scheme.

9.4 Discussion and Conclusion

The results of the two methods, which can be used to increase the thermal efficiency of fluidized bed, are presented. The results show that partial recycling of the exit gas to the

bed can increase the thermal efficiency of the bed considerably. The effect of recycling the exit air on the thermodynamic condition of gas is the increase of relative humidity of inlet air. Since the relative humidity effect is of secondary importance, the partial recycling of air will not have a very important effect on the drying time. This can result in a major advantage in the drying system because the enthalpy of recycled gas is not wasted, and at the same time, the amount of heating supply to the bed is reduced. Practical implementation of recycling approach is an easy task and it does not need special equipment.

Intermittency is another approach that can improve the efficiency of the bed and the quality of the products. In this approach, one can use the existing gradient of moisture as a driving force for the moisture migration from the inner layer to the outer layer of the particle. Increasing the thermal efficiency in this approach is limited and cannot be improved as much as in the case of recycling. However, it should be noted that the actual drying time, the time when particle is exposed to the hot air, (aerating time) is reduced in this approach. For example for the conditions presented earlier, the increase in the thermal efficiency is about 30% and the reduction in actual drying time (total of "on" periods) is about 25%. Practical implementation of this approach is also an easy task and can be done without using special equipment.

Another approach that could be used is the combination of recycling and intermittency. There is no obstacle to apply both approaches simultaneously. This means that during the "on" period of the drying, exit gas can be recycled into the bed. During the "off" period there will be no gas flow, therefore, recycling is not applicable. This approach has the advantage of both the recycling and intermittency and it can be used if the extended drying time is not a problem for the specific application.

CHAPTER 10

Conclusions and Recommendations

Various aspects related to the hydrodynamics and kinetics of fluidized bed drying systems has been studied and analyzed in this work. In this chapter, the main findings from this work are summarized and the recommendations for future work are given.

10.1 Conclusions

The following conclusions have been drawn from the present study:

1. Swirling induced distributor plate may affect the hydrodynamic characteristics of fluidized bed and gas-solid contacting pattern. For group D particles, the effect of swirling outlet is noticeable as the bubbles size inside the bed is reduced. For group B particles the effect of the swirling outlet is only important in shallow beds.

2. Increasing the bed height or particle density decreases the effect of swirling induced distributor on the hydrodynamics of the bed due to an increase in the static bed pressure.

3. The general pattern of pressure drop versus gas velocity diagram for fluidization of moist particles is different from those of dry particles. In the case of moist particles, bed pressure drop may increase gradually by increasing the gas velocity above the minimum fluidization velocity.

4. Increasing the moisture content of particles increases the minimum fluidization velocity of particles due to increased adhesive forces inside the bed. This suggests that in predicting the minimum fluidization velocity, the conventional balance of drag with gravity forces is not fully applicable and that the effect of interparticle cohesive

force caused by a liquid bridge between isolated capillaries must be taken into account.

5. The type of correlation between minimum fluidization velocity and moisture content may vary at different ranges of moisture content. For some ranges the correlation might be linear but for some other ranges it may be nonlinear, depending on the physical properties of material and the degree of liquid saturation.

6. Increasing the moisture content of materials in fixed bed conditions reduces the bed pressure drop along the bed due to the creation of low-resistance microchannels in the bed.

7. Since Ergun's equation does not consider the effect of moisture content of particles, it overestimates the bed pressure drop in the case of moist particles in the fixed bed.

8. A comprehensive mathematical model has been developed to simulate drying of different particle groups in fluidized beds, considering the different hydrodynamics models for each group of particles. The model also takes into account the contribution of different phases inside the bed throughout the general form of partial differential equations for each phase.

9. Results of model predictions exhibit a very good agreement with a large number of experimental data obtained in drying of grains (wheat and corn) without using any adjustable parameters (Average relative error 3%). The model is fully predictable for fluidized bed drying of other materials in the fluidized bed with no restriction on the range of operational condition such as air temperature and relative humidity.

10. The inlet air temperature has the most important effect on the drying rate of materials. Increasing the inlet air temperature increases the drying rate of the material.

11. Increasing the bed hold up does not significantly change the drying rate of materials, therefore, one can use as much material in the bed to increase the thermal efficiency of drying, as long as fluidization is maintained.

12. Gas velocity has no significant effect on the drying rate of the materials in the falling rate period.

13. The effect of initial moisture content of materials on the drying rate may vary for different particles depending on the physical properties of the materials. For wheat particles, where the diffusion coefficient is only a function of the temperature, the effect of initial moisture content is not tangible. For corn particles, where the diffusion coefficient depends on the temperature and the moisture content, increasing the initial moisture content increases the drying rate.

14. The distributions of moisture and temperature inside the particle are highly dependent on the mass and heat transfer Biot numbers. In the case of wheat and corn particles with high mass transfer Biot number, there are large gradients of moisture concentration contrary to the temperature profiles which are nearly flat due to a small heat transfer Biot number.

15. Air temperature gradient inside the bed is found to be significant within a fairly short distance from the distributor plate above which there is nearly uniform temperature distribution in the bed.

16. The type of hydrodynamic modeling of fluidized bed drying may have an important effect on the drying process of particles even in the falling rate. The degree of importance depends on the physical properties of particle and conditions of drying

medium. Using two-phase theory of fluidization for group B and D particles, underestimates the drying rate of particles in the bed.

17. Partial recycling of exit air from the fluidized bed, up to 97 %, can be used in drying process to increase the thermal efficiency. Although, recycling increases the drying time due to increasing the relative humidity of inlet air, the rate of energy reduction is much higher, and therefore, the overall thermal efficiency increases considerably.

18. Intermittent scheme can improve the thermal efficiency of the fluidized bed and the quality of dried products. The amount of increase in thermal efficiency depends on the intermittency scheme but it is usually lower than the recycling scheme.

10.2 Recommendations

For the future works in this area the following outlines are recommended:

1. Extending the mathematical model to consider the existence of heating surfaces inside the bed and conducting the experiments for its validation.

2. Extending the mathematical model to consider the binary particles in the bed as the heating medium and conducting the experiment for its validation.

3. Extending the mathematical model to simulate the steam fluidized bed drying and conducting the experiments for its validation.

4. Extending the mathematical model for continuous fluidized bed and conducting experiments for its validation.

5. Conducting experiments to investigate the effect of recycling scheme on the drying rate and the thermal efficiency of the bed and comparing them with the available results of the mathematical model.

6. Conducting experiments to investigate the effect of intermittent scheme on the drying rate and thermal efficiency of the bed and comparing them with the available results of the mathematical model.

7. Considering the real shape of particles in the mathematical model by using the body fitted coordinate and grid generation approaches.

8. Considering the effect of different scheme of discretization equations on the results of drying process.

9. Using the two-phase flow theory for predicting the velocity flow field in the bed by solving the Navier-Stokes equations.

10. Investigating the effect of swirling induced distributor plate on the hydrodynamics of the circulating fluidized bed systems and other regime of fluidization.

11. Investigating the effect of vibration on the hydrodynamics of moist particles inside the bed.

REFERENCES

- Abid, M., Gibert, R., Laguerie, C., 1990, "An Experimental and Theoretical Analysis of the Mechanism of Heat and Mass Transfer During the drying of Corn Grains in a Fluidized Bed", International Chemical Eng., Vol. 30 (4), pp. 632-642.

- Alebregtse, J.B., 1986, "Fluidized Bed Drying: A Mathematical Model for Hydrodynamics and Mass Transfer", In Heat and Mass transfer in fixed and Fluidized Bed; W. P. M. Van Swaajj, N. H. Afgan, Eds., Hemisphere Publishing Corp., New York, pp. 511-521.

- Alvarez, P. and Shene, C., 1996, "Experimental Study of the Heat and Mass Transfer Drying in a Fluidized Bed Dryer", Drying Technology, Vol. 14, (3,4), pp. 701-718.

- Bahu, R.E., 1991, "Energy Consumption in Dryer Design", In Drying 91, Eds. A.S. Mujumdur and I. Filkova, Elsevier Science Publishers, Amesterdam, pp. 553-557.

- Basu, P., 1984, "Design of Gas Distributors for Fluid Bed Boilers", In Fluidized Bed Boilers: Design and Application", Ed. Basu, P., Pergamon Press, pp. 45-61.

- Becken, D.W., 1960, "Thermodrying in Fluidized Beds", British Chem. Eng., Vol. 5, pp. 484-495.

- Becker, H. A., 1959, "A Study of Diffusion in Solids of Arbitrary Shape, with Application to the Drying of the Wheat Kernel", J. of Appl. Polym. Sci., Vol. 1 (2), pp. 212-226.

- Becker, H.A. and Isaacson, R..A., 1970, "Wheat Drying in Well Stirred Batch and Continuous Moving Bed Dryers", Can. J., Chem. Eng.. Vol. 48, pp. 560-567.

- Bejan, A., 1993, "Heat Transfer", John Wiley & Sons Inc., New York, pp. 352.

- Brooker, D. B., Bakker-Arkema, F. W. and Hall, C. W., 1974, Drying Cereal Grain, The AVI Publishing Company, Connecticut.

- Chandran, A.N., Rao, S.S. and Varma, Y.B.G., 1990, "Fluidized Bed Drying of Solids", AIChE J., Vol. 36 (1), pp. 29-38.

- Chaouki, J., Chavarie, D., and Klvana, D., 1985, "Effect of Interparticle Forces on the Hydrodynamic Behaviour of Fluidized Aerogels", Powder Technology, Vol. 43, pp. 117-125.

- Chu, S.T. and Hustrulid, A., 1968, "Numerical Solution of Diffusion Equations", Trans. ASAE, Vol. 11, pp. 705-708.

- Ciesielczyk, W., 1996, "Analogy of Heat and Mass Transfer During Constant Rate Period in Fluidized Bed Drying", Drying Technogy, Vol. 14, (2), pp. 217-230.

- Cook, M.E., 1997, "Drying of Wet Solids and Solids in Liquids", In Handbook of Separation Technology for Chemical Engineers, Ed. P.A. Schweitzer, McGraw-Hill, New York.

- Darton, C., LaNauze, R. D., Davidson, J. F., and Harrison, D., 1977, "Bubble Growth Due to Coalescence in Fluidized Beds", Trans. IChemE., Vol. 55, pp. 274-280.

- Dhodapkar, S.V., Klinzing, G.E, 1993, "Pressure Fluctuation Analysis for a Fluidized Bed," AIChE Symposium Serial, Vol. 89, No. 296, pp. 170-183.

- DiMattia, D. G., 1992, Onset of Slugging in Fluidized Bed Drying of Large Particles, M.Sc. Thises, Technical University of Nova Scotia, Halifax, Canada.

- Dhodapkar, S.V. and Klinzing, G.E, 1993, "Pressure Fluctuation Analysis for a Fluidized

- Ergun, S., 1952, "Fluid Flow Through Packed Columns", Chem. Eng. Prog. Vol. 48, pp. 89-94.

- Evan, P.L., J. P. K. Seville and Clift, R, 1989, "Mobilisation of Cohesive Particles in A Novel Spouted Bed", Fluidization VI, Eds., Grace, J.R., Shemilt, L.W., Bergougnou, M.A., Engineering Foundation, New York, pp. 253-260.

- Fan, L.T., Ho, T.C., Hiroaka, S. and Walawender, S.P., 1981, "Pressure Fluctuations in a Fluidized Bed," AIChE J., Vol. 27, pp. 388-396.

- Fortes, M., Okos, M.R. and Barrett, J.R., 1981, "Heat and Mass Transfer Analysis of Intra-kernel Wheat Drying and Rewetting", J. Agric. Engng. Res., Vol. 26, pp. 109-125.

- Geldart, D., 1986, Gas Fluidization Technology, Wiley & Sons, New York.

- Giner, S.A. and Calvelo, A., 1987, "Modeling of Wheat Drying in Fluidized Bed", J. of Food Sci., Vol. 52 (5), pp. 1358-1363.

- Grabowski, S., Mujumdar, A.S., Ramaswamy, H.S. and Strumillo, C., 1997, "Evaluation of Fluidized Versus Spouted Bed Drying of Baker's Yeast", Drying Technology, Vol. 15, (2), pp. 625-634.

- Hall, C. W., 1980, Drying and Storage of Agricultural Crops, The AVI Publishing Company, Connecticut.

- Hamdullahpur, F., Zayed, R.S. and El Khawaja, E., 1989, "NOx Reduction in Fluidized Bed Combustors", Proceeding of the American Flame Research Committee's, International Symposium on Combustion in Industrial Furnaces and Boilers, New Jersey.

- Hartman, M. and Svoboda, K., 1986, "Predicting Minimum Fluidization Velocities for Fluidized Beds", In Encyclopedia of Fluid Mechanics, N. P. Cheremisinoff, Ed. Gulf Publishing Co. Huston, Vol. 4, pp. 756-780.

- Hemati, M., Mourad, M., Steinmetz, D. and Laguerie, C., 1992, "Continuous and Intermittent Drying of Maize in a Flotation Fluidized Bed", Fluidization VII, Eds. Potter, O.E., Nicklin, D.J., Engineering Foundation, New York, pp. 831-839.

- Henderson, S.M., 1952, "A Basic Concept of Equilibrium Moisture", Agric. Engng. Vol. 33, pp.29-32.

- Hilligardt, K., Werther, J., 1986, "Local Bubble Gas-Hold up and Expansion of Gas/Solid-Fluidized Beds", German Chem. Eng., Vol. 9, pp. 215.

- Hoebink, J.H.B.J. and Rietema, K., 1980a, "Drying Granular Solids in Fluidized Bed-I", Chem. Eng. Sci., Vol. 35, pp. 2135-2140.

- Hoebink, J.H.B.J. and Rietema, K., 1980b, "Drying Granular Solids in Fluidized Bed-II", Chem. Eng. Sci., Vol. 35, pp. 2257-2265.

- Hovmand, S., 1987, "Fluidized Bed Drying", In Handbook of Industrial Drying, Ed. A.S. Mujumdar, Marcel Dekker Inc., New York.

- Howard, J. R., 1989, Fluidized Bed Technology, Adam Hilger, New York.

- Israelachvili, J., 1992, Intermolecular & Surface Forces, 2nd ed., Academic Press, London.

- Jaraiz, E., Kimura, S., and Levenspiel, 1992, "Vibrating Beds of Fine Particles: Estimation of Interparticle Forces from Expansion and Pressure Drop Experiments" Powder Technology, Vol. 72, pp. 23-30.

- Jumah, R.Y., Mujumdar, A.S. and Raghavan, G.S.V., 1997, "A Mathematical Model for Constant and Intermittent Batch Drying of Grains in a Novel Rotating Jet Spouted Bed", In Mathematical Modeling and Numerical Technique in Drying Technology, Eds., I., Turner, A.S. Mujumdar, Marcel Dekker Inc., New York.

- Kazarian, E.A. and Hall, C.W., 1965, "Thermal Properties of Grain", Transaction of the ASAE, Vol. 8, pp. 33-37.

- Kiranoudis, C.T., Maroulis, Z.B. and Marinos-Kouris, D., 1997, "Modeling and Optimazation of Fluidized Bed and Rotary Dryers", Drying Technology, Vol. 15, (3,4), pp. 735-763.

- Kunii, D., Levenspiel, O., 1991, Fluidization Engineering, Butterworth-Heinemann, Boston.

- Lee, K.J., Hu, C.G., Shin, Y.S. and Chun, H.S., 1990, "Combustion Characteristics of a Two-Stage Swirl-Flow Fluidized Bed Combustor," The Canadian J. of Chem. Eng., Vol. 68, pp. 824-830.

- Lirag, R. and Littman, H., 1971, "Statistical Study of the Pressure Fluctuations in a Fluidized Bed", AIChE Symposium Serial, Vol. 67, No. 116, pp. 11-22.

- Luikov, A. V., 1966, Heat and Mass Transfer in Capillary-Porous Bodies, Pergamon Press, London.

- Maroulis, Z.B., Kremalis, C. and Kritikos, T., 1996, "A Learning Process Simulator for Fluidized Bed Dryers, Application to Bentonite", Drying Technology, Vol. 13, (8,9), pp. 1763-1788.

- Masrers, K., 1993, "Importance of Proper Design of the Air Distributor Plate in Fluidized Bed Drying System", AIChE Symposium Series, Vol. 89, No. 297, pp. 118-126.

- Massimilia, L. and Donsi, G., 1976, "Cohesive Force Between Particles of Fluid-Bed Catalysts", Powder Technology, Vol. 15, pp. 253-260.

- Molerus, O., 1982, "Interpretation of Geldart's Type A, B, C, and D Powders by Taking Into Account Interparticle Cohesion Forces", Powder Technology, Vol. 33, pp. 81-87.

- Mujumdar, A.S., 1987, Handbook of Industrial Drying, Marcel Dekker Inc., New York.

- Nieh, S. and Yang, G., 1987, "Particle Flow Pattern in the Freeboard of a Vortexing Fluidized Bed," Powder Technology, Vol. 50, pp. 121-131.

- Patankar, S. V., 1980, Numerical Heat Transfer and Fluid Flow, Hemisphere Publising Corp., London.

- Pfost, H.B., Maurer, S.G., Chung, D.S. and Milliken, G.A., 1976, "Summarising and Reporting Equilibrium Moisture Data for Grains, ASAE Paper No. 76-3520.

- Plancz, B., 1983, "A Mathematical Model for Continuous Fluidized Bed Drying", Chem. Eng. Sci., Vol.38 (7), pp. 1045-1059.

- Ranz, E., 1952, "Fixation and Transfer Coefficients for Single Particles and Packed Bed", Chem. Eng. Prog., Vol. 48, pp. 247-253.

- Reay, D. and Allen, R.W.K., 1982, "Predicting the Performance of a Continuous Well-Mixed Fluid Bed Dryer From Batch Tests", Proceeding of the third International Drying Symposium, Vol. 2, pp. 130-140.

- Sadasivan, N., Barreteau, D. and Laguerie, C., 1980, "Studies on Frequency and Magnitude of Fluctuations of Pressure Drop in Gas-Solid Fluidized Beds," Powder Technology, Vol. 26, pp. 67-74.

- Saxena, S.C., Chatterjee, A. and Patel, R.C., 1979, "Effect of Distributors on Gas-Solid Fluidization," Powder Technology, Vol. 22, pp. 191-198.

- Schubert, H., Herrmann, W., and Rumf, H., 1975, "Deformation Behaviour of Agglomerates under Tensile Stress", Powder Technology, Vol. 11, pp. 121-131.

- Schubert, H., 1984, "Capillary Forces-Mdelingand Application in Particulate Technology", Powder Technology, Vol. 37, pp. 105-116.

- Simmonds, W.H.C, Ward, G.T. and McEwen, E., 1953, "The Drying of Wheat Grain. Part I: The Mechanism of Drying; Part II. Through Drying of Deep Beds", Trans. Ins. Chem. Engrs., Vol. 31, (3), pp. 265-288.

- Soponronnarit, S., Pongtornkulpanich, A. and Prachayawarakorn, S., 1997, "Drying Characteristics of Corn in Fluidized Bed Dryer", Drying Technology, Vol. 15, (5), pp. 1603-1625.

- Srinivasa Kannan, C., Rao, S.S. and Varma, Y.B.G., 1994, "A Kinetic Model for Drying of Solids in Batch Fluidized Beds", Ind. Eng. Chem. Res., Vol. 33, pp. 363-370.

- Srinivasa Kannan, C., Thomas, P.P. and Varma, Y.B.G., 1995, "Drying of Solids in Fluidized Beds", Ind. Eng. Chem. Res., Vol. 34, pp. 3068-3077.

- Stakic, M.B. and Milojevic, D.Z., 1992, "Numerical Simulation of Fluidized Bed Drying Process", In Drying 91, A. S. Mujumdar, I. Filkova, Eds., Elsevier, pp. 248-256.

- Thomas, P.P. and Varma, Y.B.G., 1992, "Fluidized Bed Drying of Granular Food Materials", Powder Technology, Vol. 69, pp. 213-222.

- Theologos, K.N., Maroulis, Z.B. and Markatos, N.C., 1997, "Simulation of Transport Dynamics in Fluidized-Bed Dryers", Drying Technology, Vol. 15, (5), pp. 1265-1291.

- Toomey, R. D., Johnstone, H. F., 1952, "Gaseous Fluidization of Solid Particles", Chem. Eng. Prog., Vol. 48, pp. 220.

- Turner, I. and Mujumdar, A.S., 1997, Mathematical Modeling and Numerical Technique in Drying Technology, Marcel Dekker Inc., New York.

- Uckan, G. and Ulku, S., 1986, "Drying of Corn Grain in a Batch fluidized Bed drier", In Drying of Solids: Recent developments; A. S., Mujumdar, Ed.; Wiley: New York, pp. 91-96.

- van Ballegooijen, W.G.E., van Loon, A.M. and van der Zanden, 1997, "Modeling Diffusion-Limited Drying Behaviour in a Batch Fluidized Bed Dryer", Drying Technology, Vol. 15, (3,4), pp. 837-1855.

- Vanecek, V., Markvart, M. and Drbohlav, R., 1966, Fluidized Bed Drying, Leonard Hill Books, London.

- Waananen, K.M., Litchfield, J.B. and Okos, M.R., 1993, "Classification of Drying Models for Porous Solids", Drying Technology, Vol. 11, (1), pp.1-40.

- Wang, C.Y. and Singh, P., 1978, "A Single Layer Drying Equation for Rough Rice", Paper No. 78-3001, Am. Soc. Agr. Eng. St. Joseph, MI.

- Zahed, A.H., Zhu, J.X., Grace, J.R., 1995, "Modeling and Simulation of Batch and Continuous Fluidized Bed Dryers", Drying Technology", Vol. 13, (1,2), pp. 1-28.

- Zayed, R. S., Hamdullahpur, F. and Al Taweel, A.M., 1990, "Mathematical Modeling of Particle Motion in the Freeboard of a Swirling Fluidized Bed", Proceeding of the 73rd Canadian Chemical Conference, Halifax, N.S.

IMAGE EVALUATION TEST TARGET (QA-3)

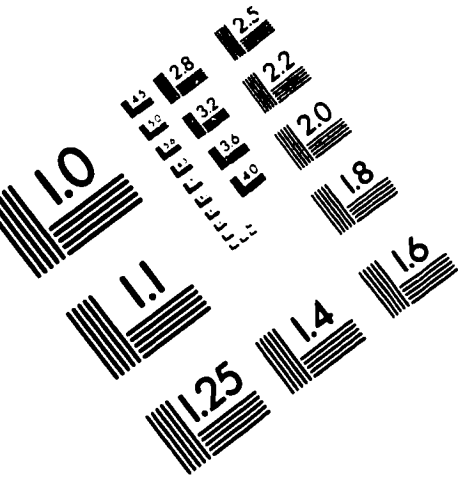

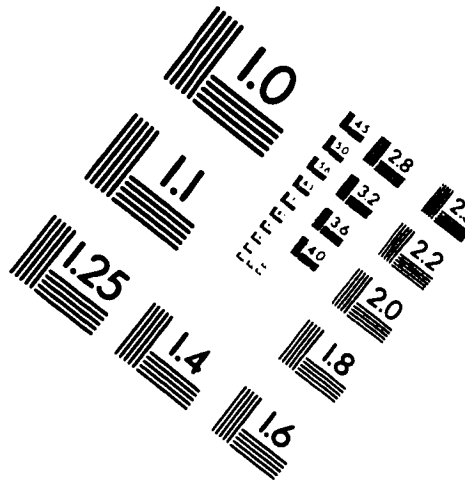

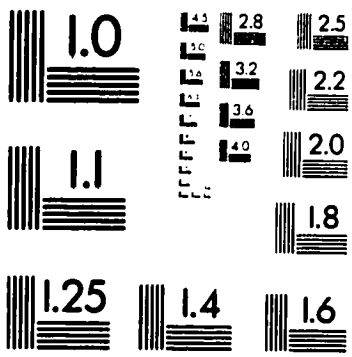

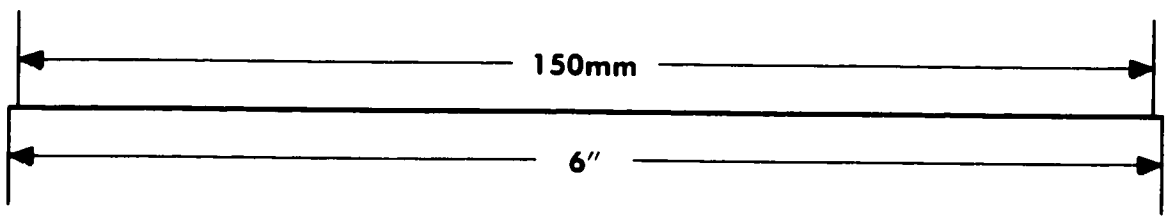

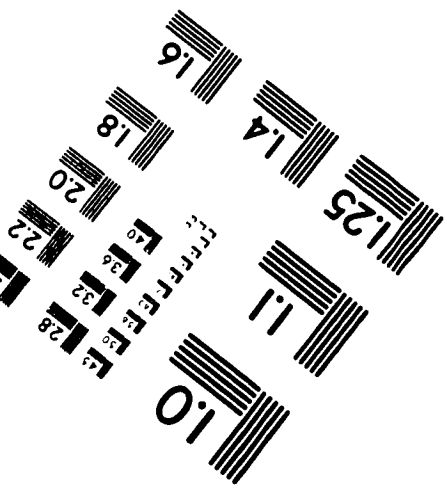

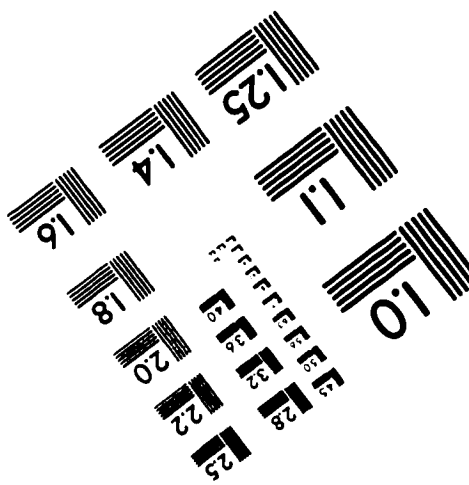

APPLIED IMAGE, Inc
1653 East Main Street
Rochester, NY 14609 USA
Phone: 716/482-0300
Fax: 716/288-5989